

Polyglycerol-Based Hydrogels For Broad-Spectrum Anti-Viral Applications

Inaugural-Dissertation
to obtain the academic degree
Doctor rerum naturalium (Dr. rer. nat.)

submitted to the Department of Biology, Chemistry,
Pharmacy
of Freie Universität Berlin

by
Antara Sharma

Berlin, 2021

The research presented in this thesis was carried out from **May 2017** to **December 2021** under the supervision of Prof. Dr. Rainer Haag at the Institute of Chemistry and Biochemistry – Organic Chemistry of the Freie Universität Berlin.

1. Examiner: Prof. Dr. Rainer Haag

2. Examiner: Prof. Dr. Nan Ma

Place: Berlin, Germany

Date of defense: 3rd March, 2022

Acknowledgements

First and foremost, I'd like to express my gratitude to Prof. Dr. Rainer Haag, for being my supervisor. His kindness, support, generosity, understanding and scientific input was invaluable during my entire time as a PhD student, and I will return to his advice again and again for my future endeavors.

I would also like to thank Prof. Dr. Nan Ma for her contribution as the second examiner in this thesis.

I would especially like to thank Dr. Sumati Bhatia for her mentorship during my time as a student in FU Berlin. She is an amazing teacher and a role model. Her inputs were valuable outside and inside the lab, she has taught me to delve deeply and with great interest into the simple question that is the beginning of every scientific story, "why?". I am very grateful for all the countless hours she made available for discussion, her support and great scientific input in all my projects.

I am grateful to the Helmholtz MacroBio School for providing funding to help in my scientific endeavors. The summer schools, seminars, and all scientific exchange in those times is greatly treasured.

I am deeply indebted to the AG Haag family, both previous and current members, for always creating the most hospitable working environment, where everyone was willing to help in even the smallest of things.

A special shout out goes to my lab and office family, Sumati, Pradip, Fang, Karolina, Michael, Lingyan, Pallavi, Shalini, Felix, Matthias, Manoj, Yong, Qingcai, Keerthana, Ehsan, Boonya, Guoxin, and Isabel, with whom countless hours were spent, perhaps equally, not only in work-related discussion, but also in pursuing (much needed) flights of fancy. Abhishek, Raju, Badri and all the members of my far too rare lunch group are thanked for their advice, (food)sharing and knowledge.

I am very thankful for my friends I made during this journey: Rotsiniaina, Keerthana, Paria, Isabel, Peng, Guoxin. Boonya Thongrom was a friend during the thick and thin, and he is thanked for being my go-to person whenever I needed advice, laugh or sometimes even a slice of cake! He is the best project-partner, office-partner and his friendship will always be cherished.

Finally, I would like to thank all my friends outside of work who are my home-away-from-home.

I am especially grateful to my family. My parents, who planted an inquisitive seed in me from the very beginning, are thanked for their unconditional love and understanding, and for making my doctoral education possible, in a myriad of ways. My sister, who has always been my best friend and my most reliable partner-in-crime. Thank you all for taking this rollercoaster with me.

Table of Contents

1. Introduction	1
1.1 Pathway of viral attack	1
1.1.1 Polymer-Based Prophylactics	2
1.1.2 Hydrogel Classification and Synthesis	4
1.1.2.1 Polymers for hydrogel synthesis.....	5
1.1.2.2 Crosslinking Chemistry.....	8
1.1.3 Antiviral and antimicrobial hydrogels	12
1.2 Mucus Biopolymers.....	14
1.2.1 Naturally occurring mucus.....	14
1.2.2 Physical and chemical structure of gel mucins	14
1.2.3 Broad spectrum antiviral approaches	15
1.2.4 Mucus as a Defense Mechanism	17
1.2.5 Lung mucus, properties and functions	19
1.2.6 Challenges in the mucus barrier efficiency.....	19
1.3 Synthetic Mucus-Like Polymers	19
2. Scientific Goals.....	21
3. Publications and Manuscripts	24
3.1 Polyglycerol-based mucus-inspired hydrogels	24
3.2 Scaffold Flexibility Controls Binding of Herpes Simplex Virus Type 1 with Sulfated Dendritic Polyglycerol Hydrogels Fabricated by Thiol-Maleimide Click Reaction	39
4. Summary.....	57
4.1 Kurzzusammenfassung	59
5. Outlook.....	62
6. Curriculum Vitae.....	72
7. Declaration of Honesty	72
8. References	63

List of Abbreviations

3D	:	3-dimensional
AMPs	:	Antimicrobial polymers
AuNPs	:	gold nanoparticles
DADMAC	:	diallyldimethylamino chloride
DPG	:	dendritic polyglycerol
DPGS	:	dendritic polyglycerol sulfate
EEGE	:	ethoxyethyl glycidyl ether
Env	:	viral envelope proteins
ETTMP 1300	:	trimethylolpropane tri(3-mercaptopropionate)
G	:	elastic modulus
G''	:	viscous modulus
GAG	:	glycosaminoglycan
GalNAc	:	N-acetyl-galactosamine
GSH	:	Glutathione
<i>H. influenza</i>	:	<i>Haemophilus influenzae</i>
HBGAs	:	Histo-blood group antigens
HIV	:	Human immunodeficiency virus
hPG	:	hyperbranched polyglycerol
hPGS	:	hyperbranched polyglycerol sulfate
HPMA	:	<i>N</i> -(2-Hydroxypropyl) methacrylamide
HSPG	:	heparan sulfate proteoglycans
HSV	:	Herpes simplex virus
IAVs	:	Influenza A viruses
KPS	:	potassium peroxydisulfate
LMWH	:	low molecular weight heparin
IPG	:	linear polyglycerol
LPG(SH) ₂	:	dithiolated linear polyglycerol
MIH	:	mucus-inspired hydrogel
NCA	:	<i>N</i> -carboxyanhydride
<i>P. aeruginosa</i>	:	<i>Pseudomonas aeruginosa</i>
PAMAM	:	poly(amidoamine)
PASP	:	poly(aspartic) acid
PBA	:	phenylboronate

PEG	:	polyethylene glycol
PEG(SH) ₂	:	dithiolated polyethylene glycol
PEI	:	polyethyleneimine
pHEMA	:	poly(2-hydroxyethyl methacrylate)
PLL	:	poly-L-lysine
PTS	:	proline-threonine-serine domain
PVA	:	polyvinyl alcohol
RSV	:	Respiratory syncytial virus
<i>S. aureus</i>	:	<i>Staphylococcus aureus</i>
SA	:	sialic acid
SARS-CoV-2	:	Severe acute respiratory syndrome coronavirus-2
SARS	:	Severe acute respiratory syndrome coronavirus
SHA	:	salicylhydroxamate
SMPs	:	synthetic mucin-like polymer systems
SPAAC	:	strain-promoted alkyne-azide cycloaddition
TEMED	:	<i>N,N,N',N'</i> -tetramethylethylenediamine
VLPs	:	virus-like particles VNTR: variable number of tandem repeats

1. Introduction

Since viruses were discovered just over a century ago, their infectiousness has become apparent. Viral epidemics and pandemics have caused a massive loss of human life around the world. Due to SARS, the scientific community has a renewed interest in investigating various ways to gain deeper insight in viral inhibition.

1.1 Pathway of viral attack

The virus life cycle comprises of attachment, entry, reproduction, and exit. Virus attachment to a host cell is a complex process, and more importantly, varies uniquely depending upon the virus. Viral attachment and subsequent entry into the host cell takes place through the viral envelope (Env) proteins or the virus capsid. Further, spike proteins facilitate the entry by allowing multiple virus-host interactions.^{1,2}

It is therefore important to understand the infection process in order to elucidate paths of intervention. Knowledge of the method and chemistry employed by the virus for entry is key for designing an anti-viral therapeutic that targets initial viral adhesion. The traditional method for viral infection inhibition dictates the use of small drugs for competitive inhibition of the receptor/ligand sites. This strategy has a number of limitations ranging from short blood-circulation time, off-target effects resulting in unwanted toxicities to healthy cells, and a high dosage requirement, which can lead to resistance. Multivalent interactions of biological molecules play an important role in many biochemical events. A multivalent therapeutic strategy, wherein several receptor sites on a pathogen are targeted at once, not only overcomes the issues of traditional drugs by using a smaller dosage, but is also more efficacious.² This process is graphically demonstrated in **Figure 1**. In this endeavor, polymeric architectures have successfully been used for multivalent targeting. Polymer conjugation with small drugs is a commonly used pharmaceutical strategy as they provide multiple advantages such as an increase in solubility and bioavailability, a larger therapeutic window, as well as an induced stealth effect, which also leads to decreased toxicity. Slower clearance rates allow for lower dosage resulting in lower susceptibility to resistance.³ Furthermore, multifunctional polymeric architectures can facilitate conjugation of multiple copies of targeting agents to scaffolds, allowing the simultaneous binding of ligands to multiple binding sites or receptors.

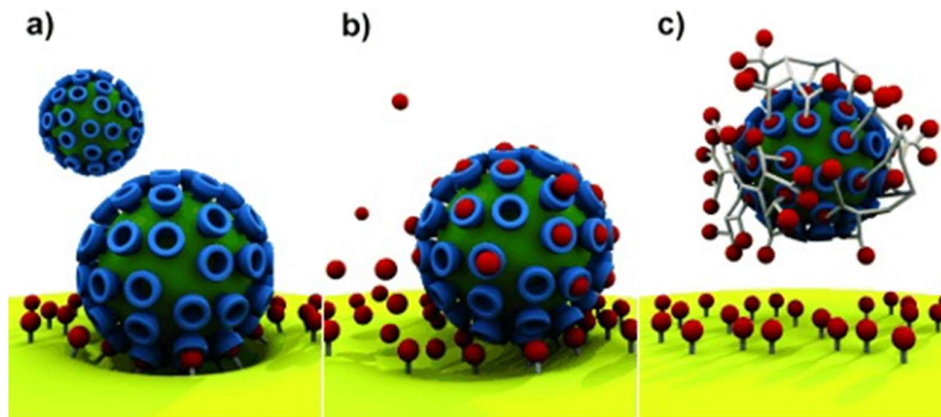


Figure 1. a) The binding of a virus to a cell surface in comparison to b) noncompetitive binding with a monovalent ligand (classical drug approach). c) Multi- and polyvalent ligands are considerably more effective in binding and shielding a virus surface than monovalent ligands, preventing viral adhesion. Reprinted with permission from Fasting, C. et al., Multivalency as a Chemical Organization and Action Principle. *Angewandte Chemie International Edition* 2012, 51 (42), 10472-10498.⁴ Copyright 2012, WILEY-VCH Verlag GmbH & Co.

1.1.1 Polymer-Based Prophylactics

The first phase of many viral infection cycles begins with relatively non-specific interactions between viruses and negatively charged cell-surface heparan sulfate proteoglycans. Sulfate mediated interactions contribute to infections caused by viruses such as herpes simplex virus (HSV) serotypes 1 and 2,⁵⁻⁷ HIV,^{8,9} respiratory syncytial virus (RSV),¹⁰ adeno-associated virus type 2,¹¹ dengue virus,¹² SARS-CoV-2,¹³ among others. The graphical representation of the SARS-CoV-2 infection cycle via heparan sulfate mediated attachment is depicted in **Figure 3**.¹⁴ Thus, there is growing interest in polyanionic substances, especially polysulfates, which can act as receptor decoys for entrapping these viruses.^{13, 15-18}

Among natural anti-viral strategies, glutamine and flucosan work against viral adhesion with the help of sulfonic groups. Chitosan, fucoidans, and antimicrobials polymers (AMPs) are also shown to behave as effective anti-viral strategies.¹⁹ Functionalized synthetic polymers such as polyethyleneimine (PEI), poly-L-lysine (PLL), poly(amidoamine) (PAMAM) dendrimers are a few examples of anti-viral synthetic polymers.¹⁹ However, polymers are often attained with a high polydispersity which can cause adverse side effects.²⁰ Another emerging class of antiviral prophylactics are hydrogels, which have the added advantage of high biocompatibility. The hydrogel scaffold circumvents all the problems associated with polymers while also exhibiting a

multivalent presentation of functional groups, which have been proven to increase viral and bacterial trapping.²¹⁻²³

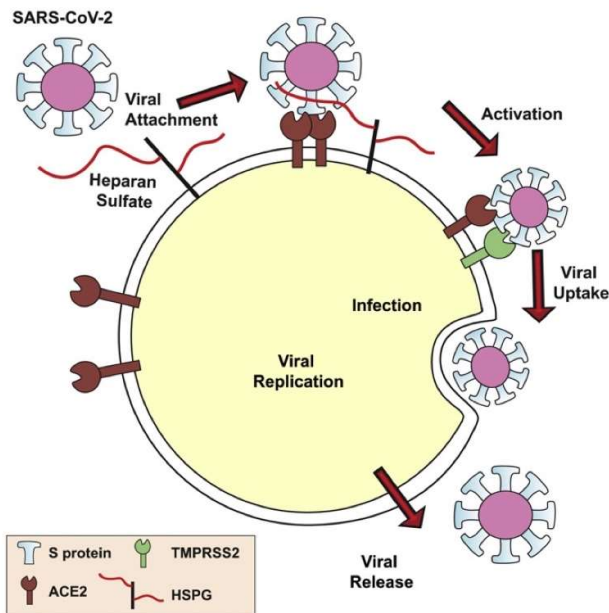


Figure 2. Graphical representation of the SARS-CoV-2 infection cycle via heparan sulfate mediated attachment. Reprinted with permission from Clausen, T. et al., SARS-CoV-2 Infection Depends on Cellular Heparan Sulfate and ACE2, *Cell* 2020, 183(4), 1043-1057.¹⁴ Copyright 2020, Elsevier Inc.

Hydrogels

Existing drugs and even polymers usually necessitate a very high dose. Polymer conjugation with small drugs is a widely-applied pharmaceutical strategy that offers multiple advantages, such as, an increase in solubility, bioavailability, specificity and the therapeutic window, as well as stealth effect, and a decrease in toxicity.³ Decreased clearance rates also allows for less dosage and lower susceptibility to resistance.³ However, polymers are often attained with a high polydispersity which can cause adverse side effects.²¹ The hydrogel scaffold circumvents all these problems while also exhibiting a multivalent presentation of functional groups, which have been proven to increase viral or bacterial trapping.²¹⁻²³

Upon their debut around the 1900s, hydrogels were defined as colloidal gels of inorganic salts.²⁴ They were redefined in 1960, in pioneering work by Wichterle and

Lim, when soft contact lenses were manufactured from poly(2-hydroxyethyl methacrylate) (pHEMA) hydrogels.²⁵

Hydrogels are three-dimensional network structures held together by either physical or chemical crosslinks, or a combination of the two. They can efficiently imbibe water or biological fluids, swelling up to thousands of times their original volume. Their physical and structural properties such as hydrophilicity and rigidity bear close semblance to the extracellular matrix in natural tissues, allowing high biocompatibility and minimal inflammatory stress on the surrounding cells.²⁴ These properties make hydrogels particularly attractive for use in the biomedical field as implantable devices, for example, in biosensors,²⁶⁻³¹ as supportive matrices for tissue engineering,³²⁻³⁴ and drug delivery.³⁵⁻³⁸ Further, hydrogels have also been designed for *in situ* gelation as a non-invasive method to form a functional macroscopic network of any shape and size at the injection size. In addition, soluble drugs and cells can be delivered with the gel precursors allowing their homogeneous distribution in the matrix.^{24, 39, 40} Naturally occurring mucus hydrogels contain a number of active functional groups including sulfate ester, sialic acid and fucose, allowing them to behave as broad-spectrum anti-viral agents.^{41, 42} Henceforth, this area of research has rapidly flourished, with hydrogels finding a multitude of applications, especially in the biomedical arena.

1.1.2 Hydrogel Classification and Synthesis

Hydrogels can be classified into two categories depending upon their network chemistry as physically or chemically crosslinked. The former constitutes of a non-covalent network while the components of the latter are crosslinked covalently. Their equilibrium swollen state results from a balance between the forces responsible for water sorption, i.e., capillary, osmotic and hydration forces and the crosslinks resisting expansion. These forces, along with polymer matrix chemistry largely influence the key properties of the hydrogel including its mechanical strength.⁴³ They may also be classified into three categories, depending upon the basis of the constituting polymers: natural, synthetic and hybrid hydrogels. As the name suggests, natural hydrogels are derived from biological sources such as the mucus hydrogel whereas synthetic polymer are derived from synthetic, generally hydrophilic polymers like polyvinyl alcohol (PVA) and polyethylene glycol (PEG). Hybrid hydrogels are a combination of the both synthetic and natural polymers. The structure of hydrogels, and the various

monomers and crosslinking agents generally used for their synthesis are shown in **Figure 4**.

The so-called “first-generation hydrogels” are fabricated by crosslinking hydrophilic polymers, or polymerization of water-soluble monomers in the presence of a crosslinking agent.²⁴ The field of the chemistry of hydrogels is very vast and only a select few can be covered herein.

1.1.2.1 Polymers for hydrogel synthesis

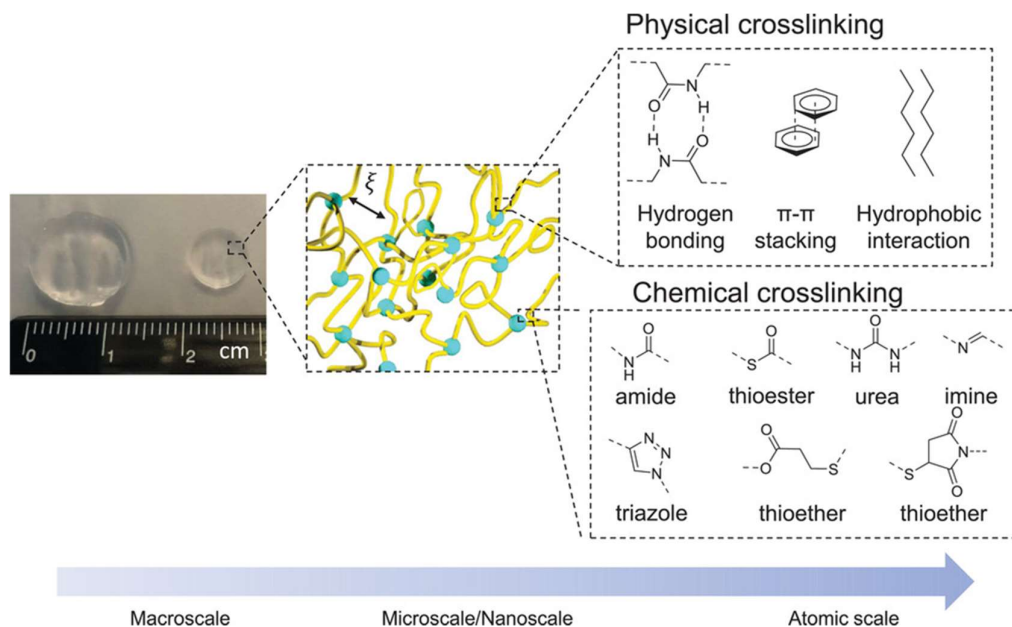


Figure 3. Representative hydrogel scheme from macro- to atomic scale. On the macroscale a prepared gel pad in a swollen (left) and freshly prepared (right) state are observed. On a micro/nanoscale, the 3D crosslinked polymeric structures with a certain pore size (micro) or mesh size ξ (nano) are displayed. On atomic scale a few typical examples of either chemical or physical crosslinking are represented. Reprinted with permission from Herrmann, A. et al., *Adv. Healthc. Mater.*, 2021, 10(11), 2100062-2100087. ⁴⁴ Copyright 2021, WILEY-VCH Verlag GmbH & Co.

Polyethylene Glycol (PEG)

PEG is used in a wide variety of pharmaceutical applications owing to its unique combination of properties. It is often conjugated to a drug to improve pharmacokinetics by imparting the stealth effect, also known as “PEGylation”, and increasing the blood circulation time.^{45, 46} Currently, there are 13 PEG-based drugs in the market.⁴⁷ Moreover, PEG chains are soluble in both water and organic solvents. It is also highly biocompatible, non-toxic and displays anti-fouling properties. Thus, PEG has been

utilized extensively in the fabrication of hydrogels.²⁴ However, it also has a number of disadvantages, for example, it only possesses two functional groups on either ends of the chain. Therefore, PEG-based hydrogels always require a second component with greater functionalization capabilities to form gel structure. This second component will also bear all the responsibility of inculcating other properties and conjugation. Moreover, there are growing anti-PEG antibodies,^{47, 48} and rapid clearance from the body's bloodstream after multiple PEG-injections.⁴⁹

Hyperbranched polyglycerols (hPG)

Due to the various drawbacks of PEG, polyglycerols have been extensively researched as their alternatives due to a structural similarity, but offering higher functionality, and higher circulation time.⁴⁹ The first attempts to polymerize glycidol were undertaken by Sandler and Berg in 1966,^{50, 51} while Vandenberg et al. were the first to characterize branched structures.⁵² hPGs are highly branched polymers which are of considerable interest for a wide variety of applications due to their high surface functionality. They possess a range of qualities which make them desirable for use in the biomedical field; they are highly biocompatible owing to their hydrophilic nature, possess anti-fouling properties and are non-toxic.⁵³⁻⁵⁷ High hydrophilicity combined with a multivalent presentation of functionalizable hydroxyl groups on their surface make hPGs ideal candidates for hydrogel constituents. hPG is prepared by a single-step anionic ring-opening, multi-branching polymerization of AB_m-type monomers by slow addition.⁵¹ This reaction produces hPGs with very narrow polydispersities.^{58, 59}

The first hPG-based hydrogels were synthesized by Oudshoorn et al. in 2006.⁶⁰ Methacrylated hPG hydrogels were synthesized by photoinitiated polymerization, wherein methacrylate-functionalized hPGs were crosslinked in the presence of potassium persulfate (KPS) as the initiator, and *N,N,N',N'*-tetramethylethylenediamine (TEMED) as the catalyst in an aqueous solution. They postulated that the low viscosity of hPGs established the formation of gels with high solid contents, fostering exceptional mechanical properties.⁶⁰ Since then, hPG-hydrogels have been explored extensively. Strain-promoted alkyne-azide cycloaddition (SPAAC) was utilized for the fabrication of sulfate-functionalized dPG (dPGS)-based hydrogels for in-situ formation to mimic the extracellular cartilage matrix for tissue-engineering (**Figure 5**).⁶¹ These hydrogels were found to promote higher cell viability than their PEG-based hydrogel counterparts. dPGS is a popular, biologically relevant dPG-

derivative as a result of its anti-inflammatory properties,⁶² while acting as an analogue to heparan sulfate, a glycoprotein receptor for many virus families.⁵

A dual-bio-responsive hydrogel prepared with PEG, dPG, sialic acid (SA) and gold nanoparticles (AuNPs) to capture Influenza A viruses (IAV) followed by a change in color and swelling has been reported. The nanocomposite hydrogel was synthesized by a click reaction between cyclooctyne-functionalized dPG and azide-functionalized PEG. Furthermore, responsiveness and viral inhibition was achieved by anchoring AuNPs to the PEG chain using thiol chemistry, and the AuNPs were in turn functionalized with sialic acid.⁶³

These studies support hPGs as a suitable platform for the synthesis of biocompatible hydrogels with tunable mechanical properties. hPG-based hydrogels are highly functionalizable, and thus can incorporate relevant properties lent by groups such as sulfates and sialic acid for anti-inflammatory and virus-binding.

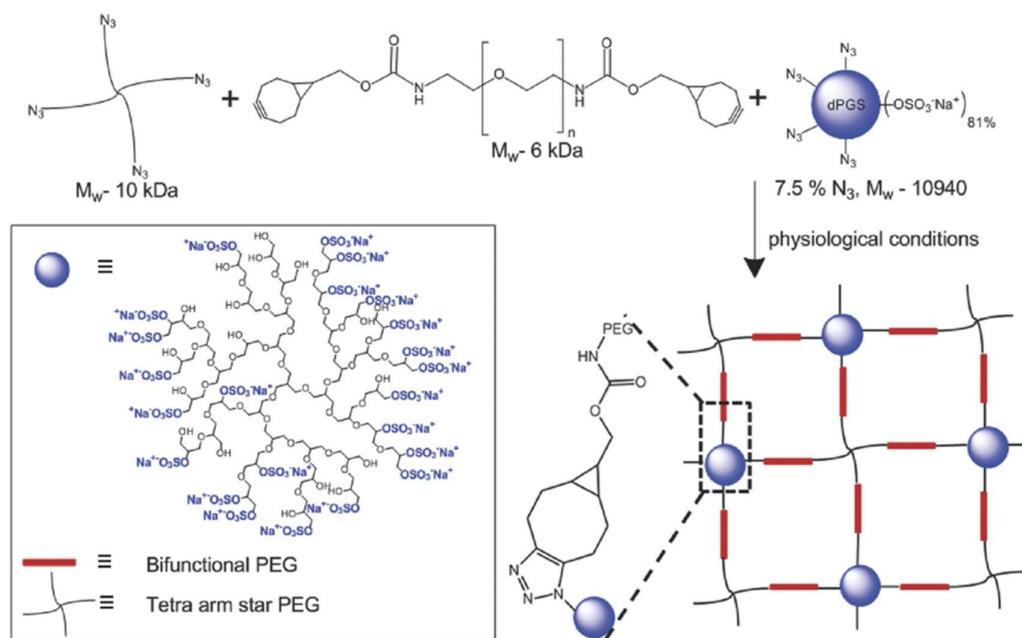


Figure 4. Fabrication of sulfate-functionalized dPG (dPGS)-based hydrogels for in-situ formation to mimic the extracellular cartilage matrix for tissue-engineering. Reprinted with permission from Dey, P. et al., Mimicking of Chondrocyte Microenvironment Using In Situ Forming Dendritic Polyglycerol Sulfate-Based Synthetic Polyanionic Hydrogels. *Macromolecular Bioscience*, 2016, 16 (4), 580-590. ⁶¹ Copyright 2016, WILEY-VCH Verlag GmbH & Co.

Linear polyglycerols (IPG)

IPG is synthesized by the polymerization of glycidol, where the occurrence of branching is prevented by protection of the hydroxyl functional group. IPGs are highly hydrophilic and display higher biocompatibility than that of PEG.⁴⁹ The American Food and Drug Administration (FDA) has approved the use of these polymers with a substantial polydispersity and degree of polymerization up to 10 for additives in dietary and pharmaceutical additives.⁴⁹ They are synthesized by oxyanionic ring-opening polymerization of protected glycidyl ethers such as ethoxyethyl glycidyl ether (EEGE). As with hPGs, IPGs also offer viable hydroxyl groups for further functionalization on their backbone. Due to their linear structure, IPG-based hydrogels offer higher flexibility and adjustable rheological properties. Supramolecular hydrogels based on IPG were synthesized by Hackelbusch et. al.⁶⁴ These hydrogels were based on non-covalent, physical crosslinks utilizing both hydrogen bonds and metal complexation to form a pH- and chelator- responsive network, which could remain stable for several weeks. By variation of the constituents, gels with various rheological properties were formed.

1.1.2.2 Crosslinking Chemistry

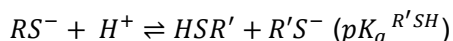
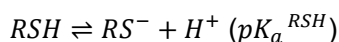
Covalently-bound hydrogels are often preferred for applications such as virus inhibition and tissue engineering, especially when they have to be applied *in vivo*, as the resulting matrix and its mechanical behavior are more manageable than physically crosslinked matrices. In order to achieve a desired biomedical response, the crosslinking chemistry is extremely important. There are several crosslinking strategies for the synthesis of hydrogels from multifunctional gel components, including various types of click reactions, thiol-disulfide and thiolene reactions, enzyme-mediated reactions, and boronic acid-diol reactions, to name a few have been reported.

Thiol-disulfide crosslinking chemistry

The growing interest in the thiol-disulfide exchange reaction stems from their widespread presence throughout biological systems, for example, in peptides and polymers as cysteine and small natural molecules.^{65, 66} However, its overall abundance compared to other naturally-occurring functional groups is still relatively low and therefore it is of high chemoselective relevance.⁴⁰ In fact, the nucleophilicity of thiol is about 1000 times higher than that of an ionized amino group at the physiological pH, and thus is an attractive functional group for the chemical modification of polymers and

their subsequent gelation for use in biomedical applications.⁴⁰ The disulfide group responds to the change in concentration of glutathione (GSH), a biologically present natural reducing agent, as it increases within the cell environment (~0.5 – 10 mM) in comparison to the extracellular conditions (~1 – 20 μ M in plasma).⁶⁷ This concentration change is enough to induce rapid intracellular degradation of the disulfide-based scaffold.⁶⁸ Redox-responsive hydrogels are designed for select applications such as self-healing materials and injectable polymer implants.⁶⁹

The thiol-disulfide exchange is an S_N2 reaction. Its general reaction scheme is summarized in **Equation 1**,⁶⁵ and its mechanism is explained with further detail in **Equation 2**.⁶⁵ Here, the thiolate anion (RS^-) is the active nucleophile, the concentration of which is pH dependent in this base-catalyzed reaction.^{65, 70}



Thiol-disulfide exchange reactions are advantageous because they are responsive, stable under circulation, readily reversible without exerting significant heat effects, and the reaction time is quite flexible and can be tuned easily according to the desired scale.⁶⁸ Different crosslinking dynamics influence the rheological properties of the hydrogel, a factor which is considerably important for designing biomimetic constructs such as mucus mimetics or synthetic extracellular matrices for tissue engineering.⁶⁹

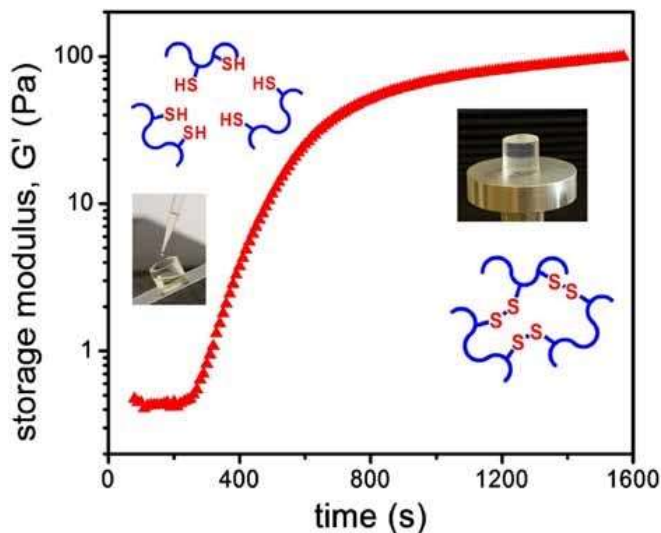


Figure 5. Oxidation induced sol-gel transition of an aqueous solution of cysteamine modified poly(aspartic acid) (PASP-SH-E, left) in PBS resulting in mechanically stable hydrogel (PASP-SS-E, right). Reprinted with permission from Gyarmati, B. et al., Redox- and pH-Responsive Cysteamine-Modified Poly(aspartic acid) Showing a Reversible Sol-Gel Transition, *Macromolecular Bioscience*, 2013, 13 (5), 633-640.⁷¹ Copyright 2013, WILEY-VCH Verlag GmbH & Co.

The mucus hydrogel is constructed from chains held together by cysteine units linked with disulfide groups, and thus contributes to its mechanical properties;⁴² responsivity to redox cues that induce structural change and degradation is fundamental in the scaffold design for tissue engineering. Reversible crosslinks impart ease of hydrogel administration without invasive surgery; the reduced hydrogel precursor responds to *in vivo* redox cues to form a gel. The sol-gel has the added advantage of allowing homogenous distribution of cells, proteins and other compounds within the network, and molds into the desired shape at the point of injection.²⁴ Gyarmati et al. reported the synthesis of pH- and redox- sensitive poly(aspartic) acid hydrogels.⁷¹ They are crosslinked using reversible thiol-disulfide chemistry and therefore can undergo sol-gel transition via thiol-disulfide interconversion, from an aqueous, injectable solution to a mechanically stable gel upon oxidation (**Figure 6**).

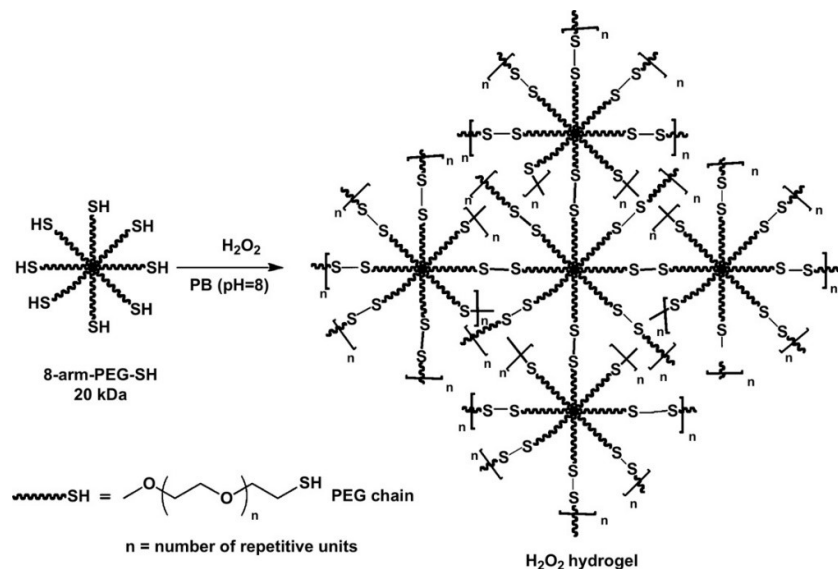


Figure 6. Schematic representation of H_2O_2 hydrogels. Intra- and inter- molecular crosslinking of the 8-arm-PEG-SH by H_2O_2 in PB (pH 8) via disulfide bridges. Reprinted with permission from Anumolu, S. S., et al., Doxycycline hydrogels with reversible disulfide crosslinks for dermal wound healing of mustard injuries. *Biomaterials* 2011, 32 (4), 1204-1217. ⁷² Copyright 2010, Elsevier Ltd.

Anumolu et al. fabricated *in situ* hydrogels for dermal wound application by crosslinking 8-arm branched thiol terminated PEG macromonomers with hydrogen peroxide under room temperature at pH 8, which were then loaded with doxycycline (**Figure 7**).⁷² They showed high mechanical strength, sustained drug release over a period of 10 days *in vitro*. The presence of disulfide groups facilitated sol-gel transition, drug release and gel degradation, while also providing mechanical strength.

Michael - Click Chemistry

The thiol-Michael addition reaction falls within the umbrella of the so-called “click” reactions. This is a powerful, highly chemoselective reaction between thiol groups and Michael acceptors such as maleimide or acrylate groups, under mild, environmentally friendly conditions. The ease of the reaction and chemoselectivity make it a popular crosslinking tool for hydrogel synthesis. The pioneering work for the use of Michael addition reactions for crosslinking systems was done by the Hubbell group wherein vinyl sulfones and acrylates were used as Michael acceptors.⁷³⁻⁷⁵ Glutathione-sensitive, degradable hydrogels were created by crosslinking maleimide-functionalized low molecular weight heparin (LMWH) with multi-arm thiol-terminated PEG molecules.⁶⁷

1.1.3 Antiviral and antimicrobial hydrogels

In light of the COVID-19 pandemic caused by the SARS-CoV-2 virus, research towards broad-spectrum anti-viral and antimicrobial materials has increased steeply, especially as currently available treatments are facing growing resistance development.^{2, 76} Recently, hydrogels are being explored as alternate antiviral and antimicrobial therapeutics such as surface and medical device coatings,^{77, 78} personal protective equipment, personal hygiene products such as disinfectants and sanitizers,⁷⁹ wound dressing and healing,⁸⁰⁻⁸⁴ and anti-viral materials that can be applied directly in the human body.^{20, 35}

Mahalingam et al. designed a pH-responsive, synthetic mucin-like polymer systems (SMPs) to enhance the barrier efficiency of naturally occurring cervical mucus (**Figure 8**).³⁵ The body's natural mucus defense mechanism weakens when it comes into contact with semen, which dilutes and neutralizes the cervical mucus. The SMP was built to kick in at this time and form a densely crosslinked network, thus inhibiting subsequent viral permeation. The pH responsiveness was generated by using boronate-diol crosslinking chemistry; the trigonal structure of the boronic acid changes to a charged, tetrahedral boronate species upon an increase in pH. The latter is more resistant to hydrolysis and therefore forms a stronger boronate ester complex, which in turn yields a highly crosslinked viscoelastic matrix. Neutralization caused the elastic modulus to jump more than 160 times, from 11 Pa at pH 4.8 to 1800 Pa, and the authors showed that HIV migration was significantly reduced. This sol-gel responsiveness allows ease of gel application at acidic pH while maintaining a semipermeable layer at neutral pH.³⁵

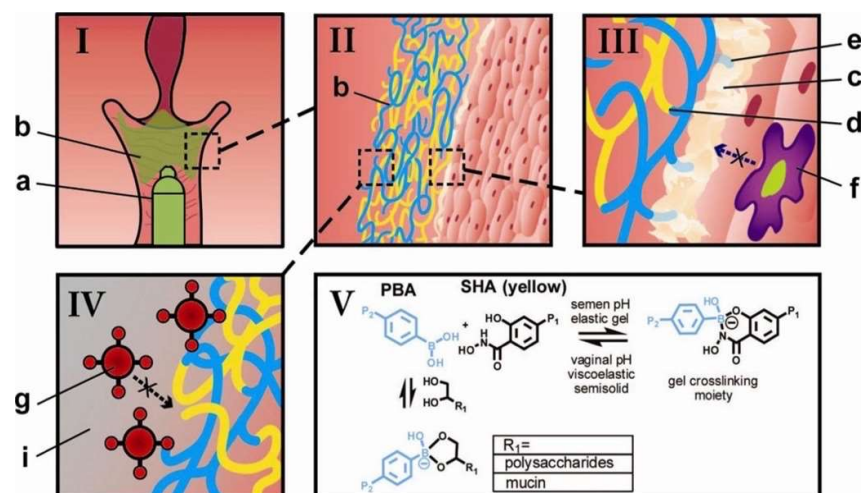


Figure 7. Schematic demonstrating the use of the phenylboronate-salicylhydroxamate crosslinked polymer (PBA-SHA, green) as a microbicide drug delivery system. (I) The two polymer solutions, pHPMAm95-PBA5 (PBA5, blue) and pHPMAm95-SHA5 (SHA5, yellow) on mixing form a weakly crosslinked viscoelastic fluid (b, green) which can be applied via an applicator (a). (II) The crosslinked polymer solutions form a pH-sensitive polymeric network, which should flow and coat the cervicovaginal epithelium at vaginal pH. (III) On a molecular scale, the gel network is comprised of chemical crosslinks between the polymer-bound PBA (blue) and SHA (yellow) (d) as well as bioadhesive interactions of PBA with diols present (e) within cervical mucus (c) and on the epithelial surface. (IV) This densely crosslinked elastic network formed at neutral pH blocks the diffusion of HIV (g), thereby generating a physical barrier between semen-borne virus and susceptible target cells in women. (V) The crosslinking chemistry utilizes the reversible covalent crosslinking between polymer-bound PBA and SHA, creating a pH-responsive network that is transient and viscoelastic at vaginal pH; and is elastic and solid-like at the seminal pH. Reprinted with permission from Mahalingam, A., et al., Inhibition of the transport of HIV in vitro using a pH-responsive synthetic mucin-like polymer system. *Biomaterials* 2011, 32 (33), 8343-55. ³⁵ Copyright 2011, Elsevier Ltd.

Zhang et al. introduced a hydrogel-based antiviral drug base to trap Noroviruses.²⁰ Human histo-blood group antigens (HBGAs) have been seen to act as ligands for the Norovirus, and were thus incorporated into the hydrogel as decoys. Human HBGA type B was reacted with diallyldimethylamino chloride (DADMAC) and acrylamide to form glycosylated poly(DADMAC)-poly(acrylamide) hydrogels. Recombinant virus-like particles (VLPs) were then introduced to the hydrogels to determine their efficacy and successfully entrapped therein.²⁰

1.2 Mucus Biopolymers

1.2.1 Naturally occurring mucus

Mucus is a complex, viscoelastic hydrogel secretion that protects the apical epithelial surfaces of the mammalian body. This includes open epithelial surfaces of the respiratory, gastrointestinal, reproductive and oculo-rhino otolaryngeal tracts, wherein it serves a plethora of functions. It prevents dryness by maintaining a hydrated layer over the epithelial façade.⁴¹ Mucus gel exhibits shear-thinning behavior which supports its role as a lubricant by warranting a smooth passage for passing materials.⁸⁵ Importantly, it serves as the external defense system of the body against pathogenic attack in mucosal immunology.^{41, 86}

The mucus coat is a heterogenous biopolymer matrix comprising of water (up to 95% by weight), mucin (typically about 5% by weight or less), inorganic salts (approximately 1% by weight), carbohydrates, and lipids. The basis of its protective functions and physical behavior relies heavily on its constituents, particularly on mucin glycoproteins which represent more than 80% of the overall organic components.⁸⁷

1.2.2 Physical and chemical structure of gel mucins

The physical and chemical properties are instrumental for mucus' biological response. Mucus behaves as a shear thinning viscoelastic material. These rheological properties are a consequence of the physical interactions which give rise to the matrix structure. The network structure with these specific characteristics arises when the rigid, fibrillar and highly entangled mucin glycoprotein components within the composite form multiple, low-affinity bonds as a function of hydrophobic interactions, hydrogen bonding, and electrostatic interactions between the mucin fibers.

The physical and chemical structure of the mucin glycoprotein contribute to the formation of a gel matrix with specific characteristics. Mucin glycoproteins are block copolymers composed of rigid subunits linked to one another in a linear fashion. Each of these subunits comprise of a central PTS domain, with variable number of tandem repeats (VNTR) of the amino acids proline, threonine, and serine, respectively.⁸⁵ Glycosyl "branches" arise from the PTS spine, connected by an N-acetyl-galactosamine (GalNAc) branching point. This results in a linear, bottlebrush structure. The terminal ends of the glycosyl branches are largely fucose, sialic acid, and sulfate

esters of galactose and N-glucosamine.⁸⁸ The chains may be charged depending upon their environment, thus prompting an augmentation in branch extension, resulting in a rigid PTS spine. The carboxy and amino terminals in this domain are flanked by, and occasionally interspersed with, cysteine-rich amino acid sequences.⁴¹ The cysteine residues are responsible for disulfide-bridge mediated end-to-end assembly of 4 – 6 of these subunits to form a single mucin molecule.⁸⁷ The “bottlebrush” domain, as well as the linear assembly account for the long, stiffened, filamentous structure of these molecules, with molecular weights in the range of 0.5 to 20 MDa.⁴¹ A schematic representation of the mucin glycoprotein structure is given in **Figure 9a**, with the formation of dimers and higher multimers shown in **Figure 9 c and d**.⁴¹

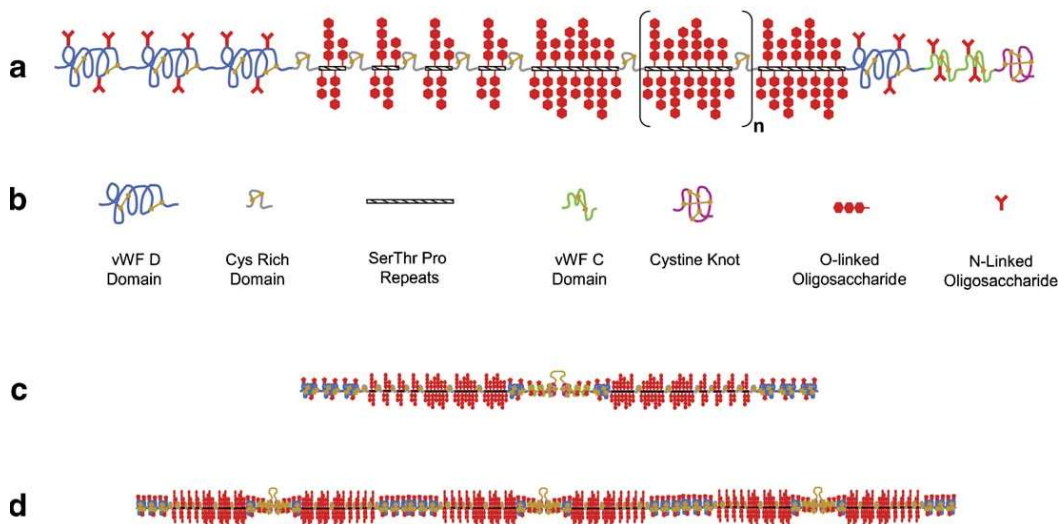


Figure 8. (a) A schematic drawing of the pig gastric mucin (PGM) monomer consisting of glycosylated regions flanked by regions with relatively little glycosylation. (b) The symbols indicate the different domains in the sketch in (a). (c) a dimer formed by two monomeric subunits linked via disulfide bonds in the non-glycosylated regions and in (d) dimers that are further disulfide linked to form higher multimers. This gives rise to the high molecular weight and polydispersity of secretory mucins. Reprinted with permission from Bansil, R. et al., Mucin structure, aggregation, physiological functions and biomedical applications, *Curr Opin Colloid Interface Sci*, 2006, 11, 164-170.⁴¹ Copyright 2006, Elsevier Ltd.

1.2.3 Broad spectrum antiviral approaches

The pathogen invasion in a biological system to initiate the infection process narrates an account of compromised mucus barrier which leads to subsequent viral proliferation. Moreover, recent developments reveal a significant and often overlooked pathway for viral infection dissemination. Associated viral systems were also found to

be significant source of other infections, for instance, the herpes causing Epstein-Barr virus may latch on to B cells to reach the epithelial cells.⁸⁹ Further studies exemplary of viral transport vehicles are motor proteins which function between the periphery and cell center; the actin system also supports virus passage with two different mechanisms.⁹⁰

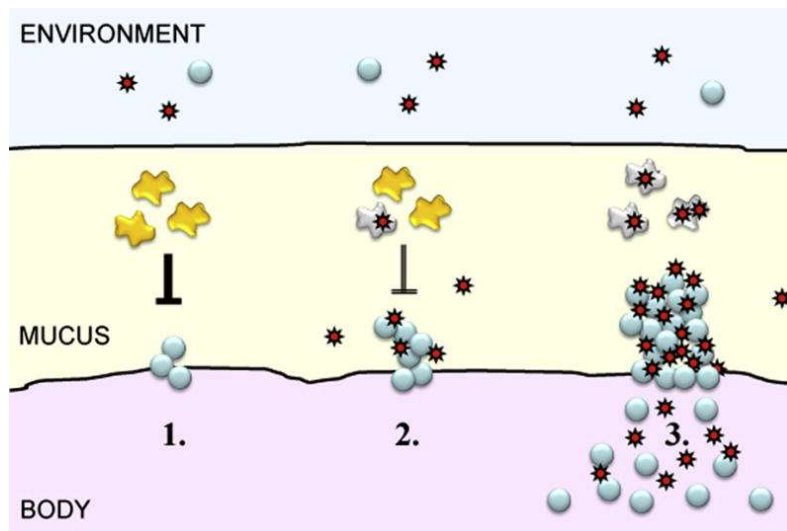


Figure 9. 1. Bacteria (blue) associated with the flu attach to mucosal cell surfaces of nose and throat and grow colonies. Immune cells (yellow) keep the density of bacteria at innocuous levels. 2. Viruses (red) adsorb to the sessile bacteria, setting the stage for viral infection. Viruses reciprocate the improved access to the host by inactivating the immune cells (grey) that chase the bacteria. 3. Bacteria exploit this temporary lack of immunological control to increase their populations to levels that result in pathogenic invasion. Reprinted with permission from Ribbeck, K., Do viruses use vectors to penetrate mucus barriers? *Biosci Hypotheses* 2009, 2 (6), 329-362.⁹¹ Copyright 2009, Elsevier Ltd.

The primary source of respiratory viral infection, for example influenza virus induced infection, are transmission through aerosols. They must pass through the mucus barrier to gain access to the underlying epithelia and initiate the viral life cycle. However, viruses themselves do not possess the ability for directed movement and therefore must rely on diffusion through the mucus gel. Based on empirical evidence, such passage is cumbersome and slow due to the inherent thickness and steric obstructions within the layer.^{85, 86, 91} Moreover, due to the constant excretion and replenishment of the mucus layer, the chances of the virus reaching the susceptible host cell are quite low. On this basis, it was proposed that viruses are enabled by motile bacterial cells residing within mucus gel by simple absorption.⁹¹

1.2.4 Mucus as a Defense Mechanism

The sugars at the terminals of the PTS domain are widely considered to behave as decoys for adhesins evolved for the interaction of pathogens with the epithelial cell surface. For example, various respiratory microbials such as *Pseudomonas aeruginosa* (*P. aeruginosa*), *Haemophilus influenzae* (*H. influenzae*), *Staphylococcus aureus* (*S. aureus*), influenza viruses, reoviruses, adenoviruses, and coronaviruses are all shown to engage with both, mucus and the epithelial surfaces through sialic acid interactions.⁹²⁻⁹⁸ Variation in the peripheral glycosyl units occur during certain immune responses and infections, serving evidence of their importance in protection against pathogenic attacks.^{99, 100} Thus, peripheral sugars are understood to interact with pathogens by the virtue of charge or hydrophobicity.

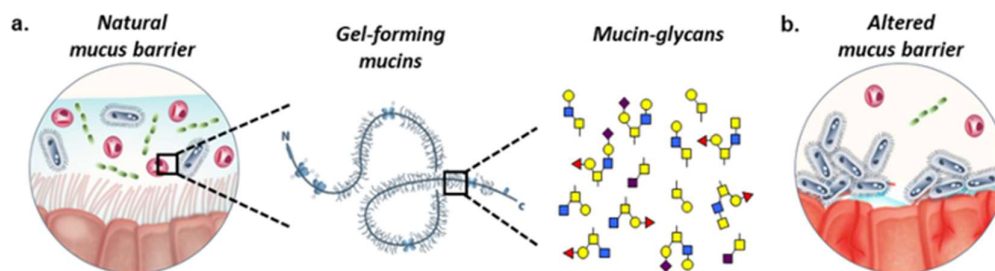


Figure 10. a. The natural mucus barrier (left) hosts a diverse range of microorganisms while limiting infections at the mucosa. Mucins (middle) are the major structural component of mucus and are densely grafted with complex glycans (right). **b.** Defects in mucus production are associated with disease and biofilm formation. Reprinted with permission from Wheeler, K. M., Mucin glycans attenuate the virulence of *P. aeruginosa* in infection. *Nature Microbiology*, 2019, 4 (12), 2146-2154.¹⁰¹ Copyright 2019, Springer Nature.

Although the exact mechanism of mucus gel formation is not fully understood, some of the major driving factors have been recognized. The length and rigidity of flexible mucin fibers is a prime feature as this allows intermolecular entanglement to form transient gels. Other proposed interactions to drive network formation are hydrophobic interactions, hydrogen bonding, and electrostatic interactions,¹⁰² graphically represented in **Figure 12**.¹⁰³ The mucin fibers essentially have alternating hydrophobic and hydrophilic areas. The hydrophobic chains fold into a globular “beads”.⁸⁵ The network crosslinks are hence formed by the intermolecular aggregation of hydrophobic groups.^{87, 102}

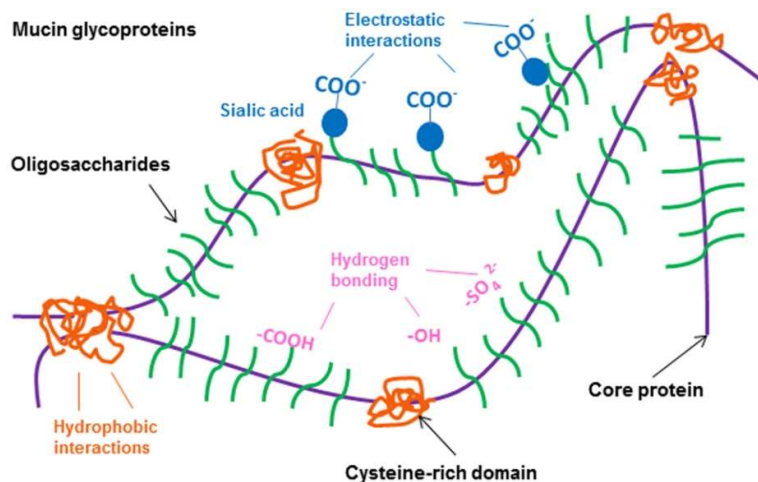


Figure 11. Crosslinking of mucin glycoproteins via electrostatic interactions, hydrogen bonding and entanglement to form the mucus hydrogel. Reprinted with permission from Yang, X. et al., Immobilization of Pseudorabies Virus in Porcine Tracheal Respiratory Mucus Revealed by Single Particle Tracking, PLOS ONE, 2012, 7 (12), e51054. ¹⁰³ Copyright 2012.

The mucus matrix is not merely a platform for displaying decoy ligands of microbes, in fact the network structure has an equally important role in mucosal immunology.¹⁰⁴ The network structure provides multiple obstructions in the path of an incoming pathogen.

The numerous active groups on mucus fibers afford multivalent interaction abilities. High viscosity is a weapon with which the flexible, entangled mucin fibers can conform to the surface of a particle, making multiple, low-affinity bonds which ensure that it remains in place.⁸⁵ These low affinity bonds lend mucus its characteristic stickiness, as well its location-specific viscoelastic behavior.

Biofilm formation associated with, and considered to play an important role in the proliferation of many diseases.¹⁰⁵ A prime example is the occurrence of *P. aeruginosa* biofilms in cystic fibrosis afflicted patients.¹⁰⁶ These biofilms are resistant to even the harshest antibacterial treatment, and further deteriorates the patient's condition.^{107, 108} In recent studies, it was determined that mucins have an ability to suppress the adhesion and consequent biofilm formation of opportunistic microbes. This inhibitory effect is specific to mucus networks and operates by promoting the motility of planktonic bacterial. A significant advantage of this method is that it limits the pressure for anti-microbial resistance.¹⁰⁴ It was speculated that the 3-dimensional network structure is responsible for such microbial motility, as it has been observed that propulsive forces may be generated by a rigid framework.¹⁰⁹

It has further been established that native gel mucus can protect the epithelial surface from particles smaller than the mucus matrix mesh size (~ 340 nm)² including HSV-1 (~ 180 nm) by mucoadhesion.^{85, 104} HSV particles specifically interact with the sulfate groups apically exposed on mucin glycoproteins,⁸⁷ which constitute about $\sim 5\%$ of the functionalities present on mucin. The role of sulfates in viral inhibition has been extensively studied. For example, highly sulfated dendritic polyglycerols (DPGS) showed high efficacy as anti-inflammatory agents.⁸⁸ In a relevant study, Dey et. al. designed DPGS-based nanogels as simple glycosaminoglycan (GAG) heparan sulfate mimics in an endeavor to inhibit HSV-1. The resulting nanogels were highly effective as broad-spectrum virus inhibition agents.¹¹⁰

1.2.5 Lung mucus, properties and functions

The MUC5B mucin glycoprotein is a major component of the airway mucus repertoire,¹¹¹ and is utilized in the processes of mucociliary clearance, assists with the control of respiratory infections, and has been shown to maintain immune homeostasis in mice.¹¹² *Muc5b* knockout mice were found to have acquired and consequently were infected by multiple bacterial species, including *S. aureus*, the pathogen species responsible for pneumonia.¹¹² These pathogens are generally unobserved in healthy, MUC5B-rich mucus. Furthermore, MUC5AC is also a major component of the lung mucus and was found to suppress biofilm formation by the *P. aeruginosa* bacteria.¹⁰⁴

1.2.6 Challenges in the mucus barrier efficiency

Another challenge to the barrier efficiency is the deviation from the normal composition of mucus, often seen in terms of differential expression of the principle glycoprotein component of gel-forming mucus, the mucin glycoproteins MUC2, MUC5AC, and MUC5B.

1.3 Synthetic Mucus-Like Polymers

Naturally occurring mucus is inept for utilization for any purpose due to erratic and unreliable composition, challenging extraction of sufficient amounts, arduous purification, and a change in performance of reconstituted mucus in terms of rheology and viscoelastic behavior.⁹⁴ These challenges can easily be overcome by the use of synthetic mucus, wherein molecular control over the structure, polymer length, viscoelastic behavior can be precisely controlled while offering a reduction in

heterogeneity typical in natural mucus. The synthetic mucus hydrogels have a promising future as antiviral agents, especially in the area to boost the effects of its natural counterpart in the human body.

Synthetic platforms for surface tethered mucins have been designed and studied by Kramer et al. (**Figure 14**).¹¹³ The authors were able to design a structure quite comparable to the peptide backbone of a mucin molecule bearing the N-GalNAc branching points native to mucus using *N*-carboxyanhydride (NCA) polymerization. However, this model is more specific to use in case of transmembrane mucins. The synthetic technique is procedurally complex, does not offer considerable flexibility with respect to system design, and is more directed towards modeling purposes than application.

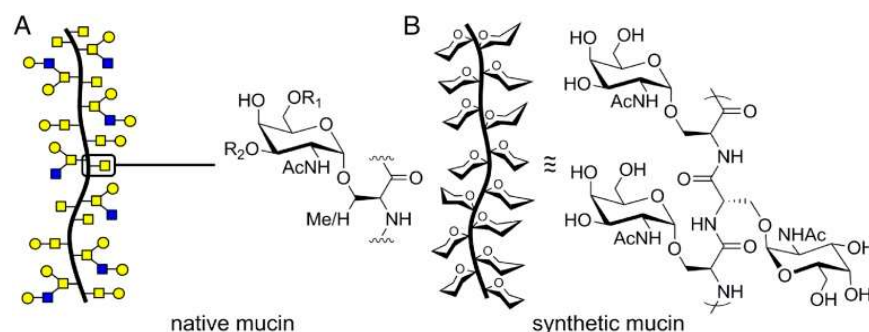


Figure 12. A) Native mucins are rich in clustered O-glycans that initiate with α -GalNAc residues attached to Ser or Thr residues that can be further elaborated with glycans (R_1 , R_2). (B) Cartoon representation and repeat unit of synthetic mucins. Reprinted with permission with from Kramer, J. R. et al., chemicallymucin chimeras asseR. RRBibCarlos BuscaCarolyn R. pg. 125751. ¹¹³ Copyright 2015, National Academy of Sciences.

Mahalingam et. al. devised an elegant platform for the fabrication of mucus gel network, where the boronate-diol condensation reaction was employed to induce a stimuli-responsive network against the HIV infection.³⁵ This has been discussed in Section 1.1.3 (**Figure 8**). This gel is exclusively aimed towards cervicovaginal mucus, consequently broad applications for this platform cannot be envisioned. Moreover, the viscoelastic behavior of natural mucus cannot be mimicked owing to a lack of interactions necessary to induce native non-Newtonian behavior essential to simulate characteristic antimicrobial properties.

2. Scientific Goals

The Covid-19 induced pandemic has highlighted the major fiscal, social and most importantly human impacts as a result of the emergence or re-emergence of viruses. The first strategy against the viral threat is the development and administration of vaccines. However, as exemplified by the corona pandemic, the time period from the development of a safe, efficacious vaccine to its deployment is lengthy and expensive affair. It is therefore pertinent to make prompt efforts to minimize the human and economic resource losses.

In such a public health crisis wherein a quick response is key, the development of broad-spectrum anti-viral agents offers a viable solution so as to minimize the time lag until vaccine administration. However, such research plans are plagued with the major problems of high virus mutation rates and inconsistencies between various virus types.

There are currently two major strategies in place when developing drugs with broad-spectrum efficacies. The first approach targets the cellular machinery or metabolic pathways that are shared by a number of viruses to infect and replicate in a host cell, while the second approach directly focuses on viruses by targeting common viral factors to develop active antiviral agents. However, a number of problems are associated with the use of small drugs e.g. low solubility, requirement of high dosages, and resistance development among others. These problems can be circumvented with the use of hydrophilic polymer-based platforms which enhance solubility, allow reduction of the dosage amount, and do not provoke resistance. Additionally, they introduce multivalency which has recently been recognized as a highly efficacious strategy in virus targeting. Multivalency also provides the added benefits of active and passive targeting, and can be tailored according to the required function.

Hydrogels are three dimensional crosslinked networks, and one of many polymer-based prophylactics. They are especially favored in the biomedical fields due to their unique viscoelastic properties, high hydrophilicity and biocompatibility. Depending on their chemistry, they can undergo sol-gel transitions and therefore can be used to form *in-situ* gels. They allow the three-dimensional presentation of a large number of functional groups, and thus may be useful for antiviral purposes. In fact, mammalian bodies use the mucus hydrogel as a broad-spectrum antiviral, among other functions.

In this PhD work, the target is to develop broad-spectrum anti-viral prophylactics based on hydrogels.

In the first project, the objective is to develop mucus-inspired hydrogels for broad-spectrum anti-viral applications. The anti-viral function of mucus stems from the structure of its main glycoprotein, i.e. mucin. The mucin glycoprotein, in turn, derives its properties from the sulfate-ester, sialic acid and fucose functional units prominently displayed on the tethered glycoprotein chains, which behave as decoys for broad-spectrum antiviral agents. The physical structure of the network is important as well, as the pore structure alters pathogen mobility and their ability to establish or maintain contact with the host cell surface. The mucin chains are linked to one-another by thiol-disulfide bonds which influences the viscoelasticity of mucus.

In this project the focus will be on the design of mucus-inspired hydrogels (MIHs) from a strictly physical perspective. In order to retain the viscoelastic properties of mucus, the hydrogels will be crosslinked with the help of a reversible thiol-disulfide bond. This bond provides a facile crosslinking reaction using redox chemistry. Linear polyglycerol (IPG) will be used as a substitute for the fibrillar mucin chain, which will provide high hydrophilicity essential for hydrogel structure. IPGs also display a large number of hydroxyl groups- a multi-functional backbone as a mucin substitute will also grant the ability to functionalize them with, if required, for future purposes. For crosslinking, the IPGs will be functionalized with thiol groups to form IPG dithiol. A tri-arm PEG molecule, functionalized with thiol on each arm will be used as the crosslinking agent. The thiol-functionalized hydrogel precursors can then be crosslinked by oxidization with hydrogen peroxide to form a disulfide-linked, multifunctional hydrogel. By changing the gel component ratios, it will be possible to influence the physical properties of the MIH. The ultimate goal here is to approach the rheological properties exhibited by the healthy human lung mucus.

In the second project, the objective will be to establish broad-spectrum antiviral properties by adopting an approach wherein several viruses which share a similar receptor binding moiety will be targeted. Heparan sulfate on the host cell surface is used by many viruses such as HSV, RSV, SARS-CoV-2 etc for initial binding. Therefore, sulfate is an appropriate candidate for virus binding and infection prevention at the initial stages. In order to provide high antiviral efficacy, a multivalent display of the sulfate groups is optimal. Thus, combining these properties, sulfate-functionalized

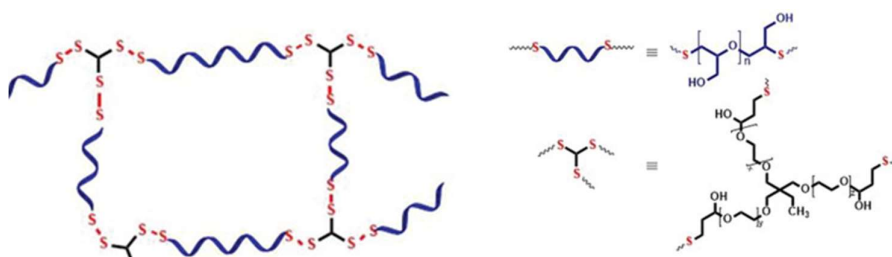
hydrogels will be constructed using maleimide-functionalized sulfated dPG and thiol-functionalized PEG, crosslinked by Michael-click chemistry. Similar to the first project, changing the ratios of the gel components will influence the properties of the hydrogels. The hydrogels will then be used in HSV-binding assays to analyze their efficacy.

3. Publications and Manuscripts

In this chapter all published articles and submitted manuscripts are listed and the contribution of the authors are stated.

3.1 Polyglycerol-based mucus-inspired hydrogels

“The mucus layer is a hydrogel network that covers mucosal surfaces of the human body. Mucus has important protective properties that are related to its unique rheological properties, which are based on mucins being the main glycoprotein constituents. Mucin macromolecules entangle with one another and form a physical network that is instrumental for many important defense functions. Mucus derived from various human or animal sources is poorly defined and thus not suitable for many application purposes. Herein, a synthetic route is fabricated to afford a library of compositionally defined mucus-inspired hydrogels (MIHs). MIHs are synthesized by thiol oxidation to render disulfide bonds between the crosslinker ethoxylated trimethylolpropane tri(3-mercaptopropionate) (THIOCURE ETTMP 1300) and the linear precursors, dithiolated linear polyglycerol (LPG(SH)₂) or polyethylene glycol (PEG(SH)₂) of different molecular weights. The mixing ratio of linear polymers versus crosslinker and the length of the linear polymer are varied, thus delivering a library of compositionally defined mucin-inspired constructs. Their viscoelastic properties are determined by frequency sweeps at 25 and 37 °C and compared to the corresponding behavior of native human mucus. Here, MIHs composed of a 10:1 ratio of LPG(SH)₂ and ETTMP 1300 are proved to be the best comparable to human airway mucus rheology.”



This work was published in:

Sharma, A.; Thongrom, B.; Bhatia, S.; Lospichl, B. V.; Addante, A.; Graeber, S. Y.; Lauster, D.; Mall, M. A.; Gradzielski, M.; Haag, R. Polyglycerol-Based Mucus-Inspired Hydrogels. *Macromol. Rapid Commun.* **2021**, *42*, 2100303.

<https://doi.org/10.1002/marc.202100303>

Author contributions

Conception, synthesis and analysis of hydrogel components and hydrogels, rheological analysis of hydrogels. Writing, editing, and revision of manuscript, and making all graphics, and galley proof.

Polyglycerol-Based Mucus-Inspired Hydrogels

Antara Sharma, Boonya Thongrom, Sumati Bhatia, Benjamin von Lospichl, Annalisa Addante, Simon Y. Graeber, Daniel Lauster, Marcus A. Mall, Michael Gradzielski,* and Rainer Haag*

The mucus layer is a hydrogel network that covers mucosal surfaces of the human body. Mucus has important protective properties that are related to its unique rheological properties, which are based on mucins being the main glycoprotein constituents. Mucin macromolecules entangle with one another and form a physical network that is instrumental for many important defense functions. Mucus derived from various human or animal sources is poorly defined and thus not suitable for many application purposes. Herein, a synthetic route is fabricated to afford a library of compositionally defined mucus-inspired hydrogels (MIHs). MIHs are synthesized by thiol oxidation to render disulfide bonds between the crosslinker ethoxylated trimethylolpropane tri(3-mercaptopropionate) (THIOcURE ETTMP 1300) and the linear precursors, dithiolated linear polyglycerol (LPG(SH)₂) or polyethylene glycol (PEG(SH)₂) of different molecular weights. The mixing ratio of linear polymers versus crosslinker and the length of the linear polymer are varied, thus delivering a library of compositionally defined mucin-inspired constructs. Their viscoelastic properties are determined by frequency sweeps at 25 and 37 °C and compared to the corresponding behavior of native human mucus. Here, MIHs composed of a 10:1 ratio of LPG(SH)₂ and ETTMP 1300 are proved to be the best comparable to human airway mucus rheology.

gastrointestinal, reproductive, and oculo-rhino-otolaryngeal tract surfaces. It is involved in a diverse range of functions as a result of its unique properties. It prevents dehydration of the mucosa by maintaining a hydrated layer on the epithelial surface,^[1] and exhibits shear-thinning rheological behavior that supports its lubricant role by warranting a smooth passage for passing objects.^[2] In the respiratory tract, mucus entraps inhaled pathogens, allergens, and irritants that are constantly removed by mucociliary clearance driven by ciliary beating on airway surfaces facilitating constant mucus clearance from the lungs.^[3] Furthermore, the mucus layer serves as the external defense system of the body against pathogen attack in mucosal immunology.^[1,4,5] The mucus coating is a complex heterogenous biopolymer matrix comprising water (up to 97% by weight), mucin (typically about 5% by weight or less), inorganic salts (≈1% by weight), carbohydrates, proteins, antimicrobial peptides, and lipids. The physical behavior and resultant protective functions

of mucus are attributed to its constituents, particularly mucin glycoproteins,^[6] which represent more than 80% of the overall organic composition.^[7] Mucin macromolecules contain regions of high glycosylation. The sulfate ester and sialic acid motifs

1. Introduction

Mucus is a complex, viscoelastic hydrogel that protects the mucosal surfaces of the mammalian body, such as the respiratory,

A. Sharma, B. Thongrom, S. Bhatia, R. Haag
 Institut für Chemie und Biochemie
 Freie Universität Berlin, Takustraße 3, Berlin 14195, Germany
 E-mail: haag@chemie.fu-berlin.de

B. von Lospichl, M. Gradzielski
 Institut für Chemie
 Technische Universität Berlin
 Straße des 17. Juni 124, Berlin 10623, Germany
 E-mail: Michael.gradzielski@tu-berlin.de

A. Addante, S. Y. Graeber, M. A. Mall
 Department of Pediatric Respiratory Medicine, Immunology and Critical Care Medicine
 corporate member of Freie Universität Berlin and Humboldt Universität zu Berlin
 Charité – Universitätsmedizin Berlin
 Berlin 13353, Germany

A. Addante, S. Y. Graeber, M. A. Mall
 Berlin Institute of Health at Charité – Universitätsmedizin Berlin
 Berlin 10178, Germany

A. Addante, S. Y. Graeber, M. A. Mall
 associated partner site
 Deutsches Zentrum für Lungenforschung e. V.
 Aulweg 130, Gießen 35392, Germany

D. Lauster
 Institut für Chemie und Biochemie
 Fachbereich Biologie, Chemie, Pharmazie
 Freie Universität Berlin
 Arnimallee 22, Berlin 14195, Germany

 The ORCID identification number(s) for the author(s) of this article can be found under <https://doi.org/10.1002/marc.202100303>

© 2021 The Authors. Macromolecular Rapid Communications published by Wiley-VCH GmbH. This is an open access article under the terms of the Creative Commons Attribution-NonCommercial License, which permits use, distribution and reproduction in any medium, provided the original work is properly cited and is not used for commercial purposes.

DOI: 10.1002/marc.202100303

decorate the glycosyl end groups, which in turn act as decoys for various virus families. In addition, the network structure of mucus has an equally important role in mucosal immunology.^[8] The long, fibrillar structure of the mucin molecules enables intermolecular entanglement as well as various covalent and electrostatic interactions to form a gel matrix. The network structure provides multiple obstructions in the path of an incoming pathogen and prevents it from reaching the epithelial cell surface by essentially affecting its motility.^[8,9]

The invasion by pathogens to initiate the infection process is typically initiated by a compromised mucus barrier and thus the subsequent proliferation of infection. Respiratory viruses, such as the influenza A virus and SARS-CoV2 must pass through the mucus barrier to access the underlying epithelia and initiate the viral life cycle.^[2,4,10]

However, naturally occurring mucus is ineffectual for antiviral purposes due to its poorly defined composition, the challenges of extracting of sufficient amounts, the arduous purification required, and performance deviation as a result of a source-dependent composition.^[11] The use of synthetic mucus offers a controlled pathway to overcome such challenges and can, therefore, help to understand the role of different mucus compositions and functional properties in health and disease. The molecular structure, polymer length, and viscoelastic behavior can be precisely controlled while offering a reduction in heterogeneity typical to natural mucus.

Synthetic platforms for surface-tethered mucins have been designed and studied by Kramer et al.^[12] An analog of the peptide backbone of a mucin molecule bearing the *N*-GalNAc branching points native to mucus was constructed using *N*-carboxyanhydride polymerization. However, this model is designed specifically for transmembrane mucin modeling rather than application purposes. Mahalingam et al. devised an elegant platform for the fabrication of a mucus gel network, wherein the boronate-diol condensation reaction was employed to induce a stimuli-responsive network against HIV infection.^[13] This gel mimics cervicovaginal mucus, rather than presenting a broader mucus-mimetic approach. Other synthetic formulations have been explored which exploit the adhesive and lubricating properties of the gel.^[14] With the multivalent presentation of hydroxyl groups on MIHs, as well as the usage of a disulfide linkage, the gels will be even more customizable and closer to natural mucus.

The aim of the present work was to synthetically fabricate linear polyglycerol (LPG) and polyethylene glycol (PEG)-based gel systems that mimic certain characteristics of gel-forming mucus, with the goal of attaining rheological characteristics approaching those of naturally occurring gel-forming mucus of healthy human sputum.

In order to synthetically combine these properties, a highly water soluble, biocompatible, multivalent, and linear core scaffold was provided by thiolated linear polyglycerol^[14–16] (LPG(SH)₂). The multivalent backbone provided ample opportunity for creating a burgeoning synthetic glycosyl domain, akin to mucin. These molecules may be functionalized as required, thereby facilitating a certain influence on the rigidity. Mucus-inspired hydrogels (MIHs) were then realized by reacting these molecules with ethoxylated trimethylolpropane tri(3-mercaptopropionate)

ETTMP 1300 crosslinkers by thiol oxidation to form disulfide bonds, whereby their rheological properties were measured (**Figure 1**). Thus, by an amalgamation of facile techniques, a library of rheologically diverse, compositionally defined mucin-inspired hydrogels was developed. This model not only approaches the structural properties of natural mucus but also attains some of its primary functions without the hassle of lengthy and difficult reactions.

2. Results and Discussion

2.1. Design and Synthesis of Building Blocks

The network structure in natural mucus arises due to the physical and chemical properties imparted by mucin glycoproteins. There are cysteine end groups on every mucin glycoprotein that allow the long, fibrillar molecules to elongate further, resulting in the formation of a mucin “chain.”^[1,7] This results in the physical entanglement of the chains and a network structure arises. The crosslinking is further secured as the chains also interact with one another by hydrophobic and electrostatic means.^[2,15]

In order to develop components for MIHs, an ideal model would be one which allows easy modulation along the lines of viscoelasticity and pore size, while offering multiple backbone functionalization groups to enable multivalent sugar modifications. A chemically crosslinked hydrogel requires a linear structure interspersed with crosslinking points, in ratios that enable a target flexibility. A linear precursor in the MIH network would correspond to the mucin glycoprotein structure in naturally occurring gel mucus, exhibiting structural and functional similarity to it. It would incorporate reactive end groups to enable chain elongation and reaction with crosslinking agents.

The nature of crosslinking in naturally occurring gel mucus is relevant in determining the rheological properties of the network. Individual mucin molecules are linked to each other by disulfide bonds.^[7] Thus, such a reversible, redox-responsive bond should be present in the MIH system. Furthermore, the components should be able to react with each other under mild conditions at room temperature.

With these tools, a library of MIHs has been created with rheological properties, network mesh sizes, and backbone structures that approach the corresponding traits of naturally occurring mucus. Homobifunctionalized linear polyglycerol chains with thiol groups at both ends, i.e., LPG(SH)₂, were prepared as analogs of mucin glycoproteins in MIH networks. Moreover, the LPG backbone structures display multiple hydroxyl groups that equip these models for functionalization with various sugars or other functional groups found in mucin to enable future modification when necessary. The structural properties of MIHs can be regulated by altering the length of the LPG backbone or by replacing it with another linear structure altogether, thus facilitating rheological comparisons on the basis of backbone structure and rigidity. For this purpose, an LPG(SH)₂ backbone of molecular weight 5 kDa was designed (**Scheme 1**). For comparison, two more MIH families were synthesized with linear dithiofunctionalized polyethylene glycol PEG(SH)₂ of molecular weights 3 and 6 kDa (**Scheme 2**).

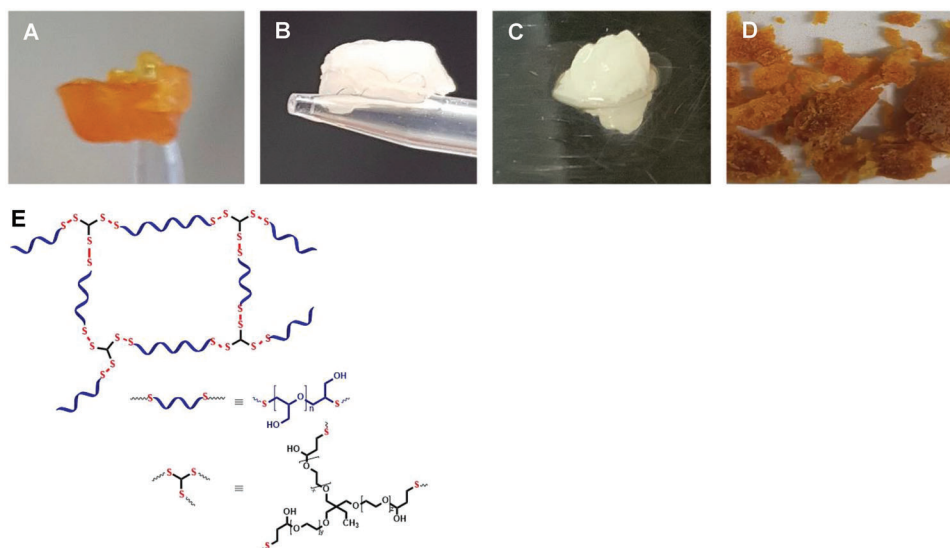
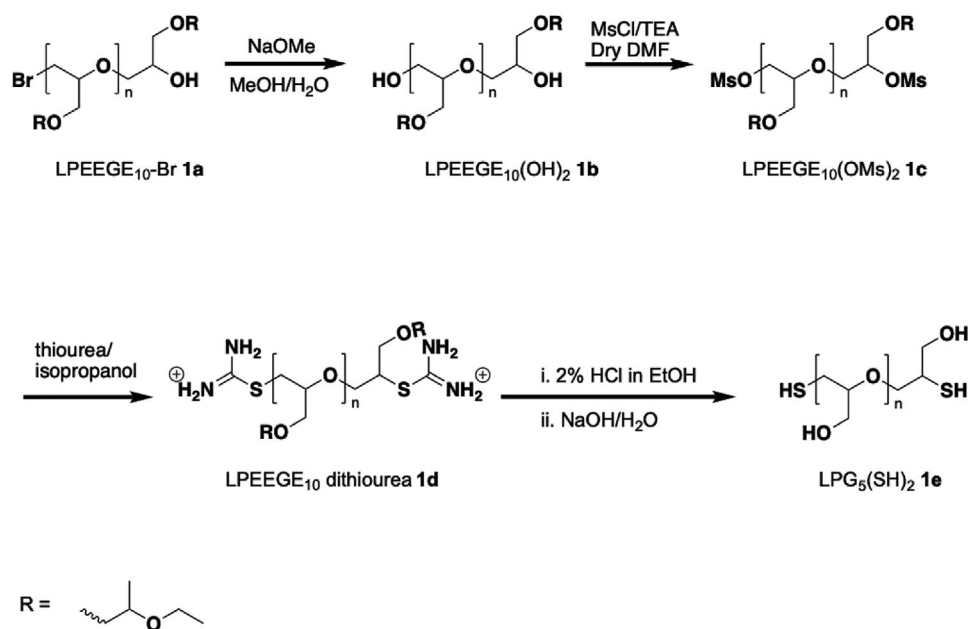
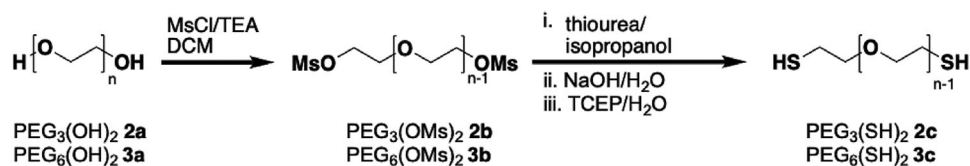


Figure 1. A) MIH-1a containing iodine traces; B) after iodine removal by PBS washing; C) the decrease in elasticity of MIH-1b with increasing linear component becomes visible by eye; D) the hard, coarse, and brittle solid formed upon oxidation of pure ETTMP; E) (right) scheme representing the network structure of MIHs composed of ETTMP 1300 and LPG(SH)₂; chemical structures of ETTMP 1300 (left) and LPG(SH)₂ (below).



Scheme 1. Synthesis of LPG(SH)₂ 1e.



Scheme 2. Synthesis of PEG(SH)₂ (2c and 3c).

2.1.1. Synthesis of Dithiolated LPG(SH)₂ 1e

The bromine-capped linear polyethoxyethyl glycidyl ether (LPEEGE-Br) was synthesized by anionic ring-opening polymerization following the procedure reported in the literature.^[16] LPG(SH)₂ was synthesized in three steps. LPEEGE-Br with molecular weight 10 kDa **1a** was hydrolyzed under basic conditions (pH > 10), resulting in the formation of linear polyethoxyethyl glycidyl ether (LPEEGE-(OH)₂ **1b** with two terminal hydroxy groups. This was followed by a mesylation reaction. The mesylated product **1c** was reacted with thiourea to obtain LPEEGE dithiourea **1d** as the substitution product. The nitrogen and sulfur contents were estimated by elemental analysis to corroborate the degree of conversion. The final compound LPG₅(SH)₂ **1e** was obtained after acidic and basic hydrolysis of ethoxyethyl and thiourea groups, respectively (Scheme 1). Tris(2-carboxyethyl)phosphine (TCEP) was added to this mixture as a reducing agent. Subsequent dialysis led to pure products. ¹H NMR analysis at each step corroborated the formation and purity of the compound. The presence of 2 thiol groups per chain was confirmed by elemental analysis and ¹H NMR studies.

2.1.2. Synthesis of PEG(SH)₂ 2c and 3c

Dithiolated PEGs with molecular weights 3 kDa PEG₃(SH)₂ and 6 kDa PEG₆(SH)₂ were synthesized following an approach modified from the original report from Mahadevegowda and Stuparu (Scheme 2).^[17] First homo-bifunctional dihydroxy PEGs, i.e., PEG₃(OH)₂ **2a** and PEG₆(OH)₂ **3a** were mesylated under anhydrous conditions. PEG₃(OMs)₂ **2b** and PEG₆(OMs)₂ **3b** were obtained as a white powder upon precipitation of the reaction mixture. Thiolation of the thus obtained PEG(OMs)₂ was then performed with thiourea under elevated temperature, followed by basic hydrolysis and reduction by TCEP to finally yield PEG₃(SH)₂ **2c** and PEG₆(SH)₂ **3c** as pale yellow powder after precipitation.

2.2. Synthesis of Mucus-Inspired Hydrogels (MIHs)

In order to assess whether hydrophilic linear polyglycerols can provide mucus-like hydrogels with matching rheological characteristics, a commercial homotrifunctionalized PEG thiol, ETTMP 1300 was used as the crosslinker. Gelation was induced by simply oxidizing the thiol groups present on both of the macromonomer components in the presence of hydrogen peroxide and NaI solution in water.^[18] A 3D matrix was consequently formed with thiol-disulfide interchange reactions facilitating certain characteristic rheological properties of such networks.

Several MIH families were synthesized and compared on the basis of their structure as well as the molecular weight of the linear scaffold. Thus, three gel families were assembled using LPG(SH)₂ and PEG(SH)₂ of varying lengths as linear precursors: LPG₅(SH)₂ **1e**, PEG₃(SH)₂ **2c**, and PEG₆(SH)₂ **3c**. Furthermore, the ratio of the crosslinker to the mucin analog component was varied while maintaining a constant gel volume of every gel family, allowing the rheological properties to be fine-tuned.

In **Table 1**, all the studied gels are listed with their corresponding synthetic details. Thiol oxidation is a sensitive procedure,

Table 1. Description of various MIH gel series studied. The gels are classified by series depending upon the linear precursors of which they are composed. Different types of MIHs within each series are fabricated by changing the ratios of ETTMP 1300 crosslinker to the linear component, thus rendering a total of 12 gels. A total gel volume of 200 μL was fixed for every composition.

MIH series	Linear precursor	Ratio of ETTMP 1300 crosslinker to linear component			
		1:3	1:7	1:10	1:14
MIH-1	LPG ₅ (SH) ₂	MIH-1a	MIH-1b	MIH-1c	MIH-1d
MIH-2	PEG ₃ (SH) ₂	MIH-2a	MIH-2b	MIH-2c	MIH-2d
MIH-3	PEG ₆ (SH) ₂	MIH-3a	MIH-3b	MIH-3c	MIH-3d

with the possibility of oxidation side products such as sulfenic, sulfinic, and sulfonic acids.^[19] These side products may have inhibitory effects on gel formation. To circumvent this problem, the amount of oxidizing agent needs to be slightly decreased with increasing linear component amounts in order to account for the disparity in the overall thiol content.

The gelation process could be visually monitored as the color of the pre-gel mixture deepened from a cloudy white solution to an orange-brown semi-solid upon oxidation. The gels were kept for some time so that an equilibrium state could be attained. Thereafter rheology studies were conducted. The color transition indicates formation of I₂ (Figure 1A). In order to remove the iodine side product from the gels, all MIHs were incubated for 24 h in phosphate-buffered saline (PBS) solution. A change of color thus followed, from the iodide-characteristic orange color to an opaque, white gel, which otherwise retained all other properties (Figure 1B).

2.3. Rheology

2.3.1. Oscillatory Rheology

The mechanical properties of a gel can be defined by its viscoelastic properties, which in turn can be determined by oscillatory rheology measurements. A study of the viscoelastic properties of the LPG- and PEG-based scaffolds was done with the aim to establish relationships between the viscoelastic properties of MIHs and their respective constitution. The results thus obtained were compared with corresponding values in naturally occurring mucus to identify systems with similar rheological properties.

The specifications of the LPG-based MIH-1 gels, and PEG-based MIH-2 and MIH-3 gels studied are listed in **Table 1**. The gels compared were based on three scaffolds—LPG₅(SH)₂, PEG₃(SH)₂, and PEG₆(SH)₂. The ratio of the linear precursor to the crosslinking component, ETTMP 1300, was varied in each case. The concentration of the crosslinker was decreased steadily while maintaining a constant amount of polymer dithiols used overall. This then should lead to increasingly less crosslinked hydrogel networks.

The rheological properties of all the hydrogels were characterized in terms of the storage *G'* and loss *G''* moduli obtained from oscillatory shear experiments. First, a strain-sweep test was conducted to determine the linear viscoelastic region (LVE).

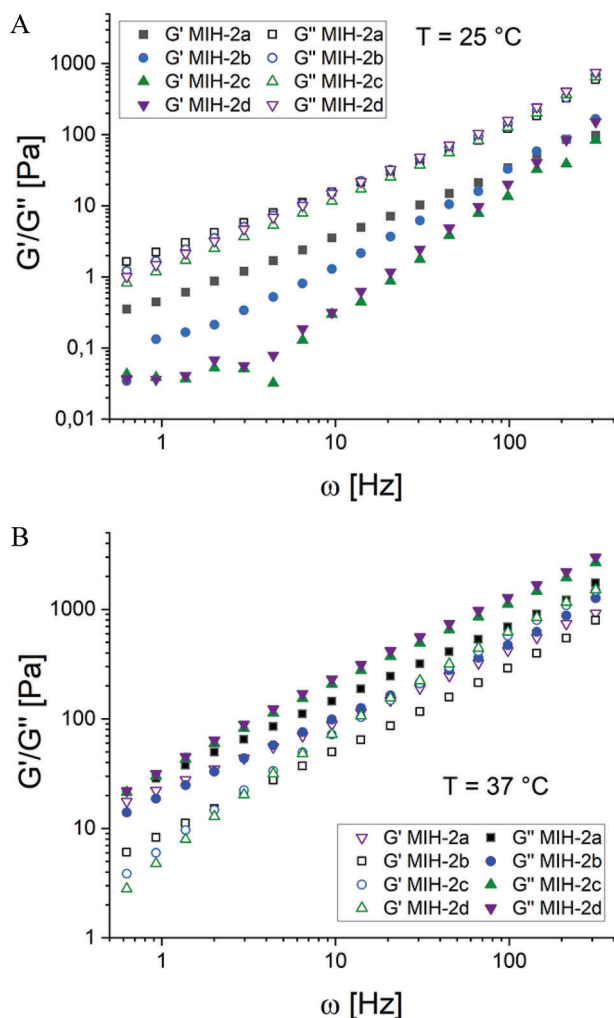


Figure 2. Storage (G') and loss (G'') modulus as function of the radial frequency ω of MIH-2 A) at 25 °C; B) at 37 °C, for samples where the crosslinker density was varied systematically.

Then oscillatory rheology experiments, specifically oscillatory shear and strain tests, were conducted in the LVE to determine G' and G'' as functions of radial frequency ω . The oscillatory rheology results for hydrogels with $\text{PEG}_3(\text{SH})_2$ and $\text{PEG}_6(\text{SH})_2$ are shown in **Figures 2** and **3**, respectively; data for gels with $\text{LPG}_5(\text{SH})_2$ are shown in **Figure 4**. Each test was conducted at 25 °C and at the physiological temperature of 37 °C.

For the PEG-based compounds (MIH-2 and MIH-3), a rather linear increase of G' and G'' can be seen in a double-logarithmic plot, where for the longer PEG spacer (MIH-3) G'' is typically higher than G' , which indicates that these systems are dominated by their viscous properties. This also indicates that these systems are not really proper gels, but at best can be classified as soft and gel-like, i.e., a viscoelastic fluid. They are not permanently crosslinked and are relaxing under a given stress proportional to the time left for this relaxation. Interestingly, with increasing temperature both moduli increase substantially (by more than a factor 10) and the increase is larger for G' , i.e., the relative elastic properties of these gels increase with rising temperature. As

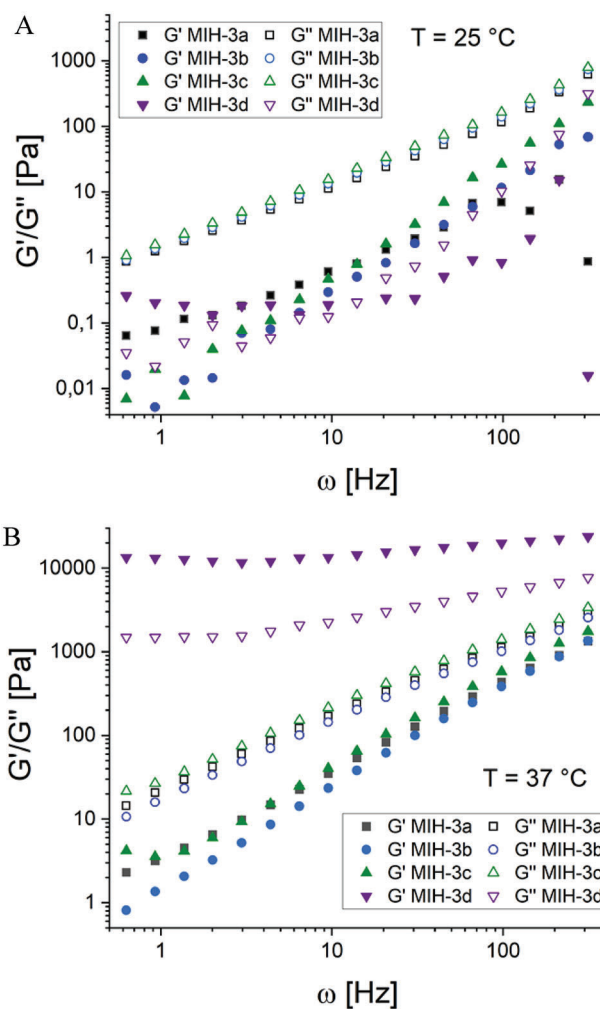


Figure 3. Storage (G') and loss (G'') modulus as function of the radial frequency ω of MIH-3 A) at 25 °C; B) at 37 °C, for samples where the crosslinker density was varied systematically.

stated before, this behavior may be attributed to the fact that PEG becomes less well soluble in water with increasing temperature and therefore the network structure would be contracting. This slope of the frequency increase was higher for G' ($\approx \omega^{1.2}$, at 37 °C) than for G'' ($\approx \omega^{0.85}$, at 37 °C) and accordingly with increasing frequency the gap between G'' and G' decreases. This suggests that the crossover point where G' would overtake G'' would take place at frequencies higher than the frequency range applied here, indicating a rather short structural relaxation time of less than 0.02 s.

Generically similar is the behavior of the PEG-based systems with the shorter PEG spacer (MIH-3), but here the relative increase of G' with rising temperature is even much more marked. Upon going from 25 to 37 °C, it increases by a factor of 30–200, while G'' only increases by a factor of 3–5. This also means that at low temperature the systems are dominated by viscous properties, but this is reversed at 37 °C, where the elastic properties become dominant. Interestingly, the scaling of both G' and G'' at 37 °C is about $\approx \omega^{0.75-0.8}$.

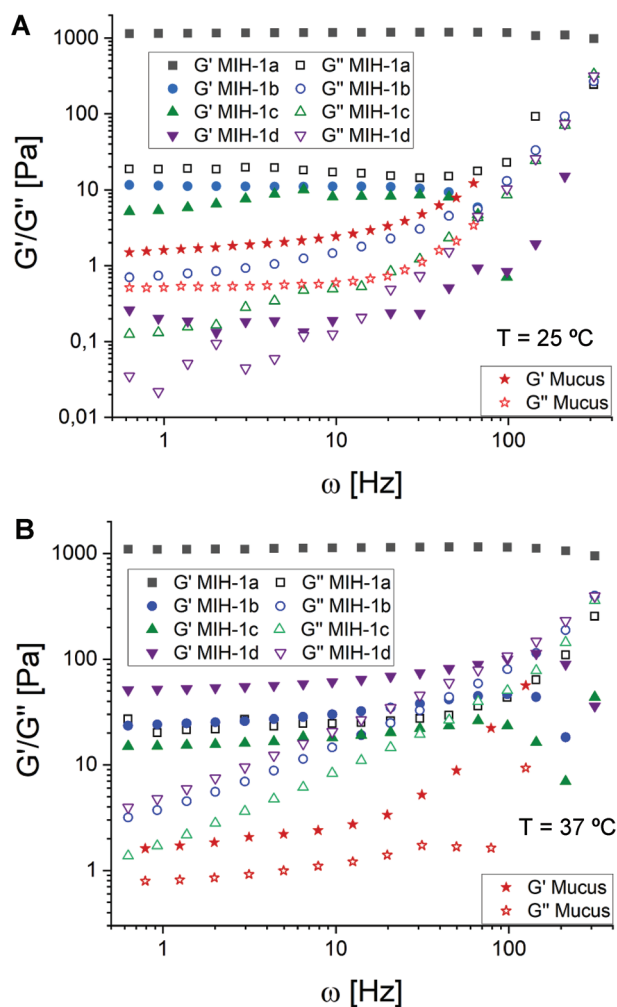


Figure 4. Storage modulus G' and loss modulus G'' as functions of the radial frequency ω of A) MIH-1 at 25 °C; B) MIH-1 at 37 °C, for samples where the crosslinker density was varied systematically. For comparison, data of fresh airway mucus obtained from healthy donors were also included in (A) (averaging over three different samples).

In contrast, for $\text{LPG}_5(\text{SH})_2$ -based MIH-1 gels, both moduli, G' and G'' , remained rather constant, with G' being much larger than G'' , i.e., they behaved like typical gels with a yield stress. For instance, for the sample with thrice the linear component as compared to the crosslinker (MIH-1a), G' remained about two orders of magnitude higher than G'' throughout the frequency range, thus showing gel-like behavior. For the other gels with less crosslinker, G' remained also constant, but at much lower frequency values. Compared to the PEG-based gels the increase of viscoelastic parameters is much less pronounced here.

Even more different is the behavior of G'' that increases markedly with rising frequency in the higher frequency range and there even bypassing G' , although also G' starts to increase somewhat for frequencies above 10 Hz. Such behavior is not very frequently seen, but has for instance similarly been reported for carrot puree.^[20] Generally, it indicates a faster relaxation process being present within the system.

Table 2. Shear modulus G_0 and estimated mesh size ξ of $\text{LPG}_5(\text{SH})_2$ -based MIHs at 25 and 37 °C.

MIH	[crosslinker]/[linear component]	25 °C		37 °C	
		Shear modulus [G_0 /Pa]	Mesh size [ξ /nm]	Shear modulus [G_0 /Pa]	Mesh size [ξ /nm]
MIH-1a	1:3	1157	15	1112	15
MIH-1b	1:7	11	72	33	52
MIH-1c	1:10	8	82	19	61
MIH-1d	1:14	0.2	286	69	40

A direct comparison of the rheological properties of healthy human airway mucus with MIHs can be very interesting in this context. Previous experiments have shown that the shear modulus of mucus in healthy lungs is ideally around 1–2 Pa.^[21] To compare synthesized MIHs with human mucus, rheological properties of healthy airway mucus from three individual donors were determined and are included in Figure 4. It can be seen that human mucus also shows such an upturn above 10 Hz in a similar fashion for G' and G'' , while at lower frequency a constant plateau is observed, with $G' \sim 2$ Pa. It is interesting to note that the rheological properties of mucus are rather insensitive to the temperature change from 25 to 37 °C (while the synthetic gels generally show some increase especially of the storage modulus, which can be attributed to the effect of entropy elasticity for covalently bound networks). Comparing the data in Figure 4, one can conclude that MIH-1 with a ratio of crosslinker to linear component in the range of 1:10 to 1:14 is showing rather similar rheological behavior as healthy airway mucus. Thus, the rheological data show that tunable hydrogels can be constructed, where storage and loss moduli, and to some extent even their frequency dependence, can be controlled via the ratio of the linear component to the crosslinking agent.

The marked decrease of the elastic properties with decreasing content of crosslinker could be attributed to a decreasing number of crosslinking points within the gel network, but given the large decrease it would not just mean less crosslinker but also a substantially reduced crosslinking efficiency. In order to quantify this further, we determined the shear modulus G_0 as the average of G' in the plateau regime and the corresponding values are given in Table 2. Especially at lower crosslinker content, an increase in temperature had a similar but smaller effect on the LPG-based MIHs as observed for the PEG-based MIHs, i.e., the elastic properties increase at the higher temperature. An explanation for that behavior would be that the linking polymer chains are less well dissolved in water with increasing temperature and therefore they swell less and correspondingly their crosslinking density increases. The effective network mesh sizes ξ were then estimated from the shear modulus G_0 from the simplified relation: $G_0 = kT/\xi^3$ and they are given in Table 2.^[22]

The mesh size ξ of a network (which is the inverse of the crosslinking density) is directly linked to its rheological properties. The rough estimate obtained from the shear modulus G_0 (Table 2, Figure 5) yields ξ values in the range of 15–80 nm, which compares well with the experimentally observed values of

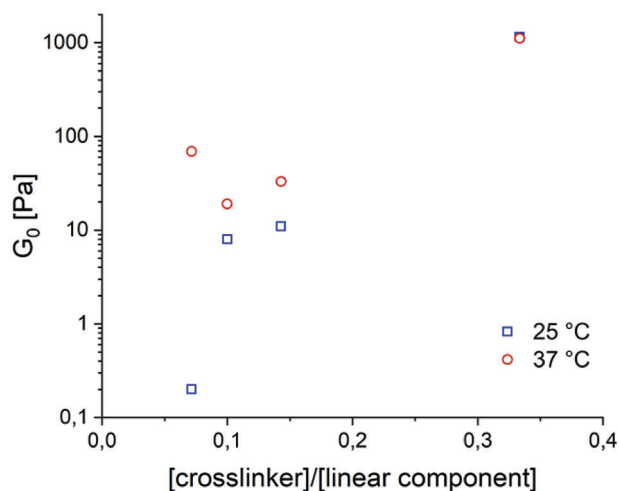


Figure 5. Shear modulus G_0 for the MIH-1 gels as a function of the ratio of crosslinker to linear component, measured at 25 and 37 °C.

Table 3. Crosslinking densities obtained by Equation (1).

MIH type	25 °C $\mu\text{mol cm}^{-3}$	37 °C $\mu\text{mol cm}^{-3}$
MIH 1a	0.44	0.45
MIH 1b	0.0099	0.0043
MIH 1c	0.0062	0.0023
MIH 1d	0.021	0.000072

20–200 nm for naturally occurring mucus.^[23] While the data differ depending upon the source and method of examination, a mesh size in the range of 100 nm up to even a few micrometers is the norm.^[24] This observation also aligns with the inferred rheological data. As shown in Table 2, for MIH-1c the effective mesh sizes at physiological temperature were about 60 nm and thus in the same range as the desired size range. With the tunable design of such systems, much larger pore sizes can be achieved by substitution of backbone structures or crosslinkers of different lengths.

The effective crosslinking density ρ can be estimated from the rheological data via Equation (1):

$$\rho = \frac{G'_{\text{plateau}}}{R \cdot T} \quad (1)$$

This equation is based on the plateau modulus G'_{plateau} obtained during frequency sweep experiments, where R is the universal gas constant, and T is the temperature. The effective rheological crosslinking density is simply the inverse of the mesh size given in Table 2, and listed in Table 3.

The observed effective crosslinking density decreases substantially with lowering the content of the crosslinker. For comparison one can also calculate the crosslinking density, as it would be expected for perfect polymerization, and for this assumption one obtains values within the limits of 2 – 20 $\mu\text{mol cm}^{-3}$, depending on the gel composition. This indicates that the chemical crosslinking is only effective to a rather low extent and correspondingly one has a much more open structure than would be

present for complete crosslinking. In addition, one has to note that Equation (1) is just a general relation and depending on the precise topology of the network one would have a prefactor different than one, which to a lesser extent may also attribute to the observed discrepancy of values.

3. Conclusion

In this work, the endeavor was to create such a mucus-inspired hydrogel in a facile, low-cost manner with a nature-inspired disulfide crosslinking chemistry. For this purpose, LPG and PEG chains of different molecular weights were utilized to produce dithiol-functionalized chains, which in turn were gelled with ETTMP 1300—a tri-PEG crosslinker, in the presence of an oxidizing agent. Of the formed gels, the most appropriate for the intended purpose was the MIH-1c gel based on a LPG-dithiol with an Mn of 5 kDa. At lower frequencies, the gel showed elastic-dominant behavior, with G' falling in the range of 5–10 Pa at 25 °C. As for all other gels, the G' increased to 15–20 Pa in the same frequency range as the temperature was increased to 37 °C. Thus, we successfully demonstrated the synthesis of mucus-like hydrogels with a range of rheological properties and achieved with MIH-1c a hydrogel that has rheological properties comparable to native human airway mucus.

4. Experimental Section

Materials: All chemicals were obtained from Merck (Darmstadt, Germany) and Acros Organics (Geel, Belgium), and used without any purification. ETTMP 1300 was received as a gift from Bruno Bock (Marschacht, Germany) and used as such. Moisture-sensitive reactions were performed under anhydrous conditions, in flame-dried glassware. Reflux reactions were performed at 115 °C in an oil bath. Dialysis was performed in Spectra Por dialysis tubing (MWCO = 2000 g mol⁻¹) (Carl Roth GmbH, Karlsruhe, Germany). The dialysate was changed five times within 2 days. ¹H NMR spectra were recorded in AV 500 spectrometer (Bruker, Massachusetts, USA). NMR chemical shifts were reported as δ values in ppm. LPEEGE with average molecular weights of 10 kDa (LPEEGE₁₀) were synthesized by following procedures reported in literature.^[15]

Methods: Synthesis and Characterization of Dithiolated Linear Polyglycerol LPG(SH)₂: **Synthesis of LPEEGE 1a:** LPEEGE-Br was synthesized as described previously.^[16] LPEEGE₁₀Br **1a** (2 g, 2.38 × 10⁻² mmol) was dissolved in a mixture of MeOH (18 mL) and H₂O (3 mL). Sodium methoxide (30 wt%, 200 μL , 0.88 mmol) was added to the solution and stirred overnight at room temperature. The crude LPEEGE product was then purified by dialysis against acetone (2 days) to remove excess sodium methoxide as well as to remove methanol and water to afford pure LPEEGE₁₀(OH)₂ **1b** (1.9 g, 95% yield).

Synthesis of LPEEGE₁₀ dithiourea 1d: Thoroughly dried LPEEGE₁₀(OH)₂ **1b** (1.9 g, 2.4 × 10⁻² mmol, 1 eq.) was dissolved in anhydrous dimethylformamide (DMF, 250 mL), followed by the addition of triethylamine (TEA, 25 μL , 1.3 mmol, 7.5 equivalent) to the stirring solution. The reaction flask was cooled over an ice bath, and subsequently a solution of MsCl (5.5 μL , 7.14 × 10⁻² mmol, 3 eq.) in DMF (1.5 mL) was added in a dropwise manner to the vigorously stirring solution. The reaction mixture was stirred over an ice bath for 1 h, after which the solution was allowed to attain room temperature and continued to be stirred for 48 h. After solvent removal, the crude product was dialyzed against a 3:1 chloroform–methanol mixture for 24 h. The resultant yellow-orange-colored LPEEGE₁₀(OMs)₂ (**1c**) had a honey-like consistency (yield: 50%) which was used for the dithiourea formation without any delay.

In order to afford thiol-functionalized LPEEGE₁₀(SH)₂, LPEEGE₁₀(OMs)₂ **1c** (1.9 g, 2.4 × 10⁻² mmol) was dried under vacuum, and then dissolved in mixture of 1-propanol (200 mL) and MeOH

(10 mL). The reaction was refluxed for 48 h after thiourea (73 mg, 9.52 × 10⁻¹ mmol, 4 eq.) was added. 1-propanol was evaporated to afford crude LPEEGE₁₀ dithiourea **1d**, which was then purified by dialysis using methanol as a solvent. Its constitution was confirmed by elemental analysis; N = 0.716; C = 46.66; S = 0.297; H = 7.578 (≈2 thiol groups per chain). LPEEGE₁₀ dithiourea **1d**, 95% isolated yield, ¹H NMR (500 MHz, MeOD, δ (ppm)): 1.17–1.30 (m, 11H), 3.88–4.11 (m, LPG backbone), 7.91 (s, 4H).

Synthesis of LPG₅(SH)₂ 1e: An acidic solution of ethanol was prepared by mixing HCl in ethanol such that the solution had a pH of 5. LPEEGE₁₀ dithiourea **1d** was dissolved in 150 mL of the prepared acidic solution and then stirred overnight, after which the pH of the solution was brought up to 8 using 1 M NaOH solution. Sodium hydroxide (4 mg, 0.1 mmol, 4 eq.) was added to an aqueous solution of the crude product, which was then refluxed for 48 h. The temperature of the reaction flask was brought down to room temperature. After the reaction, crude product was dialyzed against deionized water for 72 h to finally obtain pure LPG(SH)₂ **1e** in ≈95% isolated yield which was stored in the presence of TCEP.

Synthesis and Characterization: Dithiolated PEG (PEG₃(SH)₂): **Synthesis of Dimesylated PEG (PEG(OMs)₂):** Dry PEG₆(OH)₂ **3a** (20 g, 3.3 mmol, 1 eq.) was dissolved in anhydrous dichloromethane (DCM, 100 mL). TEA (2.77 mL, 20 mmol, 6 equiv.) was injected in this solution. The reaction flask was then cooled over ice bath followed by subsequent dropwise addition of methane sulfonyl chloride (1.03 mL, 13.3 mmol, 4 equiv.). The reaction was allowed to run for 1 day. Afterward the crude product was purified by first washing the reaction mixture thrice with brine, drying the DCM layer, and then precipitating the resultant product in cooled diethylether. The precipitate so obtained was collected and dried in vacuo over 24 h to obtain PEG(OMs)₂ as a white colored powder.

PEG₃(OMs)₂ **2b**: 90% isolated yield, ¹H NMR (700 MHz, CDCl₃, δ (ppm)): 3.07 (3H, s), 3.63–3.76 (m), 4.36 (2H, t, J = 7 Hz)

PEG₆(OMs)₂ **3b**: 95% isolated yield, ¹H NMR (500 MHz, CDCl₃, δ (ppm)): 3.07 (3H, s), 3.48–3.78 (m), 4.37 (2H, t, J = 5 Hz)

Synthesis of Dithiolated PEG (PEG(SH)₂): To a solution of dimesylated PEG (PEG₆(OMs)₂ **3b** (19 g, 3.2 mmol, 1 eq.) in 1-propanol (100 mL), thiourea (1.02 g, 13.3 mmol, 4 eq.) was added and the solution was refluxed for 24 h to obtain diisothiuronium PEGintermediate. 1-propanol was then removed from the crude mixture and NaOH (0.53 g, 13.3 mmol, 4 eq.) and water (100 mL) were added. This solution was then refluxed for 24 h. Afterward, the crude mixture was neutralized to pH 7. TCEP (1.67 g, 6.7 mmol, 2 eq.) was consequently added, and the reaction was stirred for a further 2 h to obtain the crude final PEG-dithiol product. The product was purified following a precipitation procedure. To this end, NaCl was first added to the reaction mixture until the saturation point was attained. The product was then extracted with DCM. Thereafter, the DCM layer was dried with Na₂SO₄. Finally, the pure product was precipitated in cooled diethylether followed by drying in vacuo so as to obtain PEG(SH)₂ as a pale yellow colored powder.

PEG₃(SH)₂ **2c**: 79% isolated yield, ¹H NMR (600 MHz, CDCl₃, δ (ppm)): 1.59 (1H, t, J = 6 Hz, 12 Hz), 2.69 (2H, quat, J = 6 Hz, 12 Hz), 3.51–3.76 (m). Elemental analysis; N = 0.24; C = 53.43; S = 2.43; H = 8.52

PEG₆(SH)₂ **3c**: 88% isolated yield, ¹H NMR (500 MHz, CDCl₃, δ (ppm)): 1.59 (1H, t, J = 5 Hz, 10 Hz), 2.69 (2H, quat, J = 5 Hz, 10 Hz), 3.48–3.78 (m). Elemental analysis; N = 0.13; C = 54.24; S = 2.02; H = 8.47

Synthesis of MIHs: LPG-based and PEG-based gels were both fabricated in a manner that resulted in gels with the same volumes. Four families of gels were prepared, differing only by their linear components, namely, LPG₅(SH)₂, PEG₃(SH)₂, and PEG₆(SH)₂, listed as gel series **MIH-1**, **MIH-2**, and **MIH-3** in Table 2, respectively. Furthermore, the crosslinker to linear component ratios within each series was varied in order to zero in on the gels with the most promising rheological properties. Three such ratios for each series were inspected, and thus a total of 12 gel types were finally examined, the specifications of which are also listed in Table 2.

First, separate 50% w/v aqueous solution of the linear component was prepared in water. Similarly, a 50% w/v solution was also prepared for

ETTMP 1300. A 10 × 10⁻³ M NaI solution was freshly prepared. The two gel components were then mixed in an Eppendorf tube, in amounts as listed in Table 2, with the final crosslinker to backbone ratios being 1:3, 1:7, 1:10, and 1:14, respectively. NaI and H₂O₂ were added consecutively. This cloudy pregel solution was then vortexed until a color change from white to yellow was observed indicating the release of iodide and consequent formation of the tri-iodide ion. The color deepened within the next 2 min to finally develop into an orange-brown semi-solid. The gel was incubated at room temperature overnight in a closed container, and rheology tests were conducted thereafter.

The saturated yellow color of the gel was a leftover of the oxidation process, and easily be removed by incubation of the formed gel in PBS buffer for 24 h to obtain a white gel (Figure 1B). All gels were synthesized following the same gelation procedure.

Human Lung Sputum Samples: Collection of airway mucus samples from healthy donors was approved by the ethics committee of the Charité – Universitätsmedizin Berlin and written informed consent was obtained from all participants. All donors were healthy nonsmokers. Lung sputum was collected after induction by inhalation of hypertonic saline (NaCl 6%) with a PARI LC PLUS nebuliser (PARI GmbH, Starnberg, Germany) according to a standard operating procedure. Macrorheology was measured immediately using the Kinexus Pro + rheometer (NETZSCH GmbH, Selb, Germany) at 25 °C.

Rheological Analysis: The hydrogels were measured using a stress-controlled MCR 501 Anton Paar rheometer with a plate–plate stainless steel geometrical setup. A 25 mm upper rotating plate diameter was used for all measurements with constant gap size of 0.15 mm. The measurements were conducted at room temperature (25 °C) as well as physiological temperature (37 °C). The samples were allowed to reach temperature equilibrium for ≈5 min prior to each measurement.

Oscillatory Rheology: First, an amplitude sweep was performed to determine the limits of the LVE for each type of hydrogel analyzed in this study. The critical deformation strain was found to be at about 1%. The shear strain (γ) is defined as the ratio of the deflection path (s) to the shear gap (h)

$$\gamma = \frac{s}{h} \quad (2)$$

Next, oscillatory shear tests were conducted within the LVE region, applying a constant strain amplitude, γ_A, of 1%. Frequency sweeps of the hydrogel samples were conducted in the range 0.1–50 Hz. From the experimentally determined shear stress τ_A, storage modulus G' and loss modulus G'' were determined, which are related to each other via the phase angle (δ)

$$\tan \delta = \frac{G''}{G'} \quad (3)$$

The loss modulus G'' describes the viscous behavior of the sample which in turn is the result of energy dissipation due to the internal friction between the moving layers. Conversely, the storage modulus G' describes the energy stored elastically within the internal material structure as it is sheared.

Moreover, the rheological data could also be used to draw information on the internal hydrogel structure and to roughly estimate an effective mesh size, ξ, from the number density, ¹N, of crosslinking points, the Boltzmann constant k_B, absolute temperature T, and the plateau modulus G₀:

$${}^1N = \frac{G_0}{k_B T} = \frac{1}{\xi^3} \quad (4)$$

Hysteresis curves were produced for all frequency sweeps in order to ascertain the reproducibility of the data. All reported results were the average of the up- and down-ramps at each data point. The rheological properties of all three families of LPG- and PEG-based hydrogels were investigated on this basis.

Supporting Information

Supporting Information is available from the Wiley Online Library or from the author.

Acknowledgements

This study was supported by the Helmholtz Graduate School for Macromolecular Bioscience and funded by the Deutsche Forschungsgemeinschaft (DFG, German Research Foundation)—SFB 1449—projects A01, B03, C04, and Z02 and by the German Federal Ministry of Education and Research (82DZL0098B1). The rheometer employed was financed by the Deutsche Forschungsgemeinschaft (DFG, German Research Foundation) via grant GR1030/24-1. S.Y.G. is participant in the BIH-Charité Clinician Scientist Program funded by the Charité – Universitätsmedizin Berlin and the Berlin Institute of Health.

Open access funding enabled and organized by Projekt DEAL.

Conflict of Interest

The authors declare no conflict of interest.

Data Availability Statement

Research data are not shared.

Keywords

bio-inspired hydrogels, linear polyglycerol, mucus, redox responsive hydrogels

Received: May 12, 2021

Revised: July 23, 2021

Published online: September 13, 2021

- [1] R. Bansil, B. S. Turner, *Curr. Opin. Colloid Interface Sci.* **2006**, *11*, 164.
- [2] R. A. Cone, *Adv. Drug Delivery Rev.* **2009**, *61*, 75.
- [3] M. A. Mall, *J. Aerosol Med. Pulm. Drug Delivery* **2008**, *21*, 13.
- [4] D. J. Thornton, *Proc. Am. Thorac. Soc.* **2004**, *1*, 54.
- [5] M. R. Knowles, R. C. Boucher, *J. Clin. Invest.* **2002**, *109*, 571.
- [6] D. Song, D. Cahn, G. A. Duncan, *Langmuir* **2020**, *36*, 12773.
- [7] N. A. Peppas, Y. Huang, *Adv. Drug Delivery Rev.* **2004**, *56*, 1675.
- [8] M. Caldara, R. S. Friedlander, N. L. Kavanaugh, J. Aizenberg, K. R. Foster, K. Ribbeck, *Curr. Biol.* **2012**, *22*, 2325.
- [9] H. C. Berg, L. Turner, *Nature* **1979**, *278*, 349.
- [10] K. Ribbeck, *Biosci. Hypotheses* **2009**, *2*, 359.
- [11] C. Nowald, A. Penk, H.-Y. Chiu, T. Bein, D. Huster, O. Lieleg, *Macromol. Biosci.* **2016**, *16*, 567.
- [12] J. R. Kramer, B. Onoa, C. Bustamante, C. R. Bertozzi, *Proc. Natl. Acad. Sci. U. S. A.* **2015**, *112*, 12574.
- [13] A. Mahalingam, J. I. Jay, K. Langheinrich, S. Shukair, M. D. Mcraven, L. C. Rohan, B. C. Herold, T. J. Hope, P. F. Kiser, *Biomaterials* **2011**, *32*, 8343.
- [14] C. Werlang, G. Cárcarmo-Oyarce, K. Ribbeck, *Nat. Rev. Mater.* **2019**, *4*, 134.
- [15] X. Cao, R. Bansil, K. R. Bhaskar, B. S. Turner, J. T. Lamont, N. Niu, N. H. Afdhal, *Biophys. J.* **1999**, *76*, 1250.
- [16] M. Gervais, A. - L. Brocas, G. Cendejas, A. Deffieux, S. Carloti, *Macromolecules* **2010**, *43*, 1778.
- [17] S. H. Mahadevegowda, M. C. Stuparu, *Eur. J. Org. Chem.* **2017**, *2017*, 570.
- [18] B. D. Fairbanks, S. P. Singh, C. N. Bowman, K. S. Anseth, *Macromolecules* **2011**, *44*, 2444.
- [19] J.-P. R. Chauvin, D. A. Pratt, *Angew. Chem., Int. Ed. Engl.* **2017**, *56*, 6255.
- [20] H. Moritaka, S.-I. Sawamura, M. Kobayashi, M. Kitade, K. Nagata, *Biosci., Biotechnol., Biochem.* **2012**, *76*, 429.
- [21] S. K. Lai, Y.-Y. Wang, D. Wirtz, J. Hanes, *Adv. Drug Delivery Rev.* **2009**, *61*, 86.
- [22] M. S. Green, A. V. Tobolsky, *J. Appl. Phys.* **1946**, *17*, 407.
- [23] H. M. Yildiz, C. A. Mckelvey, P. J. Marsac, R. L. Carrier, *J. Drug Targeting* **2015**, *23*, 768.
- [24] J. Leal, H. D. C. Smyth, D. Ghosh, *Int. J. Pharm.* **2017**, *532*, 555.

Supporting Information

Polyglycerol based mucin inspired hydrogels

Antara Sharma, Boonya Thongrom, Sumati Bhatia, Benjamin von Lospichl, Annalisa Addante, Simon Y. Graeber, Daniel Lauster, Marcus A. Mall, Michael Gradzielski, Rainer Haag**

Antara Sharma, Boonya Thongrom, Dr. Sumati Bhatia, Prof. Dr. Rainer Haag
Institut für Chemie und Biochemie, Freie Universität Berlin, Takustraße 3, 14195 Berlin,
Germany

Benjamin von Lospichl, Prof. Dr. Michael Gradzielski
Institut für Chemie, Technische Universität Berlin, Straße des 17. Juni 124, 10623 Berlin,
Germany

Dr. Daniel Lauster
Institut für Chemie und Biochemie, Fachbereich Biologie, Chemie, Pharmazie, Freie
Universität Berlin, Arnimallee 22, 14195 Berlin, Germany

Annalisa Addante^{1,3}, Simon Y. Graeber^{1,2,3}, Marcus A. Mall^{1,2,3}

¹Department of Pediatric Respiratory Medicine, Immunology and Critical Care Medicine,
Charité - Universitätsmedizin Berlin, corporate member of Freie Universität Berlin and
Humboldt Universität zu Berlin, Berlin, Germany

²Berlin Institute of Health at Charité – Universitätsmedizin Berlin, Berlin, Germany

³German Center for Lung Research (DZL), associated partner site, Berlin, Germany

Table S 1. Description of MIH families: monomer ratios, compositions, concentration and amount of catalyst and oxidizing agent.

MIH Gel	Crosslinker: Linear component Ratio	Gel Macromonomers (50% w/v in DI water)				Oxidizing agent		Gelation time (minutes)
		ETTMP 1300 (μL)	LPG ₅ (SH) ₂ (μL)	PEG ₃ (SH) ₂ (μL)	PEG ₆ (SH) ₂ (μL)	5M NaI solution (μL)	H ₂ O ₂ 30% w/v (μL)	
1a	1 : 3	50	150	-	-	5.5	2	8
1b	1 : 7	25	175	-	-	5.5	2	8.5
1c	1 : 10	18	182	-	-	7.5	1	10
1d	1 : 14	13.4	186.6	-	-	7.5	1	13
2a	1 : 3	50	-	150	-	5.5	2	-
2b	1 : 7	25	-	175	-	5.5	2	-
2c	1 : 10	18	-	182	-	7.5	1	-
2d	1 : 14	13.4	-	186.6	-	7.5	1	-
3a	1 : 3	50	-	-	150	5.5	2	-
3b	1 : 7	25	-	-	175	5.5	2	-
3c	1 : 10	18	-	-	182	7.5	1	-
3d	1 : 14	13.4	-	-	186.6	7.5	1	-

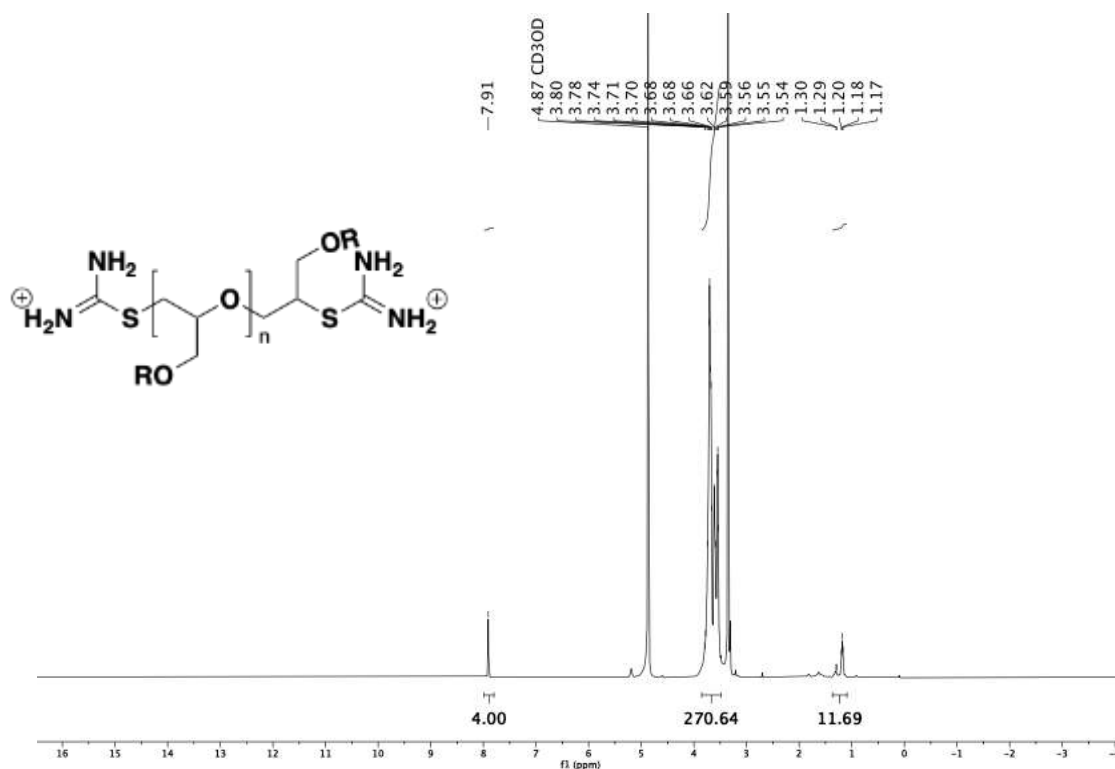


Figure S 1. ¹H NMR (500 MHz, MeOD) of LPEEGE_{10kDa} dithiourea **1d**.

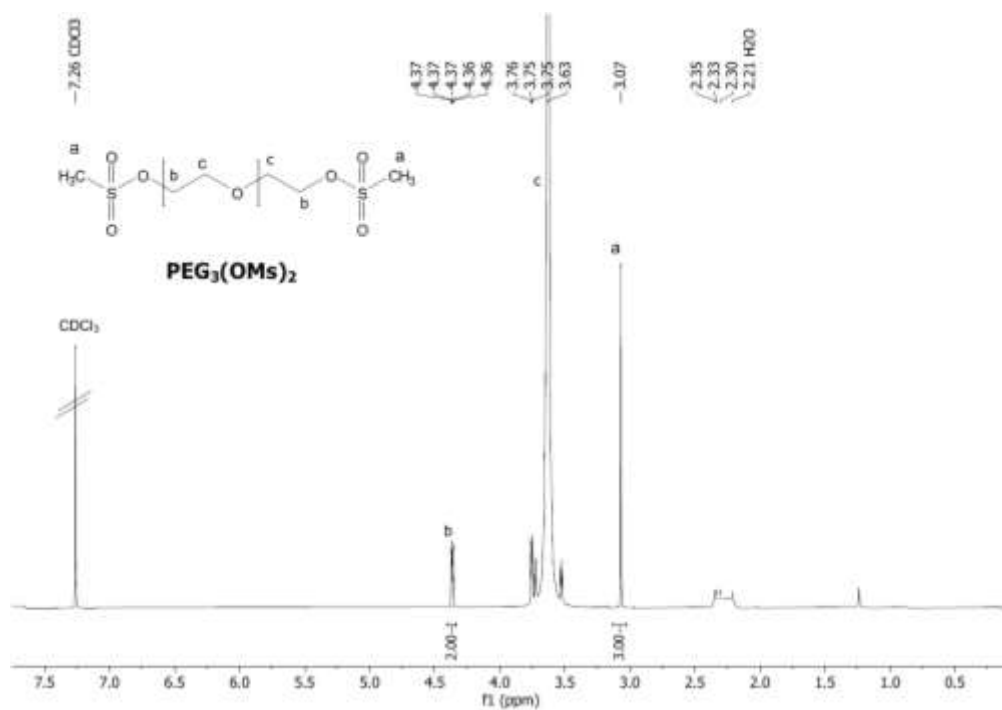


Figure S 2. ^1H NMR (700 MHz, CDCl_3) of $\text{PEG}_3(\text{OMs})_2$ **2b**.

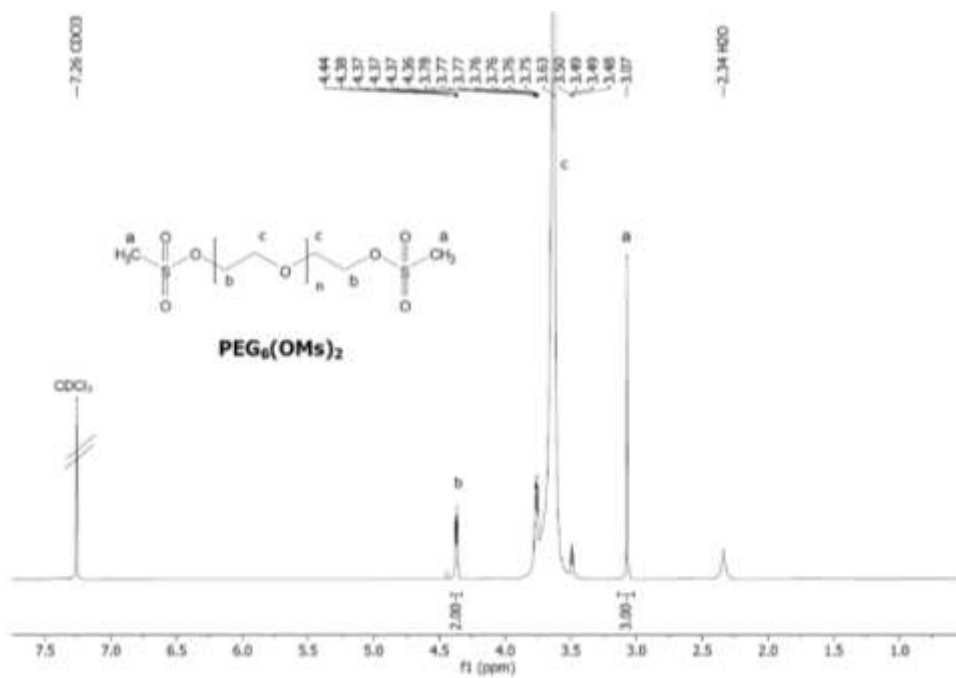


Figure S 3. ^1H NMR (500 MHz, CDCl_3) of $\text{PEG}_6(\text{OMs})_2$ **3b**.

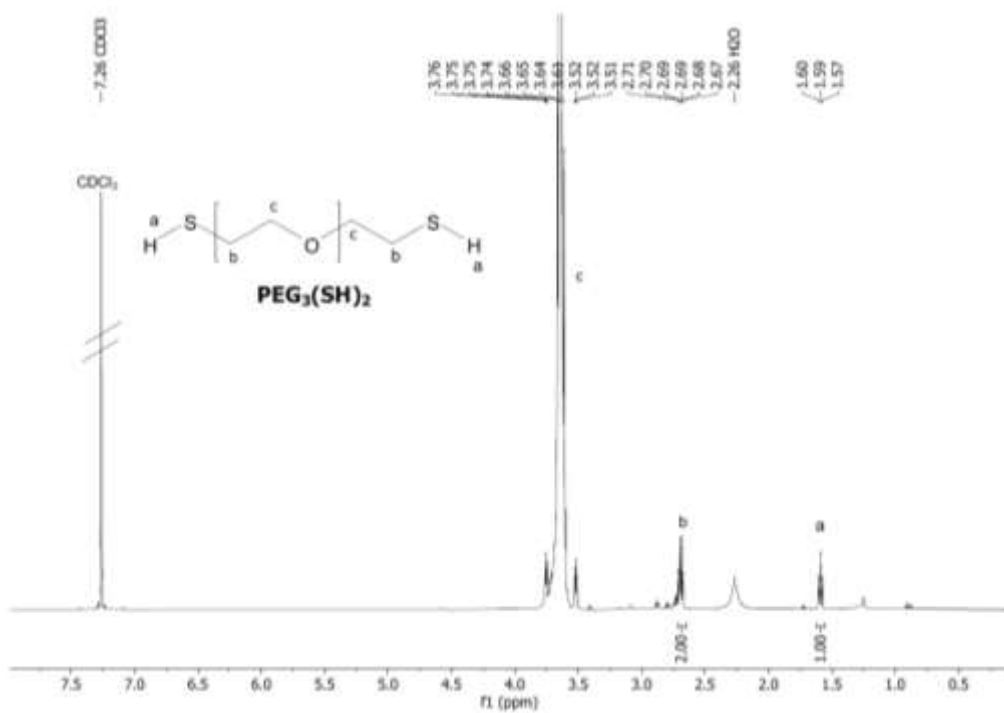


Figure S 4. ^1H NMR (600 MHz, CDCl_3) of $\text{PEG}_3(\text{SH})_2$ 2c.

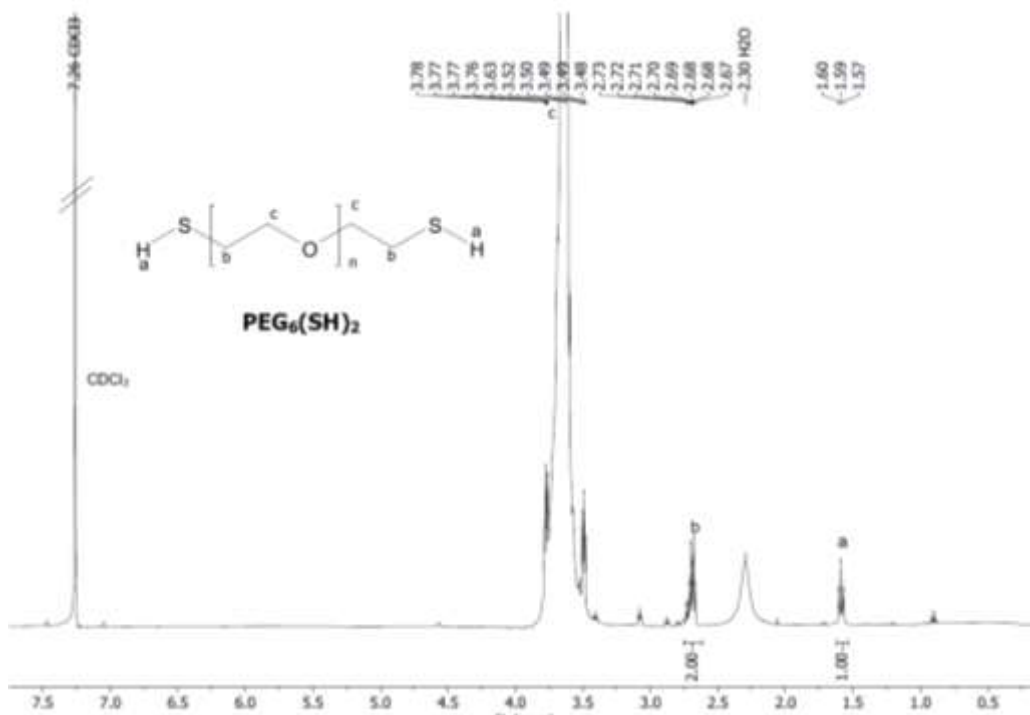
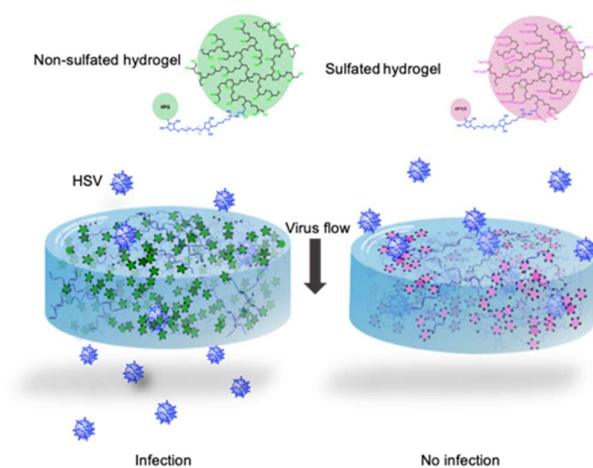


Figure S 5. ^1H NMR (500 MHz, CDCl_3) of $\text{PEG}_6(\text{SH})_2$ 3c.

3.2 Scaffold Flexibility Controls Binding of Herpes Simplex Virus Type 1 with Sulfated Dendritic Polyglycerol Hydrogels Fabricated by Thiol-Maleimide Click Reaction

“Herpes Simplex Virus -1 (HSV) with a diameter of 155 - 240 nm uses electrostatic interactions to bind with the heparan sulfate present on the cell surface to initiate infection. In this work, we aim to deter the initial contact using polysulfate-functionalized hydrogels. The hydrogels provide a large contact surface area for viral interaction and sulfated hydrogels are good mimics for the native heparan sulfate. In this work, we have synthesized hydrogels of different often prescribed to reduce the frequency, duration, and severity of infection.



HSV-1 uses its surface glycoprotein to bind to heparan sulfate proteoglycans (HSPG) to start the infection in host cells. Because the virus entry is primarily driven by electrostatic flexibilities, determined by rheology. We prepared gels within an elastic modulus range of 10 – 1119 Pa with a mesh size of 80 – 15 nm, respectively. The virus binding studies carried out with the plaque assay show that the most flexible sulfated hydrogel performs the best in binding HSV viruses. These studies prove that polysulfated hydrogels are a viable option as HSV-1 antiviral compounds. Furthermore, such hydrogel networks are also physically similar to naturally occurring mucus gels and therefore may be used as mucus substitutes.”

This work was published in:

Thongrom, B.; **Sharma, A.**; Nie, C.; Quaas, E.; Raue, M.; Bhatia, S.; Haag, R. Scaffold Flexibility Controls Binding of Herpes Simplex Virus Type 1 with Sulfated Dendritic

Polyglycerol Hydrogels Fabricated by Thiol-Maleimide Click Reaction, *Macromolecular Bioscience*. **2022**, 22, 2100507.

<https://doi.org/10.1002/mabi.202100507>

Author contributions

Conception, and analysis of hydrogel components and hydrogels, rheological analysis of hydrogels. Writing, editing, and revision of manuscript, and making all graphics, and galley proof.

Scaffold Flexibility Controls Binding of Herpes Simplex Virus Type 1 with Sulfated Dendritic Polyglycerol Hydrogels Fabricated by Thiol-Maleimide Click Reaction

Boonya Thongrom, Antara Sharma, Chuanxiong Nie, Elisa Quaas, Marwin Raue, Sumati Bhatia,* and Rainer Haag*

Herpes Simplex Virus-1 (HSV-1) with a diameter of 155–240 nm uses electrostatic interactions to bind with the heparan sulfate present on the cell surface to initiate infection. In this work, the initial contact using polysulfate-functionalized hydrogels is aimed to deter. The hydrogels provide a large contact surface area for viral interaction and sulfated hydrogels are good mimics for the native heparan sulfate. In this work, hydrogels of different flexibilities are synthesized, determined by rheology. Gels are prepared within an elastic modulus range of 10–1119 Pa with a mesh size of 80–15 nm, respectively. The virus binding studies carried out with the plaque assay show that the most flexible sulfated hydrogel performs the best in binding HSV viruses. These studies prove that polysulfated hydrogels are a viable option as HSV-1 antiviral compounds. Furthermore, such hydrogel networks are also physically similar to naturally occurring mucus gels and therefore may be used as mucus substitutes.

HSV-1 uses its surface glycoprotein to bind to heparan sulfate proteoglycans (HSPG) to start the infection in host cells. Because the virus entry is primarily driven by electrostatic interactions, many drug designs have been inspired by the sulfate-dominant interactions.^[5] This deals with the problem on the long-term scale, disabling the formation of a virus-reservoir. Previously, Dey et al. fabricated sulfated dendritic polyglycerol (dPGS) nanogels as synthetic heparan sulfate mimics of a range of flexibilities as well as sizes.^[6] While all the nanogels were successful in inhibiting virus, the more flexible nanogels showed higher efficacy. Recently, our group has also published a new series of dendronized linear polysulfates as multivalent inhibitors to prevent HSV entry. However, in this case, highly flexible sulfated linear polyglycerol (IPGS)

was compared with more rigid sulfated architectures. Here also, the flexible IPGS was highly successful in intervening with the infection process, showing 295 times greater efficacy than heparin.^[7]


Recently, hydrogels are emerging as important platforms for multiple applications in the biomedical arena.^[8,9] Hydrogels are formed when macromolecules crosslink by physical or chemical means to form water-swollen networks. They have a number of characteristics which make them particularly attractive for biomedical applications. For example, due to their structural similarity to living tissues, they are highly biocompatible; moreover they are able to provide low interfacial tension with the nearby tissues in the body.^[10] They can also be non-invasively injected and fill in any required shape at the injection point.^[11] In addition to other biomedical applications, they have been used in virus-trapping and containment. Zhang et al. used glycosylated hydrogels to trap the Norovirus.^[12] Importantly, mucus hydrogels within the body, function in a similar way providing the first line of defense against pathogenic attack.^[13]

The role of scaffold flexibility for virus binding is very important, yet, macroscopic materials with different stiffness have not been studied for this application. In this paper, we extend the understanding of scaffold flexibility with polyglycerol-based hydrogels. We have designed sulfated hydrogels by a click conjugation approach. Here we have employed polyethylene gly-

1. Introduction

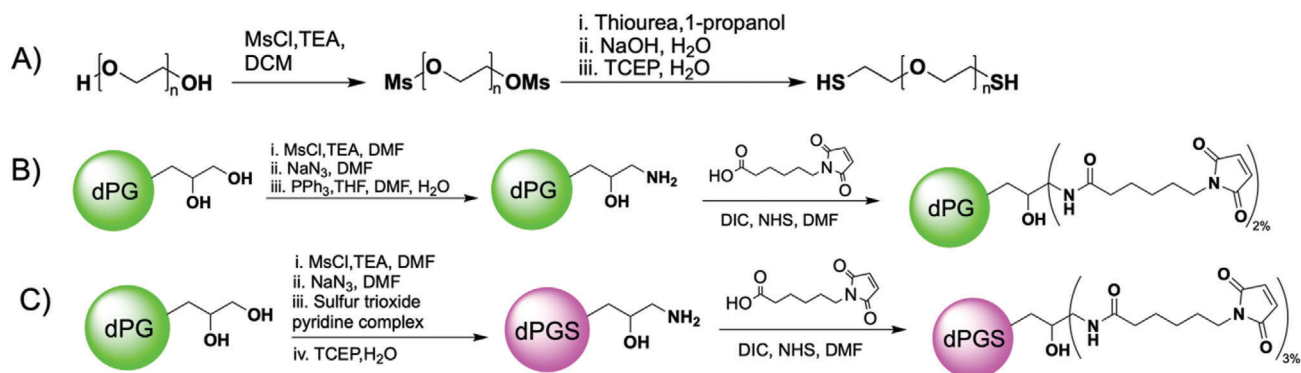
Herpes Simplex Virus-1 (HSV-1) is a part of the Herpesviridae family, which is known to target oral, pharyngeal, and genitals.^[1] The virus is supported by a wide range of hosts, including humans. HSV-1 has a high seroprevalence of $\approx 80\%$ in adults. It is an enveloped virus around 155–240 nm in diameter.^[1,2] HSV-1 can be a cause of morbidity and mortality in newborns and immunocompromised patients, and antivirals such as acyclovir (ACV) and ganciclovir are often prescribed to reduce the frequency, duration, and severity of infection.^[3,4]

B. Thongrom, A. Sharma, C. Nie, E. Quaas, M. Raue, S. Bhatia, R. Haag
 Institut für Chemie und Biochemie
 Freie Universität Berlin
 Takustraße 3, Berlin 14195, Germany
 E-mail: sumati@zedat.fu-berlin.de; haag@chemie.fu-berlin.de

 The ORCID identification number(s) for the author(s) of this article can be found under <https://doi.org/10.1002/mabi.202100507>

© 2022 The Authors. Macromolecular Bioscience published by Wiley-VCH GmbH. This is an open access article under the terms of the Creative Commons Attribution-NonCommercial License, which permits use, distribution and reproduction in any medium, provided the original work is properly cited and is not used for commercial purposes.

DOI: 10.1002/mabi.202100507



Scheme 1. Synthesis of A) PEG dithiol, B) dPG maleimide, C) dPGS maleimide.

col (PEG) dithiol and (dendritic polyglycerol sulfate) dPGS-maleimide as the macromolecular components to linear and crosslinking units, respectively. This ball-and-chain type system forms a hydrogel as a Michael-click reaction occurs between the linear PEG-dithiol and the maleimides decorating dPGs. These new sulfated hydrogels were studied by rheology and could prevent viral infection depending on the scaffold flexibility. The large surface area and highly negatively charged system allow virus binding by multivalent polyelectrolyte interactions.

2. Discussion

2.1. Design of Gel Components

We hypothesized that a ball-and-chain type polymers would further interconnect and crosslink to form a hydrogel matrix. Thus, two gel components need to be synthesized with the perspective of a facile and quick hydrogel reaction recipe. Hence, while the linear PEG “chain” component was functionalized with thiol groups, the crosslinking dPG and dPGS units were both decorated with maleimide functional groups such that the Michael addition click reaction would occur between the thiol and the maleimide units, respectively. Furthermore, in order to quantify the effect of the sulfate groups as well as to observe the individual efficacy of the matrix itself, hydrogels without sulfate, i.e., with PEG and dPG were also synthesized. These gels were then compared in separate rheology and virus binding assays.

2.1.1. Synthesis of PEG Dithiol

Commercially available PEG with a molecular weight of 6 kDa was first mesylated and subsequently purified by precipitation resulting in $\text{PEG}(\text{OMs})_2$ in the form of a white powder. In order to synthesize PEG dithiol, $\text{PEG}(\text{OMs})_2$ was first allowed to react with dithiourea, wherein the intermediate diisothiuronium PEG was formed. This was immediately followed by basic hydrolysis to finally obtain PEG dithiol, $\text{PEG}(\text{SH})_2$. Tris(2-carboxyethyl) phosphine (TCEP) was added as reducing agent at this point, and purification thereafter by extraction and precipitation resulted in pure $\text{PEG}(\text{SH})_2$, as confirmed by ^1H NMR spectroscopy. The synthesis is depicted in **Scheme 1A**.

2.1.2. Synthesis of dPG Maleimide

dPG was synthesized following the procedure in literature: dPG maleimide was synthesized in four steps. First of all, dPG was mesylated. To the mesylated product, sodium azide was added to form dPGN_3 , following a substitution reaction. The resulting mixture containing the product was purified by dialysis. dPG amine was synthesized by the reduction of dPGN_3 with triphenylphosphine (TPP). Dichloromethane (DCM) wash and dialysis of the crude product resulted in pure dPGNH_2 . This was corroborated by ^1H NMR and ^{13}C NMR spectroscopy results. Finally, the amine group was reacted with the active (*N*-hydroxy Succinimid)NHS ester formed by the reaction of NHS and *N,N*-Diisopropylcarbodiimide (DIC) resulting in the formation of dPG maleimide. Pure dPG maleimide was obtained by dialysis of the crude product against water, confirmed thereafter by ^1H NMR studies. The synthetic steps are shown in **Scheme 1B**.

2.1.3. Synthesis of dPGS Maleimide

dPGS maleimide was prepared in a similar fashion to dPG maleimide, as depicted in **Scheme 1C**. dPGN_3 was synthesized in the same manner as mentioned above. To the same reaction mixture, sulfur trioxide pyridine complex was added and subsequently the crude mixture was first neutralized and then purified by dialyzing it against first brine, followed by water. The obtained product was then reduced and purified by dialysis. The consequent dried dPGS amine was obtained in the form of a yellow powder, the purity of which was determined by ^1H NMR spectroscopy. Afterward, dPG maleimide was synthesized by the reaction of dPGS amine with NHS and DIC. After purification by dialysis against water, the final product was obtained as a pale yellow powder. The synthetic purity and 84% degree of sulfation were confirmed by ^1H NMR spectroscopy and elemental analysis, respectively.

2.2. Synthesis of Gels

Two types of gel series were constructed. dPG maleimide gels, i.e., gels represented by “HG” were created from PEG dithiol and dPG maleimide. Further, to identify the importance of the decorating functional groups, dPGS maleimide gels (represented by

Table 1. Composition of different non-sulfated (HG) and sulfated (HGS) gel types depicting the amounts and ratios of the gel components (10% w/v PEG, 16% w/v dPG, and 10% w/v dPGS) used per 100 μL volume.

Gel code	Gel type	PEG:dPG/dPGS Mol ratio	Gel components volume [μL]		Total gel volume [μL]	Gel concentration [% w/v]
			PEG	dPG/dPGS		
HG 8%	dPG maleimide	2.5:1	48	20	100	8.0
HG 7%	dPG maleimide	2.5:1	42	17.5	100	7.0
HG 6%	dPG maleimide	2.5:1	36	15	100	6.0
HG 5%	dPG maleimide	2.5:1	30	12.5	100	5.0
HG 4%	dPG maleimide	2.5:1	24	10	100	4.0
HGS 8%	dPGS maleimide	2.5:1	34.3	45.7	100	8.0
HGS 6%	dPGS maleimide	2.5:1	25.8	34.2	100	6.0
HGS 5%	dPGS maleimide	2.5:1	21.5	28.5	100	5.0
HGS 4%	dPGS maleimide	2.5:1	17.2	22.8	100	4.0
HGS 3%	dPGS maleimide	2.5:1	12.9	17.1	100	3.0

“HGS”) were synthesized from the reaction between PEG dithiol and dPGS maleimide. The synthetic procedure was rapid and simple: the Phosphate buffer saline (PBS) solution of two gel components as well as an additional PBS were vortexed together so as to amount to a total of 100 μL gel volume in the ratios indicated in **Table 1**. Further, the gels at 37 $^{\circ}\text{C}$ were allowed to swell for 1 h, and oscillatory rheology experiments were carried out to determine their mechanical properties and pore sizes. The ratio of the two reacting components in this case, PEG-dithiol and dPG maleimide was maintained to be the same as 2.5:1, respectively, in every gel decreasing the overall gel components concentration.

Increasing dilution of gel components allowed a decrease in the number of crosslinks, and thus gel elasticity decreased and conversely its viscosity increased, as can also be clearly visualized in **Figure 1B–E**. Initially, with an overall gel concentration of 8%, the rigidity of the HGS 8% gels (**Figure 1B**) is very high. For this reason, it maintains a quite rigid structure which does not flow within the measured time period.^[14] Spinnability or the ability of thread-formation is a unique property arising from non-Newtonian flow, where the existence of both elastic and viscous properties is an important prerequisite. As such, spinnability increases in viscoelastic compounds with an increase in viscosity.^[14] As the gel concentration decreases from 5% to 3% (**Figure 1C–E**), their viscosity increases. Gel HGS 5% (**Figure 1C**) is also quite elastic as it hardly flows when pressure is applied and quickly recoils to its previous position as pressure is removed. It does not display spinnability suggesting a very low viscous characteristic as well. Conversely gels HGS 4% and HGS 3% (**Figure 1D,E**, respectively), are both soft flowable gels. They are not able to maintain their conformation with the increasing pressure. In fact HGS 3% appears to be a viscous liquid; however, as evidenced by its very high spinnability, it maintains some elasticity and thus its network structure as well.

2.3. Oscillatory Rheology

A substance’s viscoelastic properties are essentially indicative of its mechanical properties and can be determined by oscillatory rheology experiments. A strain-sweep test was carried out over

the entire series to establish the linear viscoelastic region (LVE) so that consecutive oscillatory rheology experiments would be conducted in this region. These viscoelastic experiments allowed the deduction of the storage modulus, G' and the loss modulus, G'' as a function of the radial frequency, ω . Moreover, the experiments were conducted at 25 $^{\circ}\text{C}$ and at the physiological temperature 37 $^{\circ}\text{C}$, where the viscoelastic properties of the swollen gels were measured as well. The results of the experiments at 37 $^{\circ}\text{C}$ are shown in **Figure 2**, while the results of the swollen gels are shown in **Figure 3**.

The rheological behavior of the non-sulfated gels “HG” is shown in **Figures 2A and 3A** at 37 $^{\circ}\text{C}$ in the initial and swollen states after 1-h incubation with excess water, respectively. All the gels displayed notable elastic-dominated behavior, thus providing ample proof of the stability of the crosslinks. In **Figure S8** (Supporting Information), the behavior of these gels at 25 $^{\circ}\text{C}$ can be seen. The difference caused by the increase in temperature to the physiological temperature is negligible. Interestingly, the swollen state causes a notable difference in the viscoelastic behavior in all these gels. As can be seen in **Table 2**, there is a general trend of decrease in the elastic character of this gel as the gels become more swollen.

The viscoelastic behavior of the sulfated “HGS” gels at 37 $^{\circ}\text{C}$ is shown in **Figures 2B and 3B** while their behavior at 25 $^{\circ}\text{C}$ can be seen in **Figure S9** (Supporting Information). All gels in this series can be seen to behave in a similar fashion. An increase in both moduli is seen for all cases with increasing frequency, as expected. Further, as with the HG series, all HGS gels are elastic-dominated, indicating the existence of permanent crosslinking in a solid gel matrix. In comparison to the non-sulfated HGs, the general trend of elasticity was more toward the lower end. This can be explained by the electrostatic repulsion present within these gels contributed by the sulfate groups. An increase in temperature from 25 to 37 $^{\circ}\text{C}$ did not affect the rheological properties in this case. However, a significant decrease was observed in the elastic modulus of all the sulfated gels when they were in the swollen state, as can be seen in **Table 2**. This occurs due to the increase in the general pore size with swelling and this affect is particularly pronounced due to the high-water attraction of charged sulfate groups, exemplified by gel HGS 4% wherein more than 2

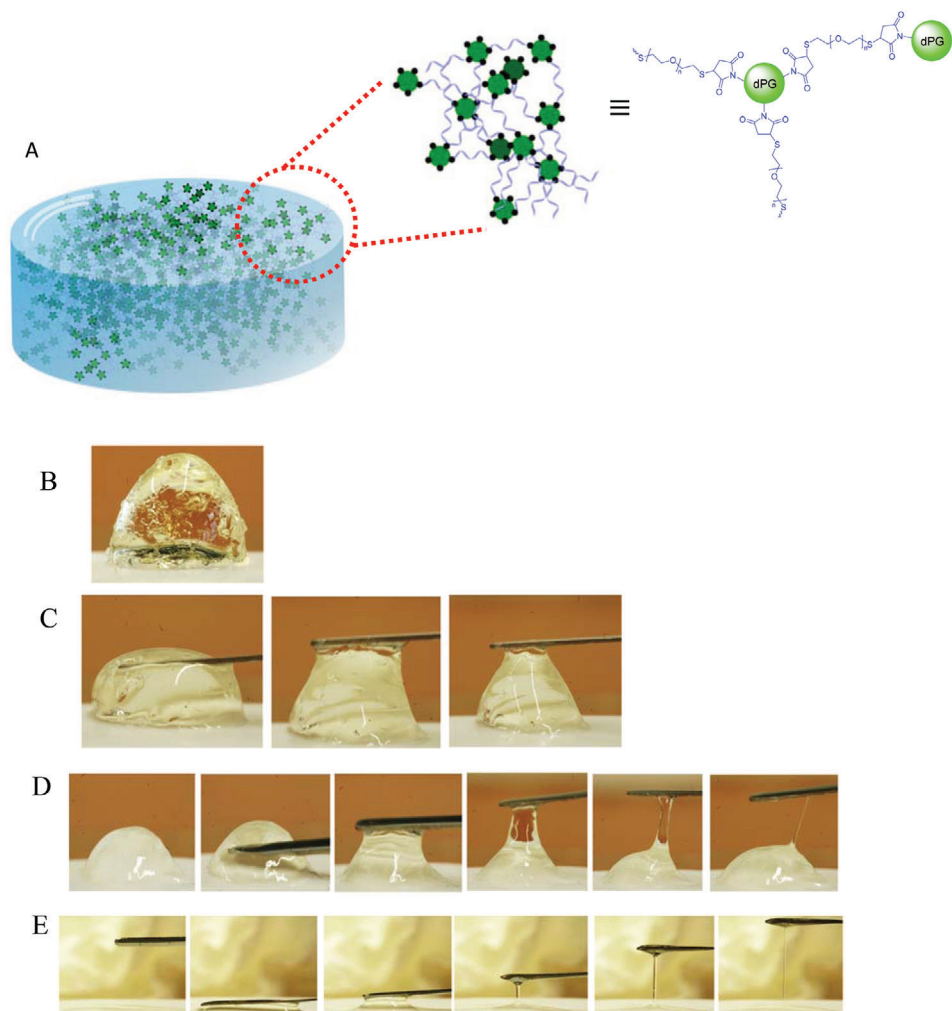


Figure 1. A) Pictorial representation of the hydrogel and its internal matrix structure (inset). The dPG units (green) are decorated with maleimide groups (black) which then react with PEG dithiol (blue) in a Michael-click reaction to result in the formation of the hydrogel. Sulfated gels B) HGS 8%, C) HGS 5%, D) HGS 4%, E) HGS 3%. Each gel displays a clear difference in its physical properties, which are dependent upon its rheological properties. Gel HGS 8% maintains a firm structure, while the viscous trait dominates in gel HGS 3%.

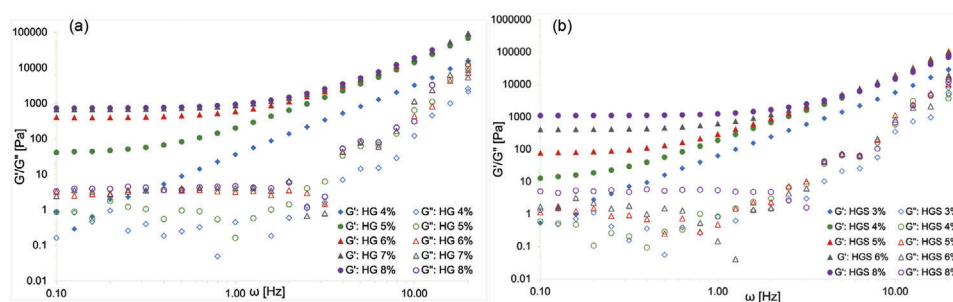


Figure 2. Storage (G') and loss (G'') moduli as a function of radial frequency (ω) of A) HG gels and B) HGS gels at 37 °C, for samples in which the gel component ratios were varied systematically.

times decrease of the elastic modulus was observed in the swollen state comparison to the initial state at 37 °C. Moreover, the change in the viscoelastic properties is more distinct in this case in comparison to the non-sulfated gels. Out of all the sulfated hydrogels, the HGS 3% was the most viscous, with its shear modulus in the

non-swollen state being only 10 Pa. The rheological behavior of the non-swollen HGS 3% network was consistent with the rest of the hydrogels in the series. For most part the elastic modulus remained higher than the viscous modulus, except for in the lower frequency range in the very beginning, as shown in Figure 2B.

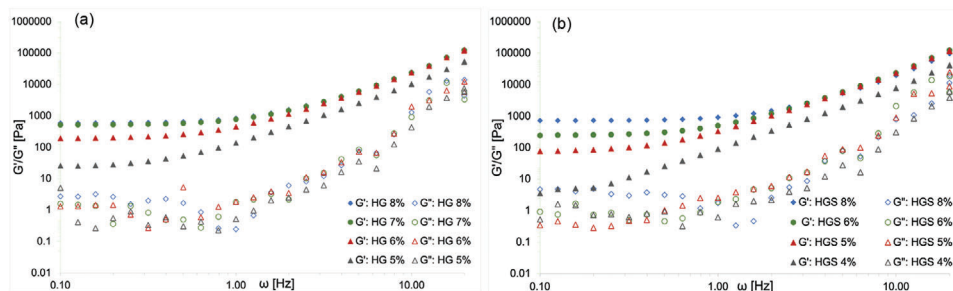


Figure 3. Storage (G') and loss (G'') moduli as a function of radial frequency (ω) of A) swollen HG gels and B) swollen HGS gels at 37 °C, for samples in which the gel component ratios were varied systematically. Gels HG 4% and HGS 3% could not be measured in a swollen state as they were too viscous and miscible when more water was introduced.

Table 2. Shear modulus G_0 and estimated mesh size of hydrogel series HG and HGS in the initial and swollen states at 37 °C.

Hydrogel ^{a)}	37 °C (Initial state)		37 °C (Swollen state)	
	Shear modulus [G_0 Pa ⁻¹]	Mesh size [ξ nm ⁻¹]	Shear modulus [G_0 Pa ⁻¹]	Mesh size [ξ nm ⁻¹]
HG 4%	5	91	–	–
HG 5%	67	39	43	46
HG 6%	433	21	234	26
HG 7%	716	18	556	19
HG 8%	766	18	630	19
HGS 3%	10	76	–	–
HGS 4%	40	47	17	62
HGS 5%	111	33	118	33
HGS 6%	442	21	283	24
HGS 8%	1119	15	748	18

^{a)} Initial state refers to the hydrogel as soon as it forms after mixing, and swollen state refers to the hydrogel after 1 h of incubation with excess water.

The existence of a stable network was also seen by spinnability. As with all other gels in this series, it is expected that its shear modulus would decrease further with swelling. For this reason, its behavior in the swollen state could not be determined, as the viscosity of the gel was quite high and therefore became miscible on the addition of PBS. However, the nature of the crosslinks remained stable as the swollen gels showed spinnability as well. In fact, the HGS 3% also show some similarities to naturally occurring gel mucus. As their shear modulus in the swollen state would be lower than 10 Pa, they would be in the approximate shear modulus range of healthy lung mucus, which is about 1–2 Pa.^[15] Moreover, lung mucus also exhibits a similar rheological pattern, maintaining a plateau at lower frequencies, and then an increase above 10 Hz.

The plateau modulus is the frequency range wherein an overall linear behavior of the storage and loss moduli is seen. Materials like hydrogels possess a complex rheological profile owing to the presence of a defined internal structure. While the macrorheology, or its bulk rheological properties such as viscoelasticity govern its functions such as lubrication and interaction with surfaces, its microrheological properties determine the diffusion behavior of small components like pathogens or drugs, within the

hydrogel matrix. While a larger mesh size allows free diffusion of a smaller component, when the two are comparable, steric hindrance on movement becomes significant. Thus precise control over the mesh size is pertinent to its application.^[16] In order to calculate the mesh size, the G' value at 0.3 Hz frequency was chosen and then substituted in the simplified equation $G' = kT/\xi^3$, where k is the Boltzmann constant, T is the temperature, and ξ is the mesh size.^[17–19] As a rule, mesh sizes increase as the crosslinking density is decreased.^[20] The lowest mesh sizes would therefore be predicted as corresponding to the least elastic hydrogel. Indeed, among the initially formed sulfated and non-sulfated hydrogel HG 4% and HGS 3% had the largest mesh size at ≈ 91 and 76 nm, respectively owing to the low crosslinking density. It was found that HSV measuring 180 nm in size were slowed down in mucus with mesh size of ≈ 100 nm, with up to a 1000-fold decrease in compared to water.^[21] The mesh size of the sulfated HGS 3% and 4% gels approaches this and can therefore be considered as suitable candidates for hindering HSV.

2.4. Cytotoxicity Studies

The cytotoxicity tests of gel components were performed against different cell types with CCK-8 kit. The Vero E6 (Figure 4A) was used, generally applied for infection assays and virus propagation studies. Moreover, the human lung cell lines A549 and HBE were also employed to diversify the study (Figure 4B,C, respectively). A slight decrease in the cell viability was observed with the addition of sulfated compounds, as expected. A high tolerance of the gel components for all the cell lines was observed, and the tolerance of dPGS decreased only at the concentration >1 mg mL⁻¹. dPG maleimide showed high cell viability throughout the tested range for all cell lines. A549, Vero E6, as well as the HeLa cell lines were treated with PEG dithiol and a high tolerance was noted in every case. These results are shown in Figure S10 (Supporting Information). Overall, all the experiments proved a high tolerance for all the gel components involved rendering them safe to be applied for future treatments.

2.5. Binding of HSV

The HSV-1 binding of the hydrogels was established by plaque reduction assays. For this purpose, the hydrogel was initially incubated with the virus solution with moderate shaking for 1 h.

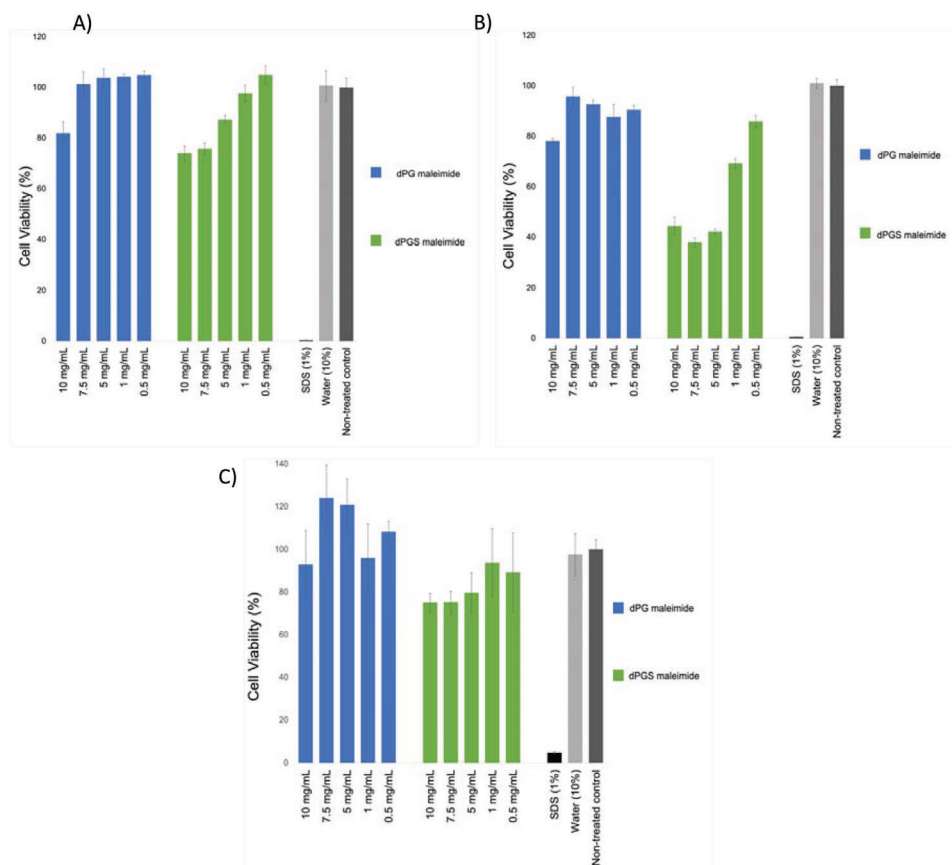


Figure 4. Cytotoxicity tests were conducted for the components of both hydrogel series, dPG-maleimide and dPGS-maleimide, as shown in A) Vero-E6 cell line, B) A549 cell line, and C) HBE cell line. For each case, the presence of sulfate groups on the gel negatively affected the cell viability results.

Afterward, the number of viral particles in the supernatant is titrated by plaque assays on Vero E6 cells. The binding with virus was revealed by reduced virus titer in the supernatant as shown in **Figure 5**.

We did not observe any significant reduction in the HSV titer with the non-sulfated control gels or gel component dPG-maleimide. The sulfated gel types (HGS 8%, HGS 6%, HGS 5%, HGS 4%, HGS 3%) showed much higher binding abilities of up to 30 times higher than their non-sulfated counterparts. HSV viruses electrostatically bind with heparan sulfate on the host cells through their surface glycoprotein. Due to the presence of sulfate groups in the HGS gels, virus binding became significantly more efficacious in comparison to HG gels. This was observed not only for every hydrogel but also for the individual sulfated and non-sulfated gel components (dPG-maleimide and dPGS-maleimide). However, as the gels HGS 8%–5% are quite stiff, their sulfate groups are less exposed even after swelling, and thus do not interact with as many HSV particles as the softer gels would. This has a negative effect on their binding performance, as can be seen in **Figure 5**. The effects of network structure on virus binding were revealed by the comparison among sulfated hydrogels with different stiffness. The more viscous gel HGS 3% being slightly better than the HGS 4%, showed a higher HSV interaction than the more elastic gels HGS 5%–8% in the series. The remaining virus titer in the supernatant treated with HGS

3% gel was 560 PFU mL⁻¹ whereas for HGS 8%, the remaining virus titer was still 1483 PFU mL⁻¹. The loosely bound network in the more flexible sulfated hydrogels might allow the exposition of more sulfate groups while binding with the virus and thus is definitely a plus for HSV binding and inhibition.

Sulfated hydrogels HGS were compared with the 2.3×10^{-3} M sulfated gel component dPGS-maleimide ($\approx 4.6\%$ w/v). As can be seen in Table S1 (Supporting Information), the concentration of sulfated gel component in the HGS 4% ($\approx 1.1 \times 10^{-3}$ M dPGS) and HGS 3% ($\approx 0.9 \times 10^{-3}$ M dPGS) are 2–2.5 times lower and all sulfate groups are not fully exposed because of 3D network formation, still the performance of these gel types were slightly higher than the dPGS-maleimide itself because of large contact surface area with the virus and high flexibility.

Thus, sulfated gels proved to be the most compelling candidates for HSV-1 binding. Moreover, the network structure also played a significant role in this study, where higher flexibility allowed higher binding capacity.

3. Conclusion

This study demonstrates the flexibility of a sulfated hydrogels network as an important parameter for its ability to bind HSV-1 virus. In order to deduce the best candidate, polyether-based hydrogels were prepared using thiol-maleimide click chemistry

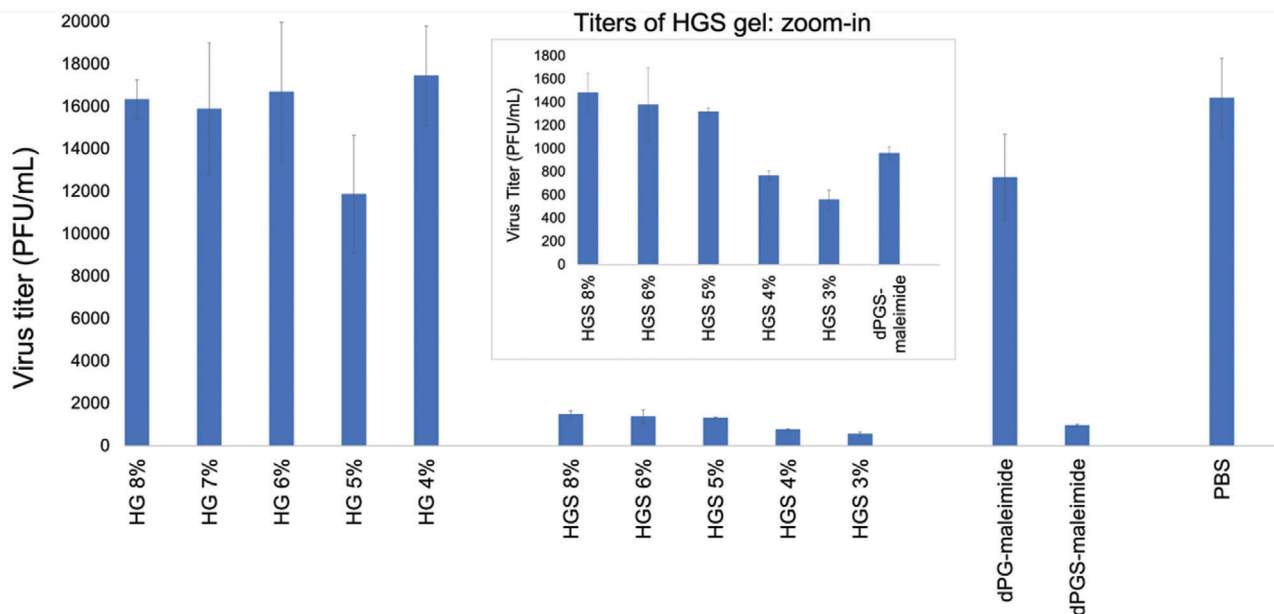


Figure 5. Efficacy of HSV-1 binding by hydrogels. The figure characterizes the virus titers after treatment with various samples. Inset: virus titers of gel series HGS, as well as dPGS-maleimide. Values are expressed as mean \pm SD, $n = 3$. dPGS-maleimide (5% w/v) and dPG-maleimide (8% w/v) were applied in the HSV binding assay.

based on dPG-maleimide as a crosslinker and PEG-dithiol as the linear component. Two sets of hydrogels were compared, distinguished by the presence of hydroxyl groups in one series and sulfate groups in the other series. Furthermore, hydrogels were prepared within each series such that their flexibility was tuned reduction of the linear component. A range of flexibilities with shear moduli between 1 and 1200 Pa were achieved. The presence of sulfate groups on hydrogels is crucial for HSV binding, rheology dependent parameters also played an important role. The sulfated hydrogels show 10–30 times stronger HSV binding than the non-sulfated controls. Furthermore, gels followed a general trend of having higher virus titer reduction as their flexibilities increased. Notably, HGS 3% proved to be the most suitable virus-binding candidate, showing an even higher binding capacity than the highly sulfated dendritic crosslinker dPGS-maleimide. These polysulfated hydrogel networks can mimic the antiviral function of mucus and may find future applications in this area.

4. Experimental Section

Materials: All chemicals were purchased from Merck KGaA, Darmstadt, Germany and/or its affiliates and used without any further purification, unless otherwise stated. The solvents used herein, i.e., diethyl ether (100%) and *N,N*-dimethylformamide (99.8%) were bought from VWR chemicals and Acros Organics, respectively, while DCM (99%) and ethyl acetate were both obtained from Fischer Scientific. Sodium hydroxide in the form of pellets, as well as in a 99.5% solution, was also procured from Fischer Scientific. Triphenylphosphine (99%) was purchased from Alfa Aesar. dPG of ≈ 6 kDa average molecular weight was prepared as previously reported^[22–24] with the improved method.^[25] For purification carried out with dialysis, Spectra Por dialysis tubing (MWCO = 2000 g mol⁻¹) (Carl Roth GmbH, Karlsruhe, Germany).

Cell viability assays were performed with a CCK-8 Kit from Sigma Aldrich according to the manufacturing instructions. A549, HBE, HeLa, and Vero

E6 cells were obtained from Leibniz-Institut DSMZ—Deutsche Sammlung von Mikroorganismen und Zellkulturen GmbH and cultured in DMEM supplemented with 10% (v/v) FBS, 100 U mL⁻¹ penicillin and 100 μ g mL⁻¹ streptomycin.

Instrumentals: The Jeol Eclipse 500 MHz (Tokyo, Japan) or a Bruker AVANCE III 700 MHz spectrometer (Billerica, MA, USA) instruments were used to measure all the NMR spectra of all the compounds (¹H and ¹³C) reported here were recorded at 300 K. Chemical shifts δ were reported in ppm and the deuterated solvent peak was used as a standard. Vario EL CHNS element analyzer (Elementar Analysensysteme GmbH (Langensfeld, Germany)) was used to carry out the elemental analysis of all relevant compounds reported in this work. All the rheology data reported here was measured and characterized by the Kinexus rheometer (NETZSCH GmbH, Selb, Germany). A parallel plate, 8 mm in diameter was used for all the measurements, with the average normal force maintained at ≈ 0.1 N at 25 and 37 °C. The data were analyzed by an oscillatory frequency sweep strain-controlled test with 1% strain (which is obtained from a linear viscoelastic range of an amplitude sweep test) and the reported storage modulus (G') of a rigid hydrogel were picked at 0.3 Hz.

Synthesis of Gel Components: PEG(OMs)₂: Dried PEG (20 g, 3.3 mmol, 1 eq., 6 kDa) was dissolved in a dichloromethane (DCM) solution (100 mL), and subsequently cooled down in an ice bath. Then triethylamine (TEA, 2.77 mL, 20 mmol, 6 eq.) was added to the solution, followed by the dropwise addition of methanesulfonyl chloride (1.03 mL, 13.3 mmol, 4 eq.). The reaction was allowed to run overnight. Afterward, the crude product was purified; the DCM layer was washed thrice with brine before drying it with Na₂SO₄. It was then precipitated in cooled diethyl ether. The purified precipitate was then allowed to dry overnight under vacuum, finally resulting in a white powder with 95% isolated yield. ¹H NMR: (500 MHz, CDCl₃, δ (ppm)): 3.07 (3H, s), 3.48–3.78 (m), 4.37 (2H, t) (Figure S1, Supporting Information).

Synthesis of PEG Dithiol (PEG(SH)₂): PEG(OMs)₂ (19 g, 3.2 mmol, 1 eq.) and thiourea (1.02 g, 13.3 mmol, 4 eq.) were added to a solution of 1-propanol. The solution was refluxed overnight to obtain diisothiuronium PEG as the intermediate product. Without any further purification, 1-propanol was immediately removed from the intermediate, followed by the addition of NaOH (0.53 g, 13.3 mmol, 4 eq.) and water (100 mL). The reaction mixture was allowed to reflux overnight. Afterward, tris(2-

carboxyethyl)phosphine (TCEP, 1.67 g, 6.7 mmol, 2 eq.) was added to the mixture and stirred for 2 h prior to the purification. To purify, NaCl was added to the mixture until the point of saturation, followed by the precipitation of the product was extracted three times into DCM. The DCM layer was then dried by Na_2SO_4 , after which it was precipitated in cooled diethyl ether. The precipitate was dried in vacuo overnight. PEG dithiol was obtained as a pale yellowish powder in 88% isolated yield. ^1H NMR (500 MHz, CDCl_3 , δ (ppm)): 1.59 (1H, t), 2.69 (2H, quat), 3.48–3.78 (m). Elemental analysis; N = 0.13; C = 54.24; S = 2.02; H = 8.47 (Figure S2, Supporting Information).

Synthesis of dPGNH₂: Dried dPG (5 g, 0.5 mmol, 1 eq.) and TEA (0.7 mL, 5 mmol, 10 eq.) were added to a solution of *N,N*-dimethyl formamide (DMF, 50 mL) and the reaction mixture was subsequently cooled using an ice bath. Methanesulfonyl chloride (0.31 mL, 4 mmol, 8 eq. to target roughly 5% mesyl groups on dPG) was added dropwise to the stirring mixture. The reaction mixture was then stirred overnight. NaN_3 (0.65 g, 10 mmol, 20 eq.) was then added to the reaction flask and thereafter heated at 60 °C for 2 days. Afterward, the crude mixture was purified in water by dialysis (MWCO = 2 kDa) for 2 days. After purification, water was first removed from the flask and DMF (40 mL) was then added to it. Separately a tetrahydrofuran (THF, 30 mL) solution of triphenylphosphine (TPP, 3.28 g, 12.5 mmol, 25 eq.) was prepared in another flask. The contents of the latter were then added gradually to the former DMF solution flask. The reaction flask was allowed to stir overnight, with additional care that phase separation did not take place. Afterward, water (5 mL) was added to the reaction mixture and stirred again overnight at room temperature overnight. Finally, the product was purified by a DCM wash, repeated three times and later dialyzed against water (MWCO = 2 kDa) for 2 days. The product obtained was then dried and collected as a pale yellowish liquid with a honey-like consistency in 70% isolated yield. ^1H NMR (700 MHz, D_2O , δ (ppm)): 0.90 (3H, broad s, initiator backbone), 1.39 (2H, broad s, initiator backbone), 2.73–4.02 (m, backbone repeating units), (Figure S3, Supporting Information). ^{13}C NMR (700 MHz, D_2O , δ (ppm)): 43.07 (s, 2nd carbon next to amino group), 60.89–79.76 (m, polymer backbone) (Figure S4, Supporting Information).

Synthesis of dPG Maleimide: dPGNH₂ (1.4 g, 0.14 mmol, 1 eq.), 6-maleimidoheptanoic acid (0.15 g, 0.7 mmol, 5 eq.), and *N*-hydroxysuccinimide (0.13 g, 1.12 mmol, 8 eq.) were added to DMF (20 mL). *N,N'*-diisopropylcarbodiimide (DIC, 0.17 mL, 1.12 mmol, 8 eq.) was then added to the mixture and it was allowed to stir overnight at room temperature. The crude mixture was afterward subjected to dialysis against water (MWCO = 2 kDa) for 2 days. The purified product was later collected and kept in an aqueous solution with 85% isolated yield. ^1H NMR (700 MHz, D_2O , δ (ppm)): 0.92 (3H, broad s, initiator backbone), 1.32 (2H, broad s), 1.61 (4H, broad s), 2.28 (2H, broad s), 3.26–4.04 (m, backbone repeating units), 6.89 (2H, broad s) (Figure S5, Supporting Information).

Synthesis of dPGSNH₂: An initial mixture was made by the addition of dPG (6 g, 0.6 mmol, 1 eq.) and TEA (0.83 mL, 6 mmol, 10 eq.) were added to DMF (60 mL). The mixture was then cooled down with the help of an ice bath. Subsequently methanesulfonyl chloride (0.37 mL, 4.8 mmol, 8 eq.) was added dropwise to the stirring solution, which was then allowed to stir overnight. Following the addition of NaN_3 (0.62 g, 9.6 mmol, 16 eq.), the reaction mixture was allowed to stir as it was heated to 60 °C. After 2 days, sulfur trioxide pyridine complex (23.87 g, 150 mmol, 250 eq.) was added to the mixture and then allowed to run for 2 days at room temperature. The crude mixture was purified by first neutralizing the solution with NaOH and then dialyzing it first against brine, followed by water for 2 more days. Dialysis tubes with a 2 kDa molecular weight cut-off were used for both these cases. After purification, TCEP (1.38 g, 4.8 mmol, 8 eq.) was added to the aqueous solution and it was allowed to stir for 3 days. The crude mixture was then purified by dialysis against water (MWCO = 2 kDa) carried out for 2 days. Finally, the aqueous solution of the product was lyophilized overnight and collected as a solid pale yellow powder with 65% isolated yield with 4% as degree of sulfation. ^1H NMR (600 MHz, D_2O , δ (ppm)): 0.93 (3H, broad s, initiator backbone), 3.45–4.74 (m, backbone repeating units), elemental analysis: N 0.84, C 20.52, S 14.94, H 3.71 (Figure S6, Supporting Information).

Synthesis of dPGS Maleimide: 6-maleimidoheptanoic acid (0.07 g, 0.35 mmol, 7 eq.), and *N*-hydroxysuccinimide (0.05 g, 0.45 mmol, 9 eq.) were added to a solution of DMF (5 mL). This was followed by the addition of DIC (0.07 mL, 0.45 mmol, 9 eq.) and the mixture was stirred. After 30 min, the aqueous solution (5 mL) of dPGSNH₂ (1 g, 0.05 mmol, 1 eq.) was added to the reaction mixture and then allowed to stir overnight at room temperature. The crude product was purified by dialyzing the mixture against water with for 2 days (MWCO = 2 kDa). Finally, the aqueous solution was lyophilized and the final product was obtained as a solid, pale yellow powder in 87% isolated yield. ^1H NMR (700 MHz, D_2O , δ (ppm)): 0.94 (3H, broad s, initiator backbone), 1.30 (2H, broad s), 1.62 (4H, broad s), 2.26–2.29 (2H, broad s), 2.48–2.52 (2H, broad s), 3.40–4.75 (m, backbone repeating units), 6.93 (2H, broad s). Elemental analysis: N 1.95, C 21.75, S 16.23, H 3.62 (Figure S7, Supporting Information).

Cytotoxicity Studies: All cell experiments were conducted according to German genetic engineering laws and German biosafety guidelines in the laboratory (safety level 1). A549, HBE, and Vero E6 cells were seeded in a 96-well plate at a density of 5×10^4 cells mL^{-1} in 90 μL DMEM medium per well over night at 37 °C and 5% CO_2 . 10 μL of sample (solved in deionized water) were added in serial dilutions including positive (1% SDS) and negative controls (medium, H_2O) and incubated for another 24 h at 37 °C and 5% CO_2 . For background subtraction, also wells containing no cells but only sample were used. After 24 h incubation the CCK8 solution was added (10 μL well⁻¹) and absorbance (450 nm/650 nm) was measured after ≈ 3 h incubation of the dye using a Tecan plate reader (Infinite pro200, TECAN-reader Tecan Group Ltd.). Measurements were performed in triplicates and repeated three times. The cell viability was calculated by setting the non-treated control to 100% and the non-cell control to 0% after subtracting the background signal using the Excel software.

Virus Binding Assay: The samples were disinfected by UV-irradiation first for 30 min. Then they were incubated with HSV-1-GFP solution (300 μL , ≈ 200 000 PFU mL^{-1}) for 1 h with constant shaking. Afterward, the virus particles in the solution was titrated by a plaque assay on the VeroE6 line with DMEM (0.9% methylcellulose) as overlay medium. The plaques were counted after 2 days with a fluorescence microscope (Axio, Zeiss, Germany).

Supporting Information

Supporting Information is available from the Wiley Online Library or from the author.

Acknowledgements

The study was funded by the Helmholtz Graduate School of Macromolecular Bioscience, by the Deutsche Forschungsgemeinschaft (DFG, German Research Foundation)—SFB 1449—431232613; subprojects A01, B03, C04, Z02 and by the German Federal Ministry of Education and Research (82DZL0098B1). SB acknowledges the financial support by DFG-project number 458564133.

Open access funding enabled and organized by Projekt DEAL.

Conflict of Interest

The authors declare no conflict of interest.

Author Contributions

B.T. and A.S. contributed equally to this work.

Data Availability Statement

The data that support the findings of this study are available in the supplementary material of this article.

Keywords

click chemistry, HSV-1, hydrogel, polysulfates, rheology, virus binding

Received: December 13, 2021

Revised: January 24, 2022

Published online: February 23, 2022

-
- [1] P. G. Arduino, S. R. Porter, *J. Oral Pathol. Med.* **2008**, *37*, 107.
- [2] R. F. Laine, A. Albecka, S. Van De Linde, E. J. Rees, C. M. Crump, C. F. Kaminski, *Nat. Commun.* **2015**, *6*, 5980.
- [3] C. Dogramatzis, H. Waisner, M. Kalamvoki, *Viruses* **2021**, *13*, 17.
- [4] S. Crimi, L. Fiorillo, A. Bianchi, C. D'Amico, G. Amoroso, F. Gorassini, R. Mastroieni, S. Marino, C. Scoglio, F. Catalano, P. Campagna, S. Bocchieri, R. De Stefano, M. T. Fiorillo, M. Cicciù, *Viruses* **2019**, *11*, 463.
- [5] B. Ziem, W. Azab, M. F. Gholami, J. P. Rabe, N. Osterrieder, R. Haag, *Nanoscale* **2017**, *9*, 3774.
- [6] P. Dey, T. Bergmann, J. L. Cuellar-Camacho, S. Ehrmann, M. S. Chowdhury, M. Zhang, I. Dahmani, R. Haag, W. Azab, *ACS Nano* **2018**, *12*, 6429.
- [7] P. Pouyan, C. Nie, S. Bhatia, S. Wedepohl, K. Achazi, N. Osterrieder, R. Haag, *Biomacromolecules* **2021**, *22*, 1545.
- [8] H. Kamata, X. Li, U.-I. Chung, T. Sakai, *Adv. Healthcare Mater.* **2015**, *4*, 2360.
- [9] A. Herrmann, R. Haag, U. Schedler, *Adv. Healthcare Mater.* **2021**, *10*, 2100062.
- [10] B. Gyarmati, B. Vajna, Á. Némethy, K. László, A. Szilágyi, *Macromol. Biosci.* **2013**, *13*, 633.
- [11] T. J. Sanborn, P. B. Messersmith, A. E. Barron, *Biomaterials* **2002**, *23*, 2703.
- [12] Y. Zhang, Q. Yao, C. Xia, X. i Jiang, P. G. Wang, *ChemMedChem* **2006**, *1*, 1361.
- [13] R. Bansil, B. S. Turner, *Curr. Opin. Colloid Interface Sci.* **2006**, *11*, 164.
- [14] N. Tsurutaro, *Bull. Chem. Soc. Jpn.* **1952**, *25*, 88.
- [15] S. K. Lai, Y.-Y. Wang, D. Wirtz, J. Hanes, *Adv. Drug Delivery Rev.* **2009**, *61*, 86.
- [16] J. Li, D. J. Mooney, *Nat. Rev. Mater.* **2016**, *1*, 16071.
- [17] A. Sharma, B. Thongrom, S. Bhatia, B. von Lospichl, A. Addante, S. Y. Graeber, D. Lauster, M. A. Mall, M. Gradzielski, R. Haag, *Macromol. Rapid Commun.* **2021**, *42*, 2100303.
- [18] B. Von Lospichl, S. Hemmati-Sadeghi, P. Dey, T. Dehne, R. Haag, M. Sittinger, J. Ringe, M. Gradzielski, *Colloids Surf., B* **2017**, *159*, 477.
- [19] Y. Tsuji, X. Li, M. Shibayama, **2018**, *4*, 50.
- [20] K. S. Anseth, C. N. Bowman, L. Brannon-Peppas, *Biomaterials* **1996**, *17*, 1647.
- [21] S. S. Olmsted, J. L. Padgett, A. I. Yudin, K. J. Whaley, T. R. Moench, R. A. Cone, *Biophys. J.* **2001**, *81*, 1930.
- [22] H. Frey, R. Haag, *J. Biotechnol.* **2002**, *90*, 257.
- [23] A. Sunder, R. Hanselmann, H. Frey, R. Mülhaupt, *Macromolecules* **1999**, *32*, 4240.
- [24] R. Haag, A. Sunder, J.-F. Stumbé, *J. Am. Chem. Soc.* **2000**, *122*, 2954.
- [25] M. Wallert, J. Plaschke, M. Dimde, V. Ahmadi, S. Block, R. Haag, *Macromol. Mater. Eng.* **2021**, *306*, 2000688.

SUPPORTING INFORMATION

Scaffold Flexibility Controls Binding of Herpes Simplex Virus Type 1 with Sulfated Dendritic Polyglycerol Hydrogels Fabricated by Thiol-Maleimide Click Reaction

Boonya Thongrom,⁺ Antara Sharma,⁺ Chuanxiong Nie, Elisa Quaas, Marwin Raue, Sumati Bhatia* and Rainer Haag*

Institut für Chemie und Biochemie, Freie Universität Berlin, Takustraße 3, 14195 Berlin, Germany.

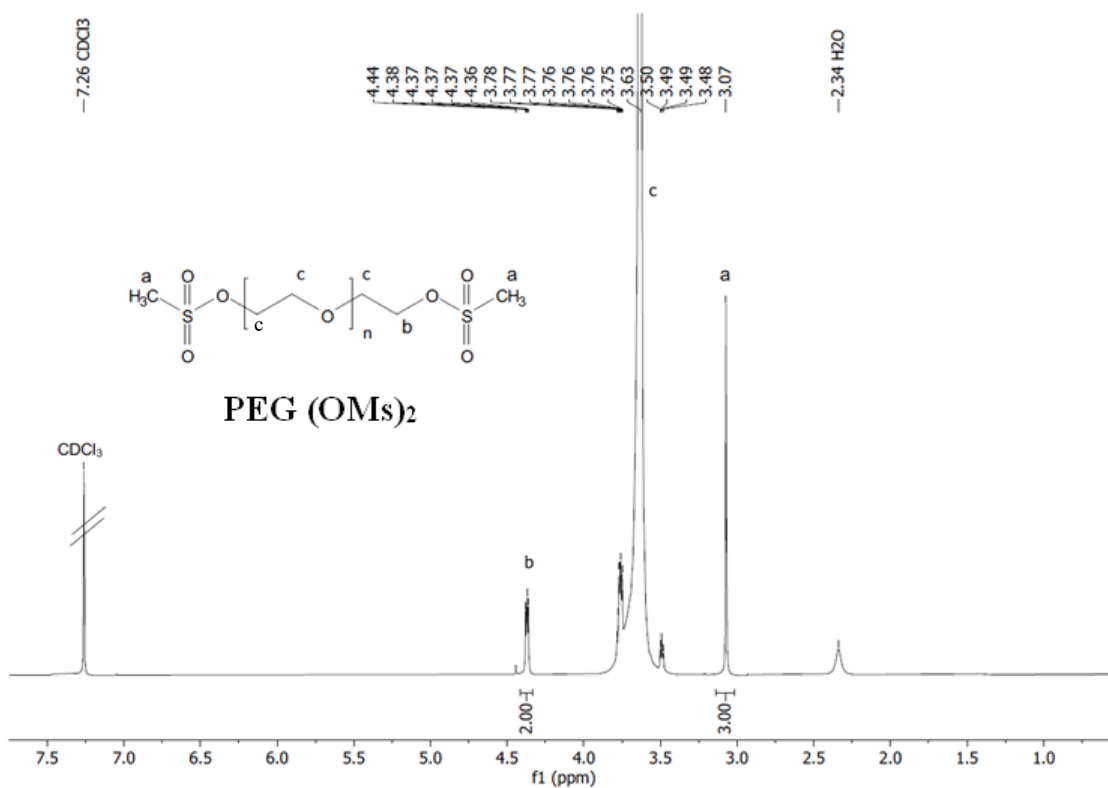


Figure S1. ¹H NMR (500 MHz, CDCl₃, δ (ppm)) of PEG (OMs)₂

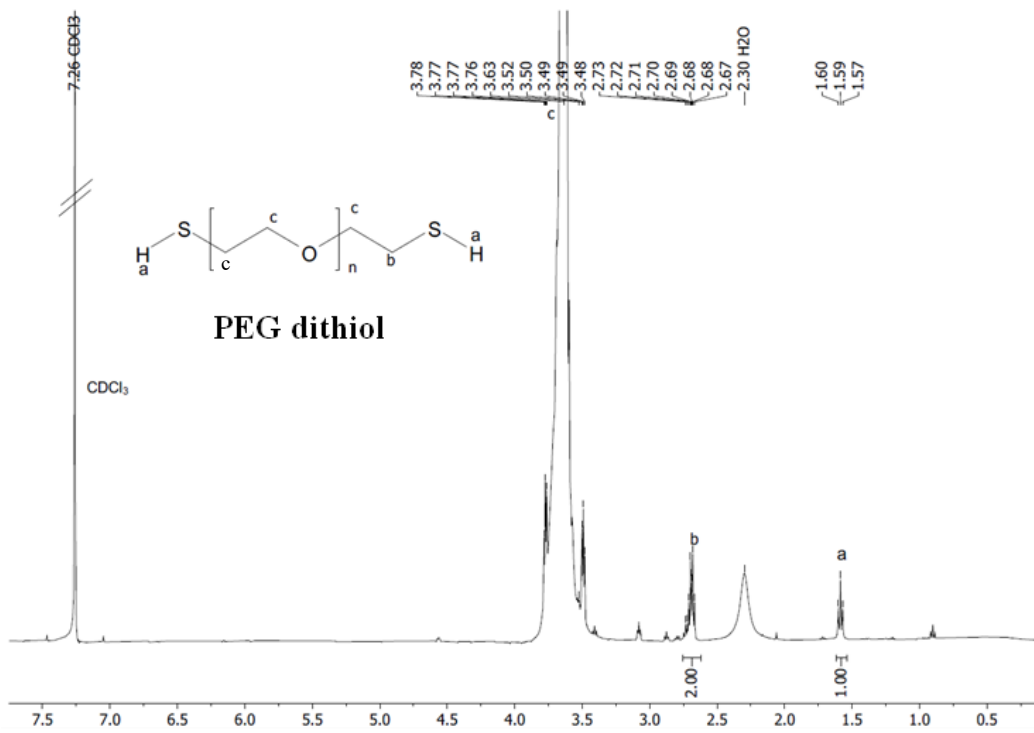


Figure S2. ¹H NMR (500 MHz, CDCl₃, δ (ppm)) of PEG dithiol

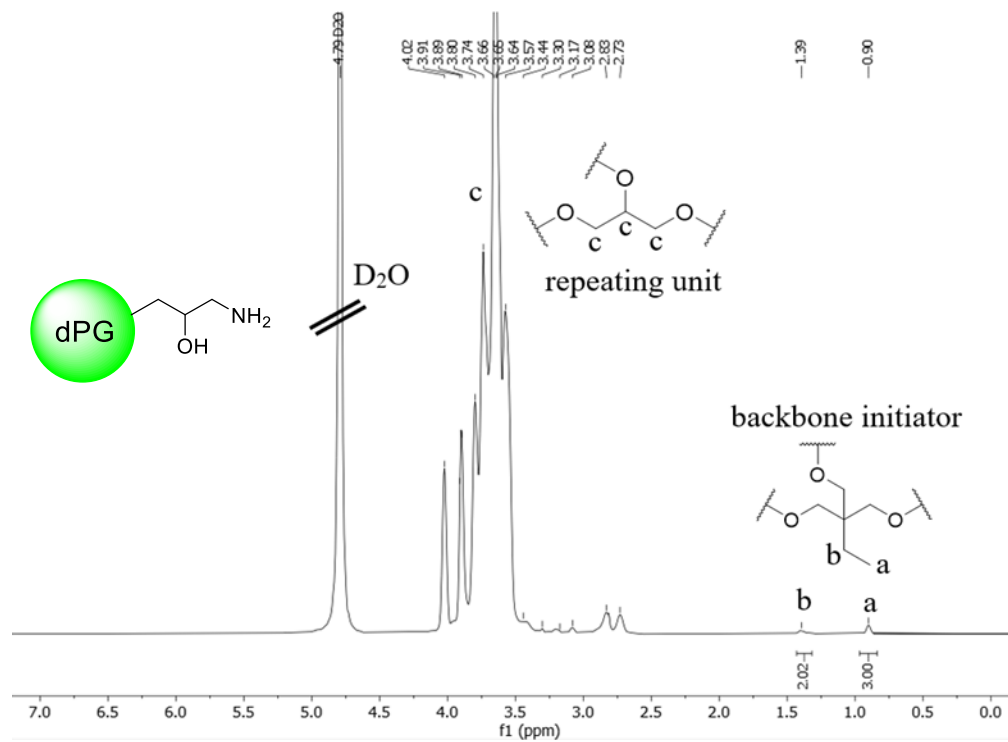


Figure S3. ¹H NMR (700 MHz, D₂O, δ (ppm)) of dPGNH₂

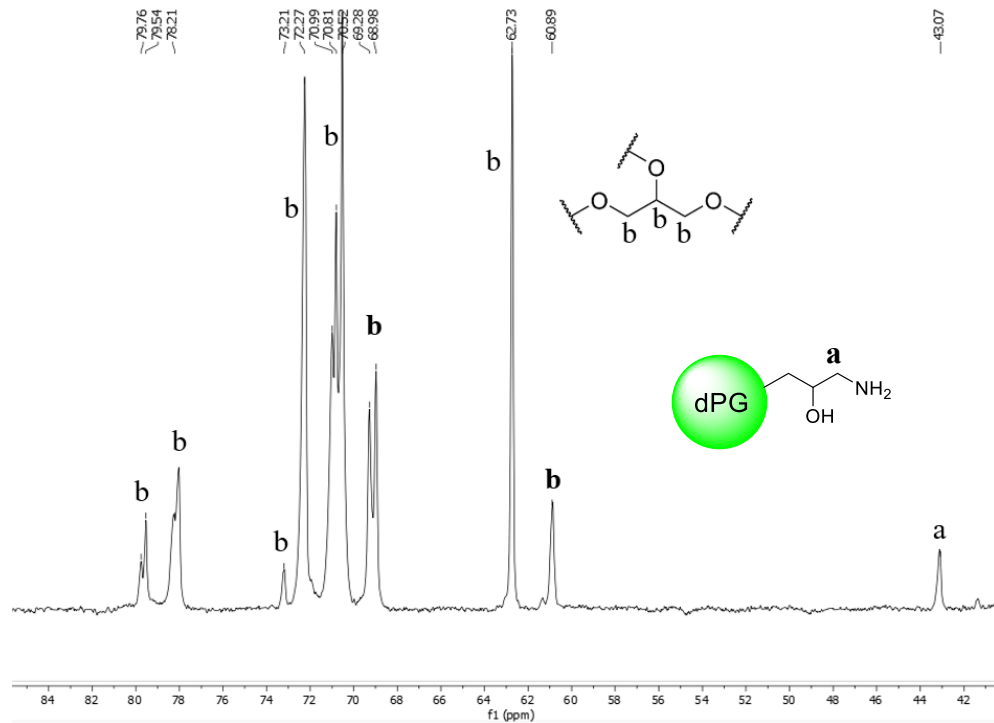


Figure S4. ^{13}C NMR (700 MHz, D_2O , δ (ppm)) of dPGNH_2

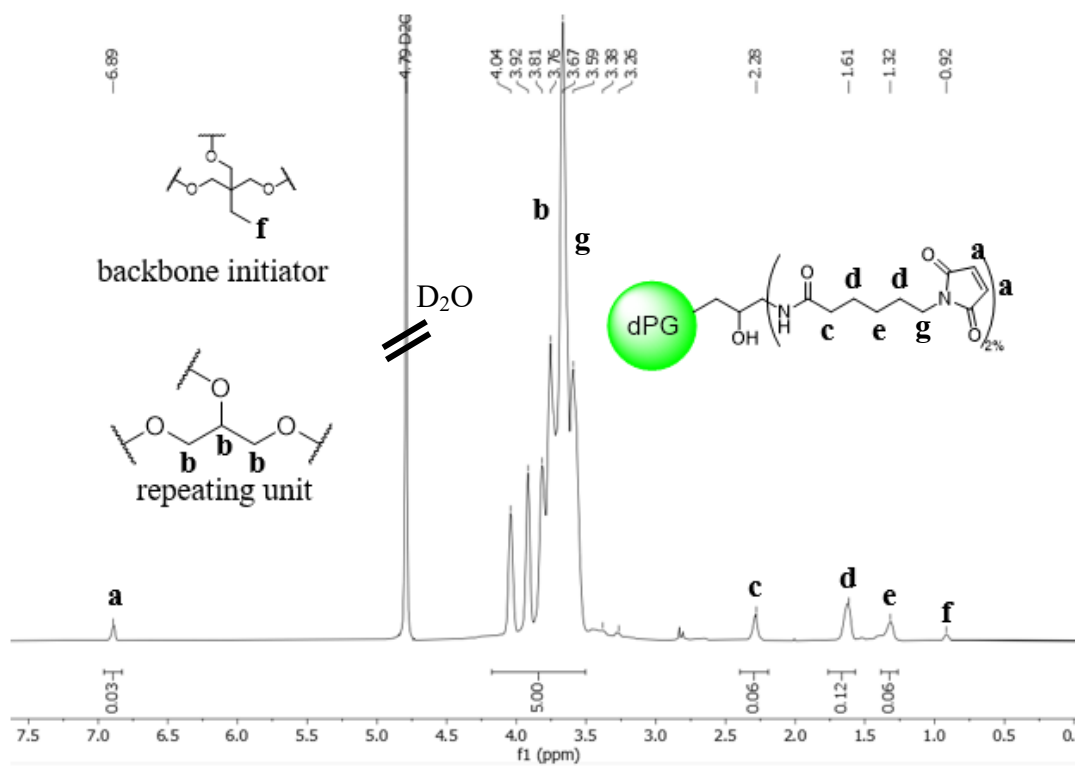


Figure S5. ^1H NMR (700 MHz, D_2O , δ (ppm)) of dPG maleimide

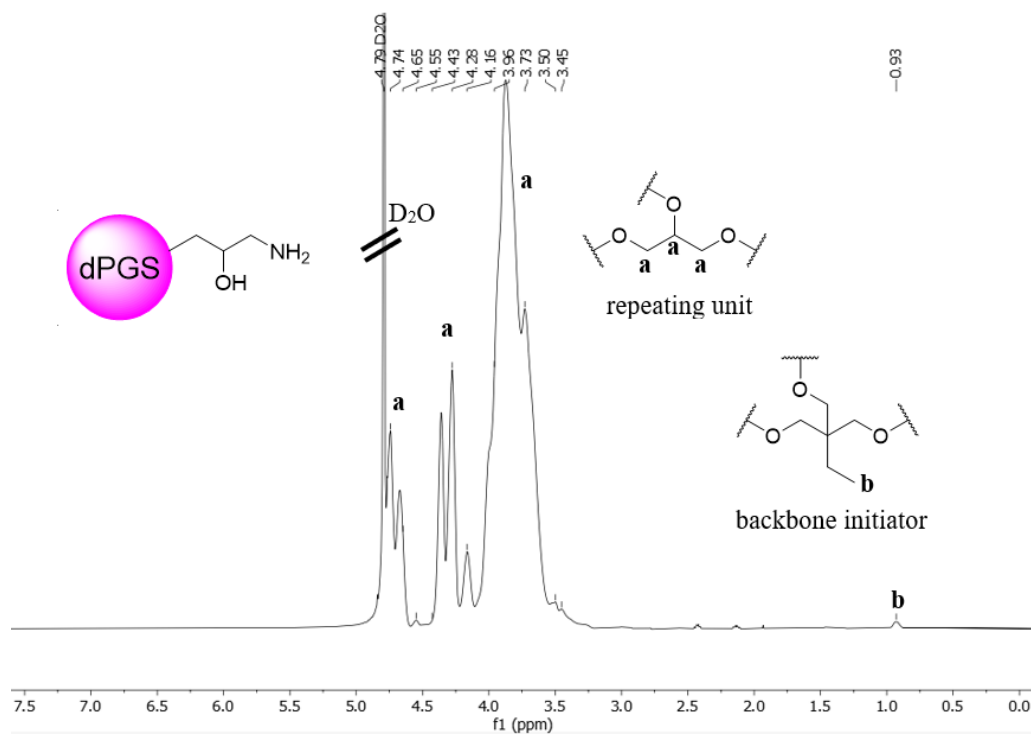


Figure S6. ^1H NMR (600 MHz, D_2O , δ (ppm)) of dPGSNH₂

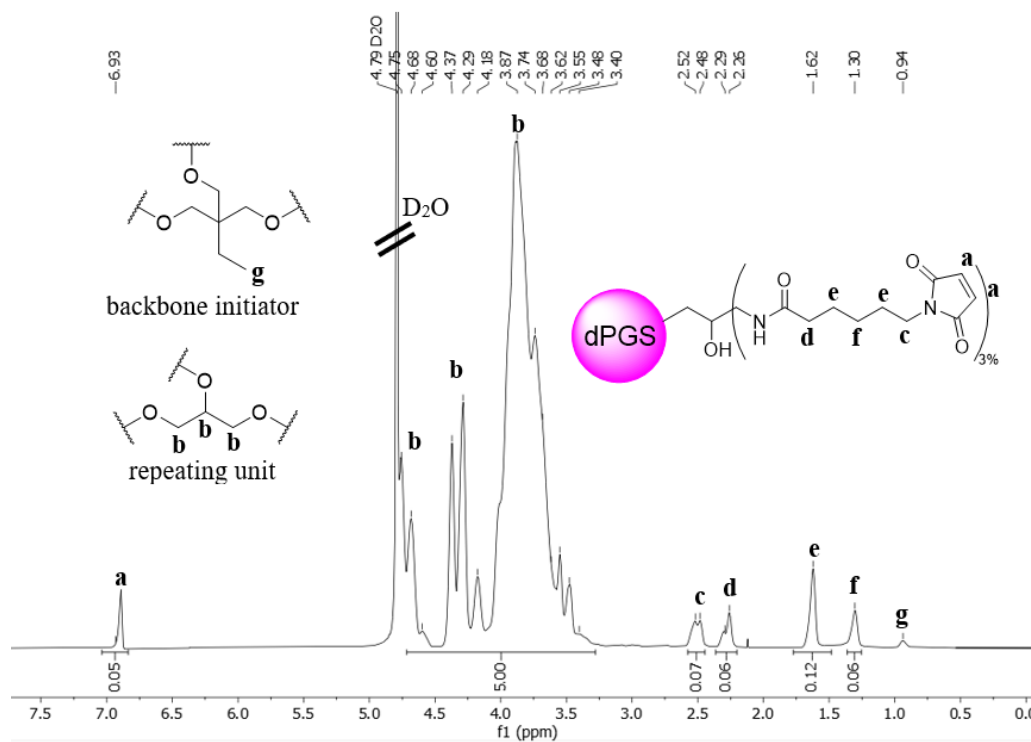


Figure S7. ^1H NMR (700 MHz, D_2O , δ (ppm)) of dPGS maleimide

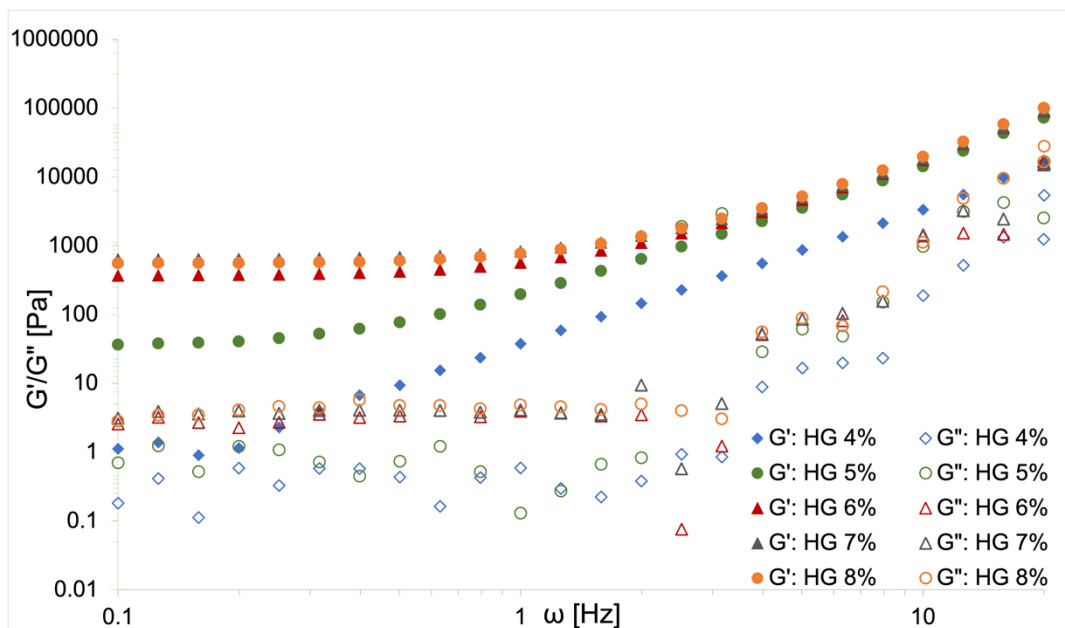


Figure S8. Storage (G') and loss (G'') moduli as a function of radial frequency (ω) of MM gels at 25 °C, for samples in which the gel component ratios were varied systemically.

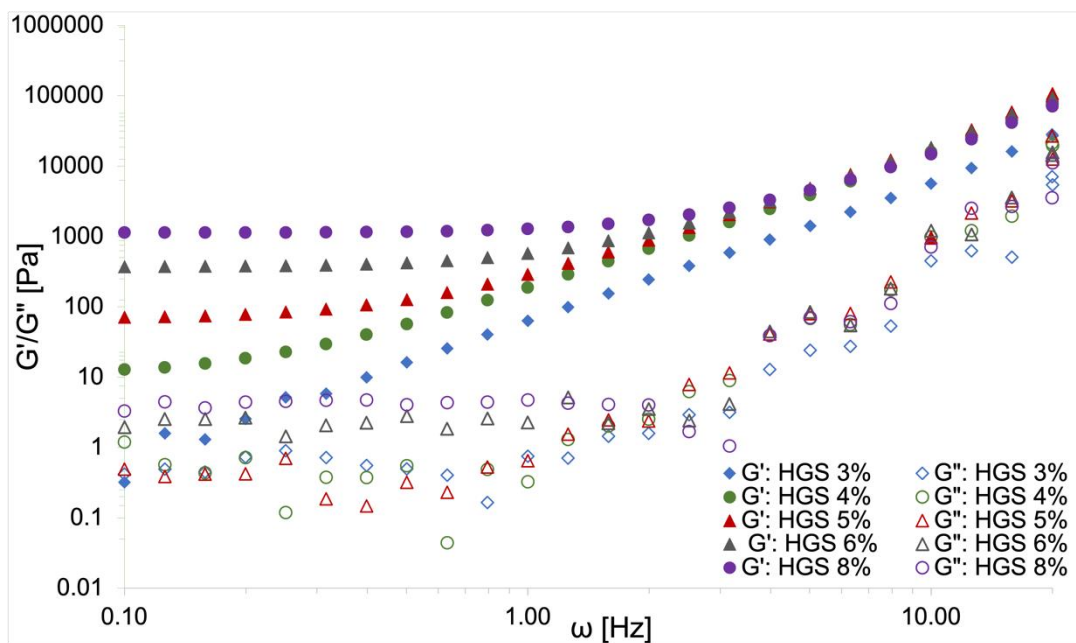


Figure S9. Storage (G') and loss (G'') moduli as a function of radial frequency (ω) of MS gels at 25 °C, for samples in which the gel component ratios were varied systemically.

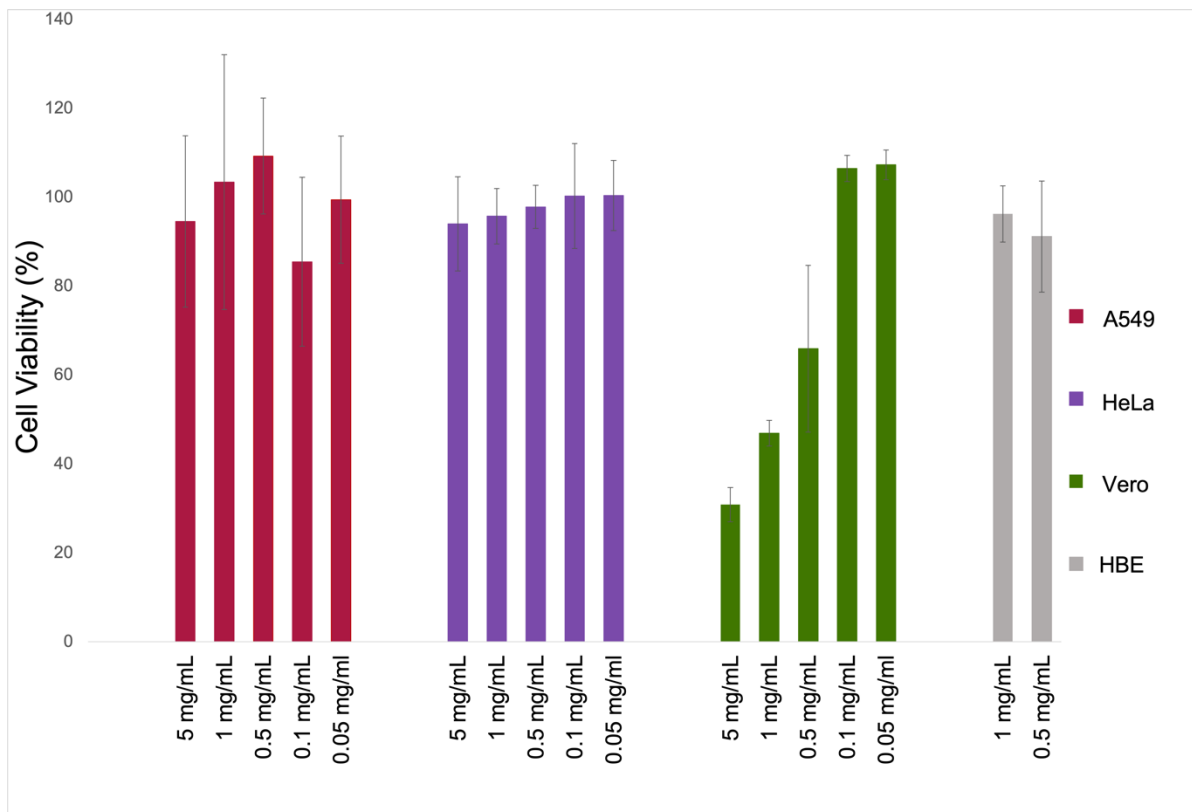


Figure S10. Cytotoxicity tests results of PEG-dithiol with A549, HeLa, Vero E6, and HBE cell lines.

Table S1. Composition of non-sulfated (HG) and sulfated (HGS) gels, depicting the amounts and ratios of the gel components used per 100 μ L gels, such as the concentration of the gel components, overall gel concentration, as well as the concentration of the dPG or dPGS gel components within each gel.

Gel Code	Gel Type	PEG:dPG Mol Ratio	Gel Components (μ mol)		Gel Concentration (% w/v)	dPG/dPGS Concentration (mM)
			PEG	dPG		
HG 8%	dPG maleimide	2.5:1	0.80	0.32	8.0	3.2
HG 7%	dPG maleimide	2.5:1	0.70	0.28	7.0	2.8
HG 6%	dPG maleimide	2.5:1	0.60	0.24	6.0	2.4
HG 5%	dPG maleimide	2.5:1	0.50	0.20	5.0	2.0
HG 4%	dPG maleimide	2.5:1	0.40	0.16	4.0	1.6
HGS 8%	dPGS maleimide	2.5:1	0.57	0.23	8.0	2.3
HGS 6%	dPGS maleimide	2.5:1	0.43	0.17	6.0	1.7
HGS 5%	dPGS maleimide	2.5:1	0.36	0.14	5.0	1.4
HGS 4%	dPGS maleimide	2.5:1	0.29	0.11	4.0	1.1
HGS 3%	dPGS maleimide	2.5:1	0.22	0.09	3.0	0.9
	dPG maleimide	-	-	0.32	3.2*	3.2
	dPGS maleimide	-	-	0.23	4.6*	2.3

*concentration of the gel component precursors

4. Summary

The focus of this PhD work is on the synthesis and characterization of different types of hydrogels using polyglycerols as the main building block. Both IPG and hPG have the advantages of good hydrophilicity and high biocompatibility which make them ideal for biological applications. In fact, the naturally present mucus hydrogel is used by the body to entrap various pathogens. Hydrogel's pores alone are responsible for the capture of many different types of viruses and the interactions involved are both physical and chemical. Moreover, previous studies have shown that the introduction of functional groups such as sulfate imparts the characteristics of heparan sulfate to the platforms which is involved in the initial binding interactions of many virus families with the gel, allowing them to behave as broad spectrum anti-viral agents.

In the first project, hydrogels were designed using naturally occurring lung mucus as the inspiration to form mucus-inspired hydrogels (MIHs). They were developed using thiol-disulfide reversible reaction chemistry that is present in natural mucus, known to influence its rheological and physiological behavior. MIHs were synthesized using $\text{H}_2\text{O}_2/\text{NaI}$ as the oxidizing agent to render disulfide bonds between the crosslinker THIOCURE® ETTMP 1300, a tri-PEG linker with thiol groups at each end, and the linear dithiolated precursors, which were used as mucin alternatives. In this study, three types of gels were created, each differing by their linear components: one series was fabricated using 5 kDa IPG(SH)₂, while the other two series were fabricated using PEG(SH)₂ of molecular weights 3 kDa and 6 kDa. Further, the ratios of the components were varied within each series such that a total of 12 different gels were obtained and these were rheologically compared in order to identify the one which is comparable by rheology to the human airway mucus. For which the shear modulus for this was observed in the range of 1 – 2 Pa. The rheology tests were performed at both 25 °C and the physiologically relevant temperature, 37 °C. The IPG-based MIHs clearly outperformed their PEG based counterparts. Moreover, by varying the composition ratios between the crosslinker and the linear components, elastic moduli could be varied widely, in the range of 19 to 1112 Pa, wherein the mesh sizes in the range of 15 – 60 Pa could be reached at 37 °C. From the variety of gels, the MIH with a crosslinker to linear component ratio of 1 : 10 was identified as the hydrogel with the rheological properties most comparable to native, healthy human airway mucus. Further studies with sulfate or sialic acid-modified MIHs are required to understand their behavior and efficacy as broad-spectrum antiviral agents.

In the second project, we endeavored to fabricate antiviral hydrogels using thiol-maleimide click chemistry. As previously mentioned, sulfated hPG (hPGS) have been shown to have analogous behavior to heparin sulfate which mediates the entry of many different virus species, including HSV. hPGS was functionalized with maleimide and then reacted with thiolated PEG chains (PEG dithiol) thus resulting in a thiol-maleimide Michael click reaction to form sulfate bearing hydrogels. In order to ascertain whether the incorporation of hPGS into the network fabric is actually pertinent to the formation of anti-HSV hydrogels, another set of hydrogels was synthesized using hPG-maleimide and PEG-dithiol. The gel component ratio was varied within each series to lead to a total of 10 different hydrogels with varying rheological and virus-binding properties, all of which showed spinnability to various extents. All the hydrogels were first studied rheologically, at both 25 °C and 37 °C. At the physiologically relevant temperature, the hydrogels were further studied in their non-swollen and swollen forms, the latter of which mimics the conditions found in vivo. In the swollen state, the shear modulus could be varied from 43 to 630 Pa for the non-sulfated gels and 17 to 748 Pa for the sulfated gels. Thus, hydrogels with a wide variety of viscoelasticities could be formed. Cytotoxicity assays were performed on the hydrogel components and did not show any toxicity. The efficacy of these compounds was examined using virus binding assays of HSV-1. Here the sulfated hydrogels exhibit up to 30 times higher binding than the non-sulfated gels. Among the sulfated gels, the most viscous network showing the highest flexibility showed the highest binding capacity among all the tested compounds, even more than the highly sulfated crosslinker dPGS-maleimide. Coincidentally, these hydrogels showed similar properties to mucus and thus could find applications as mucus mimics.

Antiviral drugs are a quick, effective way to circumvent public health crisis caused by the emergence of new virus species. However, the constantly-evolving nature of virus particles renders specific drugs obsolete and thus a requirement for broad-spectrum drugs is emerging. In this PhD work we attempt to fulfil this requirement by the synthesis of broad-spectrum anti-viral hydrogels. IPG and dPG offer a number of advantages including high hydrophilicity, biocompatibility and degree of functionalization, and therefore they can serve as ideal hydrogel building blocks.

4.1 Kurzzusammenfassung

Diese Doktorarbeit konzentriert sich auf die Synthese und Charakterisierung verschiedener Arten von Hydrogelen unter Verwendung von Polyglycerinen als Hauptbaustein. Sowohl IPG als auch hPG haben die Vorteile einer guten Hydrophilie und einer hohen Biokompatibilität, was sie ideal für biologische Anwendungen macht. Das natürlich vorkommende Schleimhydrogel wird vom Körper genutzt, um verschiedene Krankheitserreger einzuschließen. Allein die Poren des Hydrogels sind für den Einschluss vieler verschiedener Virentypen verantwortlich, und die beteiligten Wechselwirkungen sind sowohl physikalischer als auch chemischer Natur. Darüber hinaus haben frühere Studien gezeigt, dass die Einführung von funktionellen Gruppen wie Sulfat den Hydrogelen die Eigenschaften von Heparansulfat verleiht, das an den anfänglichen Bindungsinteraktionen vieler Virusfamilien mit dem Gel beteiligt ist, wodurch sie sich als Breitspektrum-Antivirenmittel verhalten können.

Im ersten Projekt wurden Hydrogele unter Verwendung von natürlich vorkommendem Lungenschleim als Inspiration für die Bildung von Schleim-inspirierten Hydrogelen (MIHs) entwickelt. Sie wurden unter Verwendung der reversiblen Thiol-Disulfid-Reaktionschemie entwickelt, die im natürlichen Schleim vorhanden ist und von der bekannt ist, dass sie sein rheologisches und physiologisches Verhalten beeinflusst. MIHs wurden unter Verwendung von H₂O₂/NaI als Oxidationsmittel synthetisiert, um Disulfidbindungen zwischen dem Vernetzer THIOCURE® ETTMP 1300, einem Tri-PEG-Linker mit Thiolgruppen an jedem Ende, und den linearen dithiolierten Vorläufern, die als Muzinersatz verwendet wurden, herzustellen. In dieser Studie wurden drei Arten von Gelen hergestellt, die sich jeweils durch ihre linearen Komponenten unterscheiden: eine Serie wurde mit 5 kDa IPG(SH)₂ hergestellt, während die beiden anderen Serien mit PEG(SH)₂ mit einem Molekulargewicht von 3 kDa und 6 kDa hergestellt wurden. Darüber hinaus wurden die Verhältnisse der Komponenten innerhalb jeder Serie variiert, so dass insgesamt 12 verschiedene Gele erhalten wurden, die rheologisch verglichen wurden, um dasjenige zu identifizieren, das rheologisch mit dem menschlichen Atemwegsschleim vergleichbar ist. Das Schermodul lag dabei im Bereich von 1 - 2 Pa. Die rheologischen Tests wurden sowohl bei 25 °C als auch bei der physiologisch relevanten Temperatur von 37 °C durchgeführt. Die IPG-basierten MIHs übertrafen ihre PEG-basierten Gegenstücke deutlich. Darüber hinaus konnten durch Variation der Zusammensetzungsverhältnisse zwischen dem Vernetzer und den linearen Komponenten die Elastizitätsmodule in

einem weiten Bereich von 19 bis 1112 Pa variiert werden, wobei bei 37 °C Maschenweiten im Bereich von 15 - 60 Pa erreicht werden konnten. Aus der Vielfalt der Gele wurde das MIH mit einem Verhältnis von Vernetzer zu linearer Komponente von 1 : 10 als das Hydrogel mit den rheologischen Eigenschaften identifiziert, die am ehesten mit dem nativen, gesunden menschlichen Atemwegsschleim vergleichbar sind. Weitere Studien mit sulfat- oder sialinsäuremodifizierten MIHs sind erforderlich, um ihr Verhalten und ihre Wirksamkeit als Breitspektrum-Antivirenmittel zu verstehen.

Im zweiten Projekt versuchten wir, antivirale Hydrogele mithilfe der Thiol-Maleimid-Click-Chemie herzustellen. Wie bereits erwähnt, hat sich gezeigt, dass sulfatiertes hPG (hPGS) ein ähnliches Verhalten wie Heparinsulfat aufweist und den Eintritt vieler verschiedener Virenarten, einschließlich HSV, verhindert. hPGS wurde mit Maleinimid funktionalisiert und dann mit thiolierten PEG-Ketten (PEG-Dithiol) umgesetzt, was zu einer Thiol-Maleimid-Michael-Click-Reaktion führte, um sulfathaltige Hydrogele zu bilden. Um festzustellen, ob die Einbindung von hPGS in das Netzwerkgewebe tatsächlich für die Bildung von Anti-HSV-Hydrogelen relevant ist, wurde eine weitere Reihe von Hydrogelen unter Verwendung von hPG-Maleimid und PEG-Dithiol synthetisiert. Das Verhältnis der Gelkomponenten wurde innerhalb jeder Serie variiert, um insgesamt 10 verschiedene Hydrogele mit unterschiedlichen rheologischen und virusbindenden Eigenschaften zu erhalten, die alle in unterschiedlichem Maße spinnbar waren. Alle Hydrogele wurden zunächst rheologisch untersucht, sowohl bei 25 °C als auch bei 37 °C. Bei der physiologisch relevanten Temperatur wurden die Hydrogele in ihrer nicht gequollenen und in ihrer gequollenen Form weiter untersucht, wobei letztere die in vivo vorgefundenen Bedingungen nachahmt. Im gequollenen Zustand konnte der Schermodul von 43 bis 630 Pa für die nichtsulfatierten Gele und von 17 bis 748 Pa für die sulfatierten Gele variiert werden. Somit konnten Hydrogele mit einer Vielzahl von Viskoelastizitäten gebildet werden. Zytotoxizitätstests wurden mit den Hydrogelkomponenten durchgeführt und ergaben keine Toxizität. Die Wirksamkeit dieser Verbindungen wurde anhand von HSV-1-Virusbindungstests untersucht. Dabei wiesen die sulfatierten Hydrogele eine bis zu 30-mal höhere Bindung auf als die nicht sulfatierten Gele. Unter den sulfatierten Gelen wies das viskoseste Netzwerk mit der höchsten Flexibilität die höchste Bindungskapazität unter allen getesteten Verbindungen auf, sogar mehr als der hoch sulfatierte Vernetzer dPGS-Maleimid. Zufälligerweise wiesen diese Hydrogele ähnliche Eigenschaften wie Schleim auf und könnten daher als Schleimnachahmer Verwendung finden.

Antivirale Medikamente sind ein schnelles und wirksames Mittel, um die durch das Auftauchen neuer Virusarten verursachte Krise der öffentlichen Gesundheit zu verhindern. Die sich ständig weiterentwickelnden Viruspartikel machen jedoch spezifische Medikamente überflüssig, so dass ein Bedarf an Breitspektrum-Medikamenten entsteht. In dieser Doktorarbeit versuchen wir, diese Anforderung durch die Synthese von antiviralen Hydrogelen mit breitem Wirkungsspektrum zu erfüllen. IPG und dPG bieten eine Reihe von Vorteilen, darunter hohe Hydrophilie, Biokompatibilität und Funktionalisierungsgrad, und können daher als ideale Hydrogelbausteine dienen.

5. Outlook

In naturally occurring mucus, the physical properties are as important as its chemical properties for antimicrobial properties. In the first project, we fabricated synthetic hydrogels inspired from naturally occurring healthy airway mucus, called MIHs. Herein we focused solely on its physical properties and were able to accomplish mechanical properties in the required viscoelastic range. The next natural step would therefore be to mimic the properties of natural mucus on a chemical scale as well to therefore realize defined mucus mimics which can be applied as broad-spectrum anti-viral agents. This can be done by the functionalization of the MIH platforms with desirable functional groups such as sulfate ester and sialic acid groups by utilizing the functionalizable hydroxyl groups on the IPG backbone. Furthermore, virus binding and trapping can be studied on these platforms, especially those which infect the airways such as HSV-1 and SARS-CoV-2.

In the second project, anti-HSV hydrogels were synthesized by the incorporation of sulfated hPGs, as heparan sulfate mimics into a crosslinked network with PEG. Here the hydrogels with the lowest elastic modulus, or the most flexible platforms showed the highest binding efficacies towards HSV-1 particles. Further tests on various other virus types sensitive to sulfate, are required in order to examine the extent broad-spectrum antiviral properties that the network can exhibit.

6. References

1. Bosch, B. J.; van der Zee, R.; de Haan, C. A.; Rottier, P. J., The coronavirus spike protein is a class I virus fusion protein: structural and functional characterization of the fusion core complex. *J Virol* **2003**, *77* (16), 8801-11.
2. Bhatia, S.; Camacho, L. C.; Haag, R., Pathogen Inhibition by Multivalent Ligand Architectures. *J Am Chem Soc* **2016**, *138* (28), 8654-66.
3. Ringsdorf, H., Ringsdorf, H.: Structure and properties of pharmacologically active polymers. *J. Polym. Sci. Polym. Symp.* 51, 135-153. *Journal of Polymer Science: Polymer Symposia* **2007**, *51*, 135-153.
4. Fasting, C.; Schalley, C. A.; Weber, M.; Seitz, O.; Hecht, S.; Kokschi, B.; Dervedde, J.; Graf, C.; Knapp, E.-W.; Haag, R., Multivalency as a Chemical Organization and Action Principle. *Angewandte Chemie International Edition* **2012**, *51* (42), 10472-10498.
5. Spillmann, D., Heparan sulfate: Anchor for viral intruders? *Biochimie* **2001**, *83* (8), 811-817.
6. WuDunn, D.; Spear, P. G., Initial interaction of herpes simplex virus with cells is binding to heparan sulfate. *Journal of Virology* **1989**, *63* (1), 52-58.
7. Dogrammatzis, C.; Waisner, H.; Kalamvoki, M., "Non-Essential" Proteins of HSV-1 with Essential Roles In Vivo: A Comprehensive Review. *Viruses* **2021**, *13* (1), 17.
8. Wilen, C. B.; Tilton, J. C.; Doms, R. W., HIV: cell binding and entry. *Cold Spring Harb Perspect Med* **2012**, *2* (8).
9. Saphire, A. C.; Bobardt, M. D.; Zhang, Z.; David, G.; Gallay, P. A., Syndecans serve as attachment receptors for human immunodeficiency virus type 1 on macrophages. *J Virol* **2001**, *75* (19), 9187-200.
10. Hallak, L. K.; Spillmann, D.; Collins, P. L.; Peeples, M. E., Glycosaminoglycan sulfation requirements for respiratory syncytial virus infection. *J Virol* **2000**, *74* (22), 10508-13.
11. Summerford, C.; Samulski, R. J., Membrane-associated heparan sulfate proteoglycan is a receptor for adeno-associated virus type 2 virions. *J Virol* **1998**, *72* (2), 1438-45.
12. Chen, Y.; Maguire, T.; Hileman, R. E.; Fromm, J. R.; Esko, J. D.; Linhardt, R. J.; Marks, R. M., Dengue virus infectivity depends on envelope protein binding to target cell heparan sulfate. *Nat Med* **1997**, *3* (8), 866-71.
13. Nie, C.; Pouyan, P.; Lauster, D.; Trimpert, J.; Kerkhoff, Y.; Szekeres, G. P.; Wallert, M.; Block, S.; Sahoo, A. K.; Dervedde, J.; Pagel, K.; Kaufer, B. B.; Netz, R. R.; Ballauff, M.; Haag, R., Polysulfates Block SARS-CoV-2 Uptake through Electrostatic Interactions**. *Angewandte Chemie International Edition* **2021**, *60* (29), 15870-15878.

14. Clausen, T. M.; Sandoval, D. R.; Spliid, C. B.; Pihl, J.; Perrett, H. R.; Painter, C. D.; Narayanan, A.; Majowicz, S. A.; Kwong, E. M.; McVicar, R. N.; Thacker, B. E.; Glass, C. A.; Yang, Z.; Torres, J. L.; Golden, G. J.; Bartels, P. L.; Porell, R. N.; Garretson, A. F.; Laubach, L.; Feldman, J.; Yin, X.; Pu, Y.; Hauser, B. M.; Caradonna, T. M.; Kellman, B. P.; Martino, C.; Gordts, P. L. S. M.; Chanda, S. K.; Schmidt, A. G.; Godula, K.; Leibel, S. L.; Jose, J.; Corbett, K. D.; Ward, A. B.; Carlin, A. F.; Esko, J. D., SARS-CoV-2 Infection Depends on Cellular Heparan Sulfate and ACE2. *Cell* **2020**, *183* (4), 1043-1057.e15.
15. Baram-Pinto, D.; Shukla, S.; Gedanken, A.; Sarid, R., Inhibition of HSV-1 attachment, entry, and cell-to-cell spread by functionalized multivalent gold nanoparticles. *Small* **2010**, *6* (9), 1044-50.
16. Lüscher-Mattii, M., Polyanions — A Lost Chance in the Fight against HIV and other Virus Diseases? *Antiviral Chemistry and Chemotherapy* **2000**, *11* (4), 249-259.
17. Lee, E.; Pavy, M.; Young, N.; Freeman, C.; Lobigs, M., Antiviral effect of the heparan sulfate mimetic, PI-88, against dengue and encephalitic flaviviruses. *Antiviral Research* **2006**, *69* (1), 31-38.
18. Bianculli, R. H.; Mase, J. D.; Schulz, M. D., Antiviral Polymers: Past Approaches and Future Possibilities. *Macromolecules* **2020**, *53* (21), 9158-9186.
19. Rakowska, P. D.; Tiddia, M.; Faruqui, N.; Bankier, C.; Pei, Y.; Pollard, A. J.; Zhang, J.; Gilmore, I. S., Antiviral surfaces and coatings and their mechanisms of action. *Communications Materials* **2021**, *2* (1), 53.
20. Zhang, Y.; Yao, Q.; Xia, C.; Jiang, X.; Wang, P. G., Trapping norovirus by glycosylated hydrogels: a potential oral antiviral drug. *ChemMedChem* **2006**, *1* (12), 1361-6.
21. Lee, Y. C.; Townsend, R. R.; Hardy, M. R.; Lönnngren, J.; Arnarp, J.; Haraldsson, M.; Lönn, H., Binding of synthetic oligosaccharides to the hepatic Gal/GalNAc lectin. Dependence on fine structural features. *J Biol Chem* **1983**, *258* (1), 199-202.
22. Lee, Y. C.; Lee, R. T., Carbohydrate-Protein Interactions: Basis of Glycobiology. *Accounts of Chemical Research* **1995**, *28* (8), 321-327.
23. Mammen, M.; Choi, S. K.; Whitesides, G. M., Polyvalent Interactions in Biological Systems: Implications for Design and Use of Multivalent Ligands and Inhibitors. *Angew Chem Int Ed Engl* **1998**, *37* (20), 2754-2794.
24. Buwalda, S. J.; Boere, K. W.; Dijkstra, P. J.; Feijen, J.; Vermonden, T.; Hennink, W. E., Hydrogels in a historical perspective: from simple networks to smart materials. *J Control Release* **2014**, *190*, 254-73.

25. Wichterle, O.; LÍM, D., Hydrophilic Gels for Biological Use. *Nature* **1960**, *185* (4706), 117-118.
26. Miyata, T.; Uragami, T.; Nakamae, K., Biomolecule-sensitive hydrogels. *Adv Drug Deliver Rev* **2002**, *54* (1), 79-98.
27. Tomatsu, I.; Peng, K.; Kros, A., Photoresponsive hydrogels for biomedical applications. *Adv Drug Deliver Rev* **2011**, *63* (14), 1257-1266.
28. Huh, K. M.; Kang, H. C.; Lee, Y. J.; Bae, Y. H., pH-sensitive polymers for drug delivery. *Macromolecular Research* **2012**, *20* (3), 224-233.
29. Meng, F.; Hennink, W. E.; Zhong, Z., Reduction-sensitive polymers and bioconjugates for biomedical applications. *Biomaterials* **2009**, *30* (12), 2180-2198.
30. Chaterji, S.; Kwon, I. K.; Park, K., Smart Polymeric Gels: Redefining the Limits of Biomedical Devices. *Prog Polym Sci* **2007**, *32* (8-9), 1083-1122.
31. Richter, A.; Paschew, G.; Klatt, S.; Lienig, J.; Arndt, K. F.; Adler, H. P., Review on Hydrogel-based pH Sensors and Microsensors. *Sensors (Basel)* **2008**, *8* (1), 561-581.
32. Censi, R.; Schuurman, W.; Malda, J.; di Dato, G.; Burgisser, P. E.; Dhert, W. J. A.; van Nostrum, C. F.; di Martino, P.; Vermonden, T.; Hennink, W. E., A Printable Photopolymerizable Thermosensitive p(HPMAm-lactate)-PEG Hydrogel for Tissue Engineering. *Advanced Functional Materials* **2011**, *21* (10), 1833-1842.
33. Zhu, J.; Marchant, R. E., Design properties of hydrogel tissue-engineering scaffolds. *Expert Review of Medical Devices* **2011**, *8* (5), 607-626.
34. Spicer, C. D., Hydrogel scaffolds for tissue engineering: the importance of polymer choice. *Polymer Chemistry* **2020**, *11* (2), 184-219.
35. Mahalingam, A.; Jay, J. I.; Langheinrich, K.; Shukair, S.; McRaven, M. D.; Rohan, L. C.; Herold, B. C.; Hope, T. J.; Kiser, P. F., Inhibition of the transport of HIV in vitro using a pH-responsive synthetic mucin-like polymer system. *Biomaterials* **2011**, *32* (33), 8343-55.
36. Hoare, T. R.; Kohane, D. S., Hydrogels in drug delivery: Progress and challenges. *Polymer* **2008**, *49* (8), 1993-2007.
37. Li, J.; Mooney, D. J., Designing hydrogels for controlled drug delivery. *Nature Reviews Materials* **2016**, *1* (12), 16071.
38. Ashley, G. W.; Henise, J.; Reid, R.; Santi, D. V., Hydrogel drug delivery system with predictable and tunable drug release and degradation rates. *Proceedings of the National Academy of Sciences* **2013**, *110* (6), 2318.

39. von Lospichl, B.; Hemmati-Sadeghi, S.; Dey, P.; Dehne, T.; Haag, R.; Sittinger, M.; Ringe, J.; Gradzielski, M., Injectable hydrogels for treatment of osteoarthritis - A rheological study. *Colloids Surf B Biointerfaces* **2017**, *159*, 477-483.
40. Su, J., Thiol-Mediated Chemoselective Strategies for In Situ Formation of Hydrogels. *Gels* **2018**, *4* (3).
41. Bansil, R.; Turner, B. S., Mucin structure, aggregation, physiological functions and biomedical applications. *Curr Opin Colloid In* **2006**, *11* (2-3), 164-170.
42. Bansil, R.; Turner, B. S., The biology of mucus: Composition, synthesis and organization. *Adv Drug Deliv Rev* **2018**, *124*, 3-15.
43. Roorda, W. E.; Boddé, H. E.; de Boer, A. G.; Junginger, H. E., Synthetic hydrogels as drug delivery systems. *Pharmaceutisch Weekblad* **1986**, *8* (3), 165-189.
44. Herrmann, A.; Haag, R.; Schedler, U., Hydrogels and Their Role in Biosensing Applications. *Adv Healthc Mater* **2021**, *10* (11), e2100062.
45. Otsuka, H.; Nagasaki, Y.; Kataoka, K., PEGylated nanoparticles for biological and pharmaceutical applications. *Adv Drug Deliv Rev* **2003**, *55* (3), 403-19.
46. Harris, J. M.; Chess, R. B., Effect of pegylation on pharmaceuticals. *Nat Rev Drug Discov* **2003**, *2* (3), 214-21.
47. Kozma, G. T.; Shimizu, T.; Ishida, T.; Szebeni, J., Anti-PEG antibodies: Properties, formation, testing and role in adverse immune reactions to PEGylated nanobiopharmaceuticals. *Adv Drug Deliver Rev* **2020**, *154-155*, 163-175.
48. Zhang, P.; Sun, F.; Liu, S.; Jiang, S., Anti-PEG antibodies in the clinic: Current issues and beyond PEGylation. *Journal of Controlled Release* **2016**, *244*, 184-193.
49. Thomas, A.; Müller, S. S.; Frey, H., Beyond Poly(ethylene glycol): Linear Polyglycerol as a Multifunctional Polyether for Biomedical and Pharmaceutical Applications. *Biomacromolecules* **2014**, *15* (6), 1935-1954.
50. Sandler, S. R.; Berg, F. R., Room temperature polymerization of glycidol. *Journal of Polymer Science Part A-1: Polymer Chemistry* **1966**, *4* (5), 1253-1259.
51. Sunder, A.; Hanselmann, R.; Frey, H.; Mülhaupt, R., Controlled Synthesis of Hyperbranched Polyglycerols by Ring-Opening Multibranching Polymerization. *Macromolecules* **1999**, *32* (13), 4240-4246.
52. Vandenberg, E. J., Polymerization of glycidol and its derivatives: A new rearrangement polymerization. *Journal of Polymer Science: Polymer Chemistry Edition* **1985**, *23* (4), 915-949.
53. Calderón, M.; Quadir, M. A.; Sharma, S. K.; Haag, R., Dendritic polyglycerols for biomedical applications. *Adv Mater* **2010**, *22* (2), 190-218.

-
54. Wei, Q.; Becherer, T.; Angioletti-Uberti, S.; Dzubielia, J.; Wischke, C.; Neffe, A. T.; Lendlein, A.; Ballauff, M.; Haag, R., Protein Interactions with Polymer Coatings and Biomaterials. *Angewandte Chemie International Edition* **2014**, *53* (31), 8004-8031.
 55. Kainthan, R. K.; Hester, S. R.; Levin, E.; Devine, D. V.; Brooks, D. E., In vitro biological evaluation of high molecular weight hyperbranched polyglycerols. *Biomaterials* **2007**, *28* (31), 4581-90.
 56. Kainthan, R. K.; Janzen, J.; Levin, E.; Devine, D. V.; Brooks, D. E., Biocompatibility testing of branched and linear polyglycidol. *Biomacromolecules* **2006**, *7* (3), 703-9.
 57. Kainthan, R. K.; Brooks, D. E., In vivo biological evaluation of high molecular weight hyperbranched polyglycerols. *Biomaterials* **2007**, *28* (32), 4779-87.
 58. Frey, H.; Haag, R., Dendritic polyglycerol: a new versatile biocompatible-material. *J Biotechnol* **2002**, *90* (3-4), 257-67.
 59. Wilms, D.; Stiriba, S. E.; Frey, H., Hyperbranched polyglycerols: from the controlled synthesis of biocompatible polyether polyols to multipurpose applications. *Acc Chem Res* **2010**, *43* (1), 129-41.
 60. Oudshoorn, M. H.; Rissmann, R.; Bouwstra, J. A.; Hennink, W. E., Synthesis and characterization of hyperbranched polyglycerol hydrogels. *Biomaterials* **2006**, *27* (32), 5471-9.
 61. Dey, P.; Schneider, T.; Chiappisi, L.; Gradzielski, M.; Schulze-Tanzil, G.; Haag, R., Mimicking of Chondrocyte Microenvironment Using In Situ Forming Dendritic Polyglycerol Sulfate-Based Synthetic Polyanionic Hydrogels. *Macromolecular Bioscience* **2016**, *16* (4), 580-590.
 62. Dervede, J.; Rausch, A.; Weinhart, M.; Enders, S.; Tauber, R.; Licha, K.; Schirner, M.; Zügel, U.; von Bonin, A.; Haag, R., Dendritic polyglycerol sulfates as multivalent inhibitors of inflammation. *Proceedings of the National Academy of Sciences* **2010**, *107* (46), 19679-19684.
 63. Randriantsilefisoa, R.; Nie, C.; Parshad, B.; Pan, Y.; Bhatia, S.; Haag, R., Double trouble for viruses: a hydrogel nanocomposite catches the influenza virus while shrinking and changing color. *Chemical Communications* **2020**, *56* (24), 3547-3550.
 64. Hackelbusch, S.; Rossow, T.; Becker, H.; Seiffert, S., Multiresponsive Polymer Hydrogels by Orthogonal Supramolecular Chain Cross-Linking. *Macromolecules* **2014**, *47* (12), 4028-4036.

65. Singh, R.; Whitesides, G. M., Thiol-Disulfide Interchange. In *The Chemistry of Sulfur-Containing Functional Groups*, Patai, S., Ed. J. Wiley and Sons, Ltd.: London, 1993; Vol. Supplement S, pp 633-658.
66. Gruhlke, M. C.; Slusarenko, A. J., The biology of reactive sulfur species (RSS). *Plant Physiol Biochem* **2012**, *59*, 98-107.
67. Baldwin, A. D.; Kiick, K. L., Reversible maleimide–thiol adducts yield glutathione-sensitive poly(ethylene glycol)–heparin hydrogels. *Polymer Chemistry* **2013**, *4* (1), 133-143.
68. Meng, F.; Hennink, W. E.; Zhong, Z., Reduction-sensitive polymers and bioconjugates for biomedical applications. *Biomaterials* **2009**, *30* (12), 2180-98.
69. Gyarmati, B.; Némethy, Á.; Szilágyi, A., Reversible disulphide formation in polymer networks: A versatile functional group from synthesis to applications. *European Polymer Journal* **2013**, *49* (6), 1268-1286.
70. Fernandes, P. A.; Ramos, M. J., Theoretical insights into the mechanism for thiol/disulfide exchange. *Chemistry* **2004**, *10* (1), 257-66.
71. Gyarmati, B.; Vajna, B.; Némethy, Á.; László, K.; Szilágyi, A., Redox- and pH-Responsive Cysteamine-Modified Poly(aspartic acid) Showing a Reversible Sol–Gel Transition. *Macromolecular Bioscience* **2013**, *13* (5), 633-640.
72. Anumolu, S. S.; Menjoge, A. R.; Deshmukh, M.; Gerecke, D.; Stein, S.; Laskin, J.; Sinko, P. J., Doxycycline hydrogels with reversible disulfide crosslinks for dermal wound healing of mustard injuries. *Biomaterials* **2011**, *32* (4), 1204-1217.
73. Vernon, B.; Tirelli, N.; Bächli, T.; Haldimann, D.; Hubbell, J. A., Water-borne, in situ crosslinked biomaterials from phase-segregated precursors. *Journal of Biomedical Materials Research Part A* **2003**, *64A* (3), 447-456.
74. Lutolf, M. P.; Hubbell, J. A., Synthesis and physicochemical characterization of end-linked poly(ethylene glycol)-co-peptide hydrogels formed by Michael-type addition. *Biomacromolecules* **2003**, *4* (3), 713-22.
75. Rizzi, S. C.; Hubbell, J. A., Recombinant Protein-co-PEG Networks as Cell-Adhesive and Proteolytically Degradable Hydrogel Matrixes. Part I: Development and Physicochemical Characteristics. *Biomacromolecules* **2005**, *6* (3), 1226-1238.
76. Coates, A. R.; Halls, G.; Hu, Y., Novel classes of antibiotics or more of the same? *Br J Pharmacol* **2011**, *163* (1), 184-94.
77. Li, P.; Poon, Y. F.; Li, W.; Zhu, H.-Y.; Yeap, S. H.; Cao, Y.; Qi, X.; Zhou, C.; Lamrani, M.; Beuerman, R. W.; Kang, E.-T.; Mu, Y.; Li, C. M.; Chang, M. W.; Jan Leong, S. S.; Chan-Park, M. B., A polycationic antimicrobial and biocompatible hydrogel with microbe membrane suctioning ability. *Nature Materials* **2011**, *10* (2), 149-156.

78. Peng, L.; Chang, L.; Si, M.; Lin, J.; Wei, Y.; Wang, S.; Liu, H.; Han, B.; Jiang, L., Hydrogel-Coated Dental Device with Adhesion-Inhibiting and Colony-Suppressing Properties. *ACS Appl Mater Interfaces* **2020**, *12* (8), 9718-9725.
79. Malmsten, M., Antimicrobial and antiviral hydrogels. *Soft Matter* **2011**, *7* (19), 8725-8736.
80. Gupta, A.; Briffa, S. M.; Swingler, S.; Gibson, H.; Kannappan, V.; Adamus, G.; Kowalczyk, M.; Martin, C.; Radecka, I., Synthesis of Silver Nanoparticles Using Curcumin-Cyclodextrins Loaded into Bacterial Cellulose-Based Hydrogels for Wound Dressing Applications. *Biomacromolecules* **2020**, *21* (5), 1802-1811.
81. Ding, C.; Tian, M.; Feng, R.; Dang, Y.; Zhang, M., Novel Self-Healing Hydrogel with Injectable, pH-Responsive, Strain-Sensitive, Promoting Wound-Healing, and Hemostatic Properties Based on Collagen and Chitosan. *ACS Biomaterials Science & Engineering* **2020**, *6* (7), 3855-3867.
82. Ninan, N.; Forget, A.; Shastri, V. P.; Voelcker, N. H.; Blencowe, A., Antibacterial and Anti-Inflammatory pH-Responsive Tannic Acid-Carboxylated Agarose Composite Hydrogels for Wound Healing. *ACS Appl Mater Interfaces* **2016**, *8* (42), 28511-28521.
83. Shu, M.; Long, S.; Huang, Y.; Li, D.; Li, H.; Li, X., High strength and antibacterial polyelectrolyte complex CS/HS hydrogel films for wound healing. *Soft Matter* **2019**, *15* (38), 7686-7694.
84. Hebeish, A.; Sharaf, S., Novel nanocomposite hydrogel for wound dressing and other medical applications. *RSC Advances* **2015**, *5* (125), 103036-103046.
85. Cone, R. A., Barrier properties of mucus. *Adv Drug Deliv Rev* **2009**, *61* (2), 75-85.
86. Thornton, D. J.; Sheehan, J. K., From mucins to mucus: toward a more coherent understanding of this essential barrier. *Proc Am Thorac Soc* **2004**, *1* (1), 54-61.
87. Peppas, N. A.; Huang, Y., Nanoscale technology of mucoadhesive interactions. *Adv Drug Deliv Rev* **2004**, *56* (11), 1675-87.
88. Macadam, A., The Effect of Gastrointestinal Mucus on Drug Absorption. *Adv Drug Deliver Rev* **1993**, *11* (3), 201-220.
89. Shannon-Lowe, C. D.; Neuhierl, B.; Baldwin, G.; Rickinson, A. B.; Delecluse, H. J., Resting B cells as a transfer vehicle for Epstein-Barr virus infection of epithelial cells. *Proc Natl Acad Sci U S A* **2006**, *103* (18), 7065-70.
90. Sodeik, B., Mechanisms of viral transport in the cytoplasm. *Trends Microbiol* **2000**, *8* (10), 465-72.
91. Ribbeck, K., Do viruses use vectors to penetrate mucus barriers? *Biosci Hypotheses* **2009**, *2* (6), 329-362.

92. Helander, A.; Silvey, K. J.; Mantis, N. J.; Hutchings, A. B.; Chandran, K.; Lucas, W. T.; Nibert, M. L.; Neutra, M. R., The viral sigma 1 protein and glycoconjugates containing alpha 2-3-linked sialic acid are involved in type 1 reovirus adherence to M cell apical surfaces. *Journal of Virology* **2003**, *77* (14), 7964-7977.
93. Matrosovich, M.; Klenk, H. D., Natural and synthetic sialic acid-containing inhibitors of influenza virus receptor binding. *Rev Med Virol* **2003**, *13* (2), 85-97.
94. Couceiro, J. N.; Paulson, J. C.; Baum, L. G., Influenza virus strains selectively recognize sialyloligosaccharides on human respiratory epithelium; the role of the host cell in selection of hemagglutinin receptor specificity. *Virus Res* **1993**, *29* (2), 155-65.
95. Arcasoy, S. M.; Latoche, J.; Gondor, M.; Watkins, S. C.; Henderson, R. A.; Hughey, R.; Finn, O. J.; Pilewski, J. M., MUC1 and other sialoglycoconjugates inhibit adenovirus-mediated gene transfer to epithelial cells. *Am J Respir Cell Mol Biol* **1997**, *17* (4), 422-35.
96. Lu, W.; Hisatsune, A.; Koga, T.; Kato, K.; Kuwahara, I.; Lillehoj, E. P.; Chen, W.; Cross, A. S.; Gendler, S. J.; Gewirtz, A. T.; Kim, K. C., Cutting edge: enhanced pulmonary clearance of *Pseudomonas aeruginosa* by Muc1 knockout mice. *J Immunol* **2006**, *176* (7), 3890-4.
97. Kubiet, M.; Ramphal, R.; Weber, A.; Smith, A., Pilus-mediated adherence of *Haemophilus influenzae* to human respiratory mucins. *Infect Immun* **2000**, *68* (6), 3362-7.
98. Scharfman, A.; Kroczyński, H.; Carnoy, C.; Van Brussel, E.; Lamblin, G.; Ramphal, R.; Roussel, P., Adhesion of *Pseudomonas aeruginosa* to respiratory mucins and expression of mucin-binding proteins are increased by limiting iron during growth. *Infect Immun* **1996**, *64* (12), 5417-20.
99. Kamio, K.; Matsushita, I.; Hijikata, M.; Kobashi, Y.; Tanaka, G.; Nakata, K.; Ishida, T.; Tokunaga, K.; Taguchi, Y.; Homma, S.; Nakata, K.; Azuma, A.; Kudoh, S.; Keicho, N., Promoter analysis and aberrant expression of the MUC5B gene in diffuse panbronchiolitis. *Am J Respir Crit Care Med* **2005**, *171* (9), 949-57.
100. Linden, S. K.; Sutton, P.; Karlsson, N. G.; Korolik, V.; McGuckin, M. A., Mucins in the mucosal barrier to infection. *Mucosal Immunol* **2008**, *1* (3), 183-97.
101. Wheeler, K. M.; Cárcamo-Oyarce, G.; Turner, B. S.; Dellos-Nolan, S.; Co, J. Y.; Lehoux, S.; Cummings, R. D.; Wozniak, D. J.; Ribbeck, K., Mucin glycans attenuate the virulence of *Pseudomonas aeruginosa* in infection. *Nature Microbiology* **2019**, *4* (12), 2146-2154.
102. Cao, X.; Bansil, R.; Bhaskar, K. R.; Turner, B. S.; LaMont, J. T.; Niu, N.; Afdhal, N. H., pH-dependent conformational change of gastric mucin leads to sol-gel transition. *Biophys J* **1999**, *76* (3), 1250-8.

103. Yang, X.; Forier, K.; Steukers, L.; Van Vlierberghe, S.; Dubruel, P.; Braeckmans, K.; Glorieux, S.; Nauwynck, H. J., Immobilization of Pseudorabies Virus in Porcine Tracheal Respiratory Mucus Revealed by Single Particle Tracking. *PLOS ONE* **2012**, *7* (12), e51054.
104. Caldara, M.; Friedlander, R. S.; Kavanaugh, N. L.; Aizenberg, J.; Foster, K. R.; Ribbeck, K., Mucin biopolymers prevent bacterial aggregation by retaining cells in the free-swimming state. *Curr Biol* **2012**, *22* (24), 2325-30.
105. Parsek, M. R.; Singh, P. K., Bacterial biofilms: an emerging link to disease pathogenesis. *Annu Rev Microbiol* **2003**, *57*, 677-701.
106. Singh, P. K.; Schaefer, A. L.; Parsek, M. R.; Moninger, T. O.; Welsh, M. J.; Greenberg, E. P., Quorum-sensing signals indicate that cystic fibrosis lungs are infected with bacterial biofilms. *Nature* **2000**, *407* (6805), 762-4.
107. Burns, J. L.; Ramsey, B. W.; Smith, A. L., Clinical manifestations and treatment of pulmonary infections in cystic fibrosis. *Adv Pediatr Infect Dis* **1993**, *8*, 53-66.
108. Hoiby, N., Antibiotic therapy for chronic infection of pseudomonas in the lung. *Annu Rev Med* **1993**, *44*, 1-10.
109. Berg, H. C.; Turner, L., Movement of microorganisms in viscous environments. *Nature* **1979**, *278* (5702), 349-51.
110. Dey, P.; Bergmann, T.; Cuellar-Camacho, J. L.; Ehrmann, S.; Chowdhury, M. S.; Zhang, M.; Dahmani, I.; Haag, R.; Azab, W., Multivalent Flexible Nanogels Exhibit Broad-Spectrum Antiviral Activity by Blocking Virus Entry. *ACS Nano* **2018**, *12* (7), 6429-6442.
111. Rose, M. C.; Voynow, J. A., Respiratory tract mucin genes and mucin glycoproteins in health and disease. *Physiol Rev* **2006**, *86* (1), 245-78.
112. Roy, M. G.; Livraghi-Butrico, A.; Fletcher, A. A.; McElwee, M. M.; Evans, S. E.; Boerner, R. M.; Alexander, S. N.; Bellinghausen, L. K.; Song, A. S.; Petrova, Y. M.; Tuvim, M. J.; Adachi, R.; Romo, I.; Bordt, A. S.; Bowden, M. G.; Sisson, J. H.; Woodruff, P. G.; Thornton, D. J.; Rousseau, K.; De la Garza, M. M.; Moghaddam, S. J.; Karmouty-Quintana, H.; Blackburn, M. R.; Drouin, S. M.; Davis, C. W.; Terrell, K. A.; Grubb, B. R.; O'Neal, W. K.; Flores, S. C.; Cota-Gomez, A.; Lozupone, C. A.; Donnelly, J. M.; Watson, A. M.; Hennessy, C. E.; Keith, R. C.; Yang, I. V.; Barthel, L.; Henson, P. M.; Janssen, W. J.; Schwartz, D. A.; Boucher, R. C.; Dickey, B. F.; Evans, C. M., Muc5b is required for airway defence. *Nature* **2014**, *505* (7483), 412-6.
113. Kramer, J. R.; Onoa, B.; Bustamante, C.; Bertozzi, C. R., Chemically tunable mucin chimeras assembled on living cells. *Proc Natl Acad Sci U S A* **2015**, *112* (41), 12574-9.

7. Curriculum Vitae

For reasons of data protection, the curriculum vitae is not included in the online version.

Declaration of Honesty

Hereby I declare and confirm that this PhD thesis is entirely the result of my own work and that no other sources than those cited have been used. All annotations, which have been used from published or unpublished sources, are identified as such. The shown illustrations have been created by me, or have been marked with the corresponding references.

Antara Sharma

January 2022

